7-23-2015

Passive Sensor Bias Estimation Using Targets of Opportunity

Djedjiga Belfadel
University of Connecticut - Storrs, djedjigabelfadel@yahoo.com

Passive Sensor Bias Estimation Using Targets of Opportunity

Djedjiga Belfadel, Ph.D.

University of Connecticut, 2015

Most of the literature pertaining to target tracking assumes that the sensor data are corrupted by measurement noises that are zero mean (i.e., unbiased) and with known variances (accuracies). However in real tracking systems, measurements from sensors exhibit, typically, biases. This thesis aims to solve several key problems in passive sensors residual bias estimation, when only targets of opportunity are available. For angle-only sensors, imperfect registration leads to systematic Line of Sight (LOS) angle measurement errors in azimuth and elevation. If uncorrected, registration errors can lead to large tracking errors and potentially to the formation of multiple tracks (ghosts) on the same target. The first step is to formulate a general bias model for synchronized optical sensors; then we use a Maximum Likelihood (ML) approach that leads to a nonlinear least-squares estimation problem for simultaneous estimation of the 3D Cartesian state of the target of opportunity and the angle measurement biases of the sensors. The evaluation of the Cramér-Rao Lower Bound (CRLB) on the covariance of the bias estimates, and the statistical tests on the results of simulations show that this method is statistically efficient.

Passive Sensor Bias Estimation Using Targets of Opportunity

Djedjiga Belfadel

B.S., Mouloud Mammeri University, 2003

M.S., Mouloud Mammeri University, 2005

M.S., University of New Haven, 2009

A Dissertation

Submitted in Partial Fullfilment of the

Requirements for the Degree of

Doctor of Philosophy

at the

University of Connecticut

2015

APPROVAL PAGE

Doctor of Philosophy Dissertation

Passive Sensor Bias Estimation Using Targets of Opportunity

Presented by

Djedjiga Belfadel,

Major Advisor

Prof. Yaakov Bar-Shalom

Associate Advisor

Prof. Peter Willett

Associate Advisor

Prof. Krishna Pattipati

University of Connecticut

2015

ACKNOWLEDGEMENTS

I would like to express my gratitude to my major advisor Dr. Yaakov Bar-Shalom. His guidance, support and encouragement have made this a thoughtful and rewarding journey. His sharp insight, clear mindset and down-to-earth attitude toward research have set an example of academic perfection, from which I will continue to benefit in the future. I would also like to thank my associate advisors, Dr. Peter Willett, and Dr. Krishna Pattipati. It has truly been a privilege working with them, and I have learned a tremendous amount.

I also would like to say thanks to my friends and colleagues, Manisha Mishra, Ali Abdollahi, Richard Osborne, Wenbo Dou, Sora Choi, Ting Yuan, and Balakumar Balasingam for their helpful discussion, support and advice.

Last, but far from least, I owe a tremendous debt of gratitude to my family. To my mother, father, brothers and sister. I cannot thank you enough for all that you have done to support me.

To Massi, and Dihya, you are the joy of my life

.

TABLE OF CONTENTS

LIST OF FIGURES

LIST OF TABLES

Chapter 1

Introduction

1.1 Background

A single-target tracking Infrared (IR) system will, typically, attempt to keep the target centered in the sensor field of view and provide Line of Sight (LOS) angle measurements of a target of opportunity to an algorithm that estimates the target state comprising position, velocity, and acceleration. Methods to enhance sensor LOS measurement accuracy will minimize track uncertainties and enhance track state estimation. Typically two sources of error exist in a target tracking problem. The first is due to random errors in the tracking system and are commonly called system dynamics and measurement noises. These errors are typically assumed Gaussian with zero mean and certain variances. The second source consists of systematic measurement errors that cause all measured values to deviate from the true value by constant or slowly varying amounts. These errors are what we refer to as bias errors. Both types of errors, if uncorrected or insufficiently characterized, can lead to significant deviations in the estimated state of the target object [16].

Multisensor systems use fusion of data (or tracks) from multiple sensors to form more accurate estimates of a target's state. To fuse multiple sensor data, the individual sensor data must be expressed in a common reference frame. A

problem encountered in multisensor systems is the presence of errors due to sensor bias. Some primary sources of bias errors include: measurement biases due to the deterioration of initial sensor calibration over time; attitude errors caused by biases in the gyros of the inertial measurement units of (airborne, seaborne or spaceborne) sensors; and timing errors due to the biases in the onboard clock of each sensor platform [20].

The effect of biases introduced in the process of converting sensor measurements from polar (or spherical) coordinates to Cartesian coordinates has been discussed extensively in [3] together with the limit of validity of the standard transformation. One of the most studied examples of using converted measurements in tracking involves the conversion from polar or spherical measurements to Cartesian coordinates for use in a linear Kalman filter. If the conversion process is unbiased, the performance of a converted measurement Kalman filter is superior to a mixed coordinate EKF (i.e. target motion in Cartesian coordinates and measurements in polar coordinates) [3]. The approaches for conversion include the conventional conversion, the Unbiased Converted Measurement (UCM), the Modified Unbiased Converted Measurement (MUCM), and the Unscented Transform (UT). Recently, a decorrelated version of the UCM technique (DUCM) has been developed to address both conversion and estimation bias [13], [14].

Another example of biased measurement conversion is the estimation of range-rate from a moving platform. To measure range rate using the Doppler effect, it is necessary to nullify the impact of platform motion. The conventional nullification approach suffers from a similar bias problem as the position measurement conversion [3]. A novel scheme was proposed in [11] and [12] by applying the DUCM technique to own-Doppler nullification to eliminate this bias.

Time varying bias estimation based on a nonlinear least squares formulation and the singular value decomposition was presented in [20]. However, this work did not discuss the CRLB for bias estimation. An approach using maximum a posteriori (MAP) data association for concurrent bias estimation and data association based on sensor-level track state estimates was proposed in [21] and extended in [22]. In [15] the effect of sensor and timing bias error on the tracking quality of a space-based IR tracking system that utilizes a Linearized Kalman Filter (LKF) for the highly non-linear problem of tracking a ballistic missile was presented. This was extended in [16] by proposing a method of using stars observed in the sensor background to reduce the sensor bias error.

We propose an algorithm that uses targets of opportunity for estimation of measurement biases. The first step is to formulate a general bias model for synchronized optical sensors; then we use a Maximum Likelihood (ML) approach that leads to a nonlinear least-squares estimation problem for simultaneous estimation of the 3 dimensional Cartesian positions of the targets of opportunity and the angle measurement biases of the sensors. The algorithm is applied to different tracking systems. The first system consists of fixed sensors with known location and perfect data association tracking ballistic targets. The second system consists of two or more satellites (on known trajectories) with perfect data association, for tracking ballistic targets. However, for the third problem, the assumption of perfect data association is relaxed. This problem deals with a system that consists of space based sensors tracking ballistic targets in the presence of measurement association uncertainty. In the last part of this thesis we propose a new methodology that uses an exoatmospheric target of opportunity seen in a satellite borne sensor's field of view to estimate the sensor's biases simultaneously with the state

of the target (i.e., its trajectory).

1.2 Outline of the Dissertation

This dissertation is organized as follows: In Chapter II, bias estimation is investigated when only targets of opportunity are available. We assume the sensor locations are known fixed and we estimate their orientation biases and that data association is correct. In the first case we use three optical sensors to observe three points on the trajectory of a single target of opportunity, in the second case we consider the estimation of the position of points on the trajectory of a single target of opportunity simultaneously with the biases of two optical sensors. We discuss the bias estimation for synchronous biased sensors and the related observability issues. It is shown that for two sensors at fixed locations there is an ambiguity due to a certain rotation that does not affect the measurements, i.e., one can not have complete observability with targets of opportunity. We evaluate the Cramer-Rao lower bound (CRLB) on the covariance of the bias estimates, which is the quantification of the available information on the sensor biases and show via statistical tests that the estimation in the completely observable case is statistically efficient — it meets the CRLB.

Chapter III examines the effect of sensor bias errors on the tracking quality of a Space Tracking and Surveillance System (STSS) for the problem of tracking a ballistic missile. The STSS constellation consists of two or more satellites (on known trajectories) for tracking ballistic targets. Each satellite is equipped with an IR sensor that provides azimuth and elevation to the target. The measurements provided by these sensors are assumed time-coincident (synchronous) and

perfectly associated. The evaluation of the Cramér-Rao Lower Bound (CRLB) on the covariance of the bias estimates, and the statistical tests on the results of simulations show that this method is statistically efficient for both the three and two sensor cases. We also show that the Root Mean Square (RMS) target position error is significantly improved with bias estimation compared with the target position estimation using the original biased measurements.

In Chapter IV, an approach to bias estimation in the presence of measurement association uncertainty using common targets of opportunity, is developed. Data association is carried out before the estimation of sensor angle measurement biases. Consequently, the quality of data association is critical to the overall tracking performance. Data association becomes especially challenging if the sensors are passive. Mathematically, the problem can be formulated as a multidimensional optimization problem, where the objective is to maximize the generalized likelihood that the associated measurements correspond to common targets, based on target locations and sensor bias estimates. Applying gating techniques significantly reduces the size of this problem. The association likelihoods are evaluated using an exhaustive search after which an acceptance test is applied to each solution in order to obtain the optimal (correct) data association solution. We demonstrate the merits of this approach by applying it to a simulated tracking system, which consists of two or three satellite borne sensors tracking a ballistic target. We assume the sensors are synchronized, their locations are known, and we estimate their orientation biases together with the unknown target locations.

In Chapter V, we provide a new methodology using an exoatmospheric target of opportunity seen in a satellite borne sensor's field of view to estimate the sensor's biases simultaneously with the state of the target. Each satellite is

equipped with an IR sensor that provides the Line Of Sight (LOS) measurements azimuth and elevation to the target. The measurements provided by these sensors are assumed to be noisy but perfectly associated, i.e., it is known perfectly that they belong to the same target. The evaluation of the Cramér-Rao Lower Bound (CRLB) on the covariance of the bias estimates, and the statistical tests on the results of simulations show that this method is statistically efficient.

Finally, Chapter VI provides conclusions and future work.

1.3 Publications

The following is a list of journal papers and conference papers that have been published/accepted, are submitted, or will be submitted as a result of this research.

1.3.1 Journal Publications

1. D. Belfadel, R. W. Osborne, and Y. Bar-Shalom, "Bias Estimation and Observability for Optical Sensor Measurements with Targets of Opportunity," *Journal of Advances in Information Fusion*, vol. 9, no. 2, pp. 59–74, Dec. 2014.
2. D. Belfadel, R. W. Osborne, and Y. Bar-Shalom, "Bias Estimation for Moving Optical Sensor Measurements with Targets of Opportunity," to appear in *Journal of Advances in Information Fusion*, vol. 10, June 2015.
3. D. Belfadel, R. W. Osborne, Y. Bar-Shalom, and K. Pattipati, "Space Based Sensor Bias Estimation in the Presence of Data Association Uncertainty," Submitted to *Journal of Advances in Information Fusion*,

Feb. 2015.

1.3.2 Conference Publications

1. D. Belfadel, R. W. Osborne, and Y. Bar-Shalom, "Bias Estimation for Optical Sensor Measurements with Targets of Opportunity," *Proc. International Conference on Information Fusion, Istanbul*, Turkey, July 2013.
2. D. Belfadel, R. W. Osborne, and Y. Bar-Shalom, "A Minimalist Approach to Bias Estimation for Passive Sensor Measurements with Targets of Opportunity," *Proc. SPIE Conf. Signal and Data Processing of Small Targets*, #8857-13, San Diego, California, Aug. 2013.
3. D. Belfadel, R. W. Osborne, and Y. Bar-Shalom, "Bias estimation for space-based optical sensors with targets of opportunity," *Proc. SPIE Conf. Signal and Data Processing of Small Targets*, #9092-25, Baltimore, MD, May 2014.
4. D. Belfadel, R. W. Osborne, and Y. Bar-Shalom, "Robust approach for space-based sensor bias estimation in the presence of data association uncertainty" *Proc. SPIE Conf. Signal and Data Processing of Small Targets,* # 9474-6, Baltimore, MD, April 2015.

Chapter 2

Bias Estimation and Observability for Optical Sensor Measurements with Targets of Opportunity

2.1 Introduction

This chapter provides a solution for bias estimation of multiple passive sensors using common targets of opportunity. The measurements provided by these sensors are assumed time-coincident (synchronous) and perfectly associated. The line of sight (LOS) measurements from the sensors can be fused into measurements which are the Cartesian target position, i.e., linear in the target state.

To fuse multiple sensor data the individual sensor data must be expressed in a common reference frame. A problem encountered in multisensor systems is the presence of errors due to sensor bias. Some sources of bias errors include: measurement biases due to the deterioration of initial sensor calibration over time; attitude errors caused by biases in the gyros of the inertial measurement units of (airborne, seaborne or spaceborne) sensors; and timing errors due to the biases in the onboard clock of each sensor platform [20].

The effect of biases introduced in the process of converting sensor measurements from polar (or spherical) coordinates to Cartesian coordinates has been discussed extensively in [3] together with the limit of validity of the standard

transformation. If the conversion process is unbiased, the performance of a converted measurement Kalman filter is superior to a mixed coordinate EKF (i.e. target motion in Cartesian coordinates and measurements in polar coordinates) [3]. The approaches for conversion include the conventional conversion, the Unbiased Converted Measurement (UCM), the Modified Unbiased Converted Measurement (MUCM), and the Unscented Transform (UT). Recently, a decorrelated version of the UCM technique (DUCM) has been developed to address both conversion and estimation bias [13], [14]. Another example of biased measurement conversion is the estimation of range-rate from a moving platform. To measure range rate using the Doppler effect, it is necessary to nullify the impact of platform motion. The conventional nullification approach suffers from a similar bias problem as the position measurement conversion [3]. A novel scheme was proposed in [11] and [12] by applying the DUCM technique to own-Doppler nullification to eliminate this bias.

Time varying bias estimation based on a nonlinear least squares formulation and the singular value decomposition using truth data was presented in [20]. However, this work did not discuss the CRLB for bias estimation. An approach using maximum a posteriori (MAP) data association for concurrent bias estimation and data association based on sensor-level track state estimates was proposed in [21] and extended in [22]. Estimation of location biases only for passive sensors was discussed in [18]. The estimation of range, azimuth and location biases for active sensors was presented in [23].

For angle-only sensors, imperfect registration leads to LOS angle measurement biases in azimuth and elevation. If uncorrected, registration error can lead to large tracking errors and potentially to the formation of multiple tracks (ghosts)

on the same target.

In this chapter, bias estimation is investigated when only targets of opportunity are available. We assume the sensors are synchronized, their locations are fixed and known, the data association is correct, and we estimate their orientation biases. We investigate the use of the minimum possible number of optical sensors (which can not be less than two sensors). Two cases are considered. In the first case we use three optical sensors to observe 3 points on the trajectory of a single target of opportunity [6], in the second case we estimate the position of 6 points on the trajectory of a single target of opportunity simultaneously with the biases of two optical sensors [5]. First, we discuss the observability issues related to the bias estimation. Namely, it is shown that for two fixed sensors there is an inherent ambiguity due to a certain rotation that does not affect the measurements, i.e., one can not have complete observability of the sensor biases with targets of opportunity. For three fixed sensors, the biases are completely observable. We evaluate the Cramér-Rao lower bound (CRLB) on the covariance of the bias estimates (for the observable biases), which is the quantification of the available information on the sensor biases and show via statistical tests that the estimation is statistically efficient — it meets the CRLB. Section II presents the problem formulation and solution in detail. Section III describes the simulations performed and gives the results. Finally, Section IV gives the conclusions.

2.2 Problem Formulation

The fundamental frame of reference used in this chapter is a 3D Cartesian Common Coordinate System (CCS) defined by the orthogonal set of unit vectors

(e_x, e_y, e_z). In a multisensor scenario, sensor platform s will typically have a sensor reference frame associated with it (measurement frame of the sensor) defined by the orthogonal set of unit vectors $(e_{\xi_s}, e_{\eta_s}, e_{\zeta_s})$. The origin of the measurement frame of the sensor is a translation of the CCS origin, and its axes are rotated with respect to the CCS axes. The rotation between these frames can be described by a set of Euler angles. We will refer to these angles $\phi_s + \phi_s^n,\ \rho_s + \rho_s^n,\ \psi_s + \psi_s^n$ of sensor s, as roll, pitch and yaw respectively [20], where ϕ_s^n is the nominal roll angle, ϕ_s is the roll bias, etc.

Each angle defines a rotation about a prescribed axis, in order to align the sensor frame axes with the CCS axes. The xyz rotation sequence is chosen, which is accomplished by first rotating about the x axis by ϕ_s^n, then rotating about the y axis by ρ_s^n, and finally rotating about the z axis by ψ_s^n. The rotations sequence can be expressed by the matrices

$$\begin{aligned} T_s(\psi_s^n, \rho_s^n, \phi_s^n) =& T_z(\psi_s^n) T_y(\rho_s^n) T_x(\phi_s^n) \\ =& \begin{bmatrix} \cos\psi_s^n & \sin\psi_s^n & 0 \\ -\sin\psi_s^n & \cos\psi_s^n & 0 \\ 0 & 0 & 1 \end{bmatrix} \\ \cdot& \begin{bmatrix} \cos\rho_s^n & 0 & -\sin\rho_s^n \\ 0 & 1 & 0 \\ \sin\rho_s^n & 0 & \cos\rho_s^n \end{bmatrix} \\ \cdot& \begin{bmatrix} 1 & 0 & 0 \\ 0 & \cos\phi_s^n & \sin\phi_s^n \\ 0 & -\sin\phi_s^n & \cos\phi_s^n \end{bmatrix} \end{aligned} \tag{2.1}$$

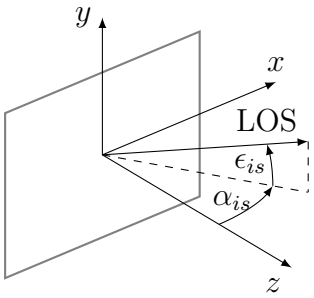

Fig. 2.1: Optical sensor coordinate system with the origin in the center of the focal plane.

Assume there are N_S synchronized passive sensors, with known fixed position in the CCS, $\boldsymbol{\xi}_s = [\xi_s, \eta_s, \zeta_s]'$, $s = 1, 2, ..., N_S$, and N_t targets, located at $\mathbf{x}_i = [x_i, y_i, z_i]'$, $i = 1, 2, ..., N_t$, in the same CCS. With the previous convention, the operations needed to transform the position of a given target i expressed in the CCS coordinate into the sensor s coordinate system ($\mathbf{x}_{is} = [x_{is}, y_{is}, z_{is}]'$) is

$$\mathbf{x}_{is}^n = T(\boldsymbol{\omega}_s)(\mathbf{x}_i - \boldsymbol{\xi}_s) \quad i = 1, 2, ..., N_t, \quad s = 1, 2, ..., N_S \tag{2.2}$$

where $\boldsymbol{\omega}_s = [\phi_s^n, \rho_s^n, \psi_s^n]'$ is the nominal orientation of sensor s and $T(\boldsymbol{\omega}_s)$ is the appropriate rotation matrix and the translation $(\mathbf{x}_i - \boldsymbol{\xi}_s)$ is the difference between the vector position of the target i and the vector position of the sensor s, both expressed in the CCS. The superscript n in (2.2) indicates that the rotation matrix is based on the nominal sensor orientation.

As shown in Figure 1, the azimuth angle α_{is} is the angle in the sensor xz plane between the sensor z axis and the line of sight to the target, while the elevation angle ϵ_{is} is the angle between the line of sight to the target and its

projection onto the xz plane, that is

$$\begin{bmatrix} \alpha_{is} \\ \epsilon_{is} \end{bmatrix} = \begin{bmatrix} \tan^{-1}\left(\frac{x_{is}}{z_{is}}\right) \\ \tan^{-1}\left(\frac{y_{is}}{\sqrt{x_{is}^2+z_{is}^2}}\right) \end{bmatrix} \tag{2.3}$$

The model for the biased noise-free LOS measurements is then

$$\begin{bmatrix} \alpha_{is}^b \\ \epsilon_{is}^b \end{bmatrix} = \begin{bmatrix} g_1(\mathbf{x_i}, \boldsymbol{\xi_s}, \boldsymbol{\omega_s}, \mathbf{b_s}) \\ g_2(\mathbf{x_i}, \boldsymbol{\xi_s}, \boldsymbol{\omega_s}, \mathbf{b_s}) \end{bmatrix} = \boldsymbol{g}(\mathbf{x_i}, \boldsymbol{\xi_s}, \boldsymbol{\omega_s}, \mathbf{b_s}) \tag{2.4}$$

where g_1 and g_2 denote the sensor Cartesian coordinates-to-azimuth/elevation angle mapping that can be found by inserting equations (2.2) and (2.3) into (2.4). The bias vector of sensor s is

$$\mathbf{b}_s = [\phi_s, \rho_s, \psi_s]' \tag{2.5}$$

For a given target, each sensor provides the noisy LOS measurements

$$\mathbf{z}_{is} = \boldsymbol{g}(\mathbf{x_i}, \boldsymbol{\xi_s}, \boldsymbol{\omega_s}, \mathbf{b_s}) + \mathbf{w_{is}} \tag{2.6}$$

where

$$\mathbf{w}_{is} = [w_{is}^{\alpha}, w_{is}^{\epsilon}]' \tag{2.7}$$

The measurement noises w_{is}^{α} and w_{is}^{ϵ} are zero-mean, white with corresponding standard deviations σ_s^{α}, σ_s^{ϵ} and are assumed mutually independent. The problem is to estimate the bias vectors for all sensors and the positions of the targets of opportunity. We shall obtain the maximum likelihood (ML) estimate of the

augmented parameter vector

$$\boldsymbol{\theta} = [\mathbf{x}'_1, ..., \mathbf{x}'_{N_t}, \mathbf{b}'_1, ..., \mathbf{b}'_{N_S}]' \tag{2.8}$$

consisting of the (unknown) position of target i and the biases of sensor s, $i = 1, ..., N_t, s = 1, ..., N_S$, by maximizing the likelihood function

$$\Lambda(\boldsymbol{\theta}) = \prod_{i=1}^{N_t} \prod_{s=1}^{N_S} p\left(\mathbf{z}_{is}|\boldsymbol{\theta}\right) \tag{2.9}$$

where

$$\begin{aligned} p\left(\mathbf{z}_{is}|\boldsymbol{\theta}\right) =& |2\pi R_s|^{-1/2} \\ & \cdot \exp\left(-\frac{1}{2}\left[\mathbf{z}_{is} - \mathbf{h}_{is}\left(\boldsymbol{\theta}\right)\right]' R_s^{-1}\left[\mathbf{z}_{is} - \mathbf{h}_{is}\left(\boldsymbol{\theta}\right)\right]\right) \end{aligned} \tag{2.10}$$

and

$$\mathbf{h}_{is}(\boldsymbol{\theta}) \stackrel{\Delta}{=} \boldsymbol{g}(\mathbf{x_i}, \boldsymbol{\xi_s}, \boldsymbol{\omega_s}, \mathbf{b_s}) \tag{2.11}$$

The ML estimate (MLE) is then

$$\hat{\boldsymbol{\theta}}^{ML} = \arg\max_{\boldsymbol{\theta}} \Lambda(\boldsymbol{\theta}) \tag{2.12}$$

In order to find the MLE, one has to solve a nonlinear least squares problem for the exponent in (2.10). This will be done using a numerical search via the Iterated Least Squares (ILS) technique [2].

2.2.1 Requirements for bias estimability

First requirement for bias estimability. For a given target we have a two-dimensional measurement from each sensor (the two LOS angles to the target). We assume that each sensor sees all the targets at a common time.[1] Stacking together each measurement of N_t targets seen by N_S sensors results in an overall measurement vector of dimension $2N_tN_S$. Given that the position and bias vectors of each target are three-dimensional, and knowing that the number of equations (size of the stacked measurement vector) has to be at least equal to the number of parameters to be estimated (target positions and biases), we must have

$$2N_tN_S \geq 3(N_t + N_S) \tag{2.13}$$

This is a necessary condition but not sufficient because (2.12) has to have a unique solution, i.e., the parameter vector has to be estimable. This is guaranteed by the second requirement.

Second requirement of bias estimability. This is the invertibility of the Fisher Information matrix (FIM) [1], to be discussed later. For example, to estimate the biases of 3 sensors (9 bias components) we need 3 targets (9 position components), i.e., the search is in an 18-dimensional space. In order to estimate the biases of 2 sensors (6 bias components) we need at least 6 targets (18 position components) to meet the necessary requirement (2.13). The rank of the FIM has to be equal to the number of parameters to be estimated (6+18=24). The full rank of the FIM is a necessary and sufficient condition for estimability, however, for the two fixed sensors situation this is not satisfied. This issue will be discussed further in the

[1] This can also be the same target at different times, as long as the sensors are synchronized.

simulation section, where an explanation will be provided.

2.2.2 Iterated Least Squares

Given the estimate $\hat{\boldsymbol{\theta}}^j$ after j iterations, the ILS estimate after the $(j+1)$th iteration will be

$$\hat{\boldsymbol{\theta}}^{j+1} = \hat{\boldsymbol{\theta}}^j + \left[(H^j)' R^{-1} H^j\right]^{-1} (H^j)' R^{-1} [\mathbf{z} - \mathbf{h}(\hat{\boldsymbol{\theta}}^j)] \tag{2.14}$$

where

$$\mathbf{z} = [z'_{11}, ..., z'_{is}, ..., z'_{N_t N_S}]' \tag{2.15}$$

$$\mathbf{h}(\hat{\boldsymbol{\theta}}^j) = [h_{11}(\hat{\boldsymbol{\theta}}^j)', ..., h_{is}(\hat{\boldsymbol{\theta}}^j)', ..., h_{N_t N_S}(\hat{\boldsymbol{\theta}}^j)'] \tag{2.16}$$

$$R = \begin{bmatrix} R_1 & 0 & \cdots & 0 \\ 0 & R_2 & \cdots & 0 \\ \vdots & \vdots & \ddots & \vdots \\ 0 & \cdots & 0 & R_{N_S} \end{bmatrix} \tag{2.17}$$

where R_s is the measurement noise covariance matrix of sensor s, and

$$H^j = \left. \frac{\partial \mathbf{h}\left(\boldsymbol{\theta}^j\right)}{\partial \boldsymbol{\theta}} \right|_{\boldsymbol{\theta}=\hat{\boldsymbol{\theta}}^j} \tag{2.18}$$

is the Jacobian matrix of the vector consisting of the stacked measurement functions (2.16) w.r.t. (2.8) evaluated at the ILS estimate from the previous iteration j. In this case, the Jacobian matrix is, with the iteration index omitted for con-

ciseness,

$$H = \begin{bmatrix} H_{11} & H_{21} & \cdots & H_{N_t 1} & H_{12} & \cdots & H_{N_t N_S} \end{bmatrix}' \tag{2.19}$$

where

$$H'_{is} = \begin{bmatrix} \frac{\partial g_{1_{is}}}{\partial x_1} & \frac{\partial g_{2_{is}}}{\partial x_1} \\ \frac{\partial g_{1_{is}}}{\partial y_1} & \frac{\partial g_{2_{is}}}{\partial y_1} \\ \frac{\partial g_{1_{is}}}{\partial z_1} & \frac{\partial g_{2_{is}}}{\partial z_1} \\ \vdots & \vdots \\ \frac{\partial g_{1_{is}}}{\partial x_{N_t}} & \frac{\partial g_{2_{is}}}{\partial x_{N_t}} \\ \frac{\partial g_{1_{is}}}{\partial y_{N_t}} & \frac{\partial g_{2_{is}}}{\partial y_{N_t}} \\ \frac{\partial g_{1_{is}}}{\partial z_{N_t}} & \frac{\partial g_{2_{is}}}{\partial z_{N_t}} \\ \frac{\partial g_{1_{is}}}{\partial \psi_1} & \frac{\partial g_{2_{is}}}{\partial \psi_1} \\ \frac{\partial g_{1_{is}}}{\partial \rho_1} & \frac{\partial g_{2_{is}}}{\partial \rho_1} \\ \frac{\partial g_{1_{is}}}{\partial \phi_1} & \frac{\partial g_{2_{is}}}{\partial \phi_1} \\ \vdots & \vdots \\ \frac{\partial g_{1_{is}}}{\partial \psi_{N_S}} & \frac{\partial g_{2_{is}}}{\partial \psi_{N_S}} \\ \frac{\partial g_{1_{is}}}{\partial \rho_{N_S}} & \frac{\partial g_{2_{is}}}{\partial \rho_{N_S}} \\ \frac{\partial g_{1_{is}}}{\partial \phi_{N_S}} & \frac{\partial g_{2_{is}}}{\partial \phi_{N_S}} \end{bmatrix} \tag{2.20}$$

The appropriate partial derivatives are given in Appendix A.

2.2.3 Initialialization

In order to perform the numerical search via ILS, an initial estimate $\hat{\boldsymbol{\theta}}^0$ is required. Assuming that the biases are null, the LOS measurements from the first and the second sensor α_{i1}, α_{i2} and ϵ_{i1} can be used to solve for each initial Cartesian target

position, in the CCS, as

$$x_i^0 = \frac{\xi_2 - \xi_1 + \zeta_1 \tan\alpha_{i1} - \zeta_2 \tan\alpha_{i2}}{\tan\alpha_{i1} - \tan\alpha_{i2}} \tag{2.21}$$

$$y_i^0 = \frac{\tan\alpha_{i1}\left(\xi_2 + \tan\alpha_{i2}\left(\zeta_1 - \zeta_2\right)\right) - \xi_1 \tan\alpha_{i2}}{\tan\alpha_{i1} - \tan\alpha_{i2}} \tag{2.22}$$

$$z_i^0 = \eta_1 + \tan\epsilon_{i1} \left| \frac{\left(\xi_1 - \xi_2\right)\cos\alpha_{i2} + \left(\zeta_2 - \zeta_1\right)\sin\alpha_{i2}}{\sin\left(\alpha_{i1} - \alpha_{i2}\right)} \right| \tag{2.23}$$

2.2.4 Cramér-Rao Lower Bound

In order to evaluate the efficiency of the estimator, the CRLB must be calculated. The CRLB provides a lower bound on the covariance matrix of an unbiased estimator as [1]

$$E\{(\boldsymbol{\theta} - \hat{\boldsymbol{\theta}})(\boldsymbol{\theta} - \hat{\boldsymbol{\theta}})'\} \geq J^{-1} \tag{2.24}$$

where J is the Fisher Information Matrix (FIM), $\boldsymbol{\theta}$ is the true parameter vector to be estimated, and $\hat{\boldsymbol{\theta}}$ is the estimate. The FIM is

$$J = E\left\{\left[\nabla_{\boldsymbol{\theta}} \ln\Lambda(\boldsymbol{\theta})\right]\left[\nabla_{\boldsymbol{\theta}} \ln\Lambda(\boldsymbol{\theta})\right]'\right\}\Big|_{\boldsymbol{\theta}=\boldsymbol{\theta}_{\text{true}}} \tag{2.25}$$

where the gradient of the log-likelihood function is

$$\lambda(\boldsymbol{\theta}) \triangleq \ln\Lambda(\boldsymbol{\theta}) \tag{2.26}$$

$$\nabla_{\boldsymbol{\theta}}\lambda(\boldsymbol{\theta}) = \sum_{i=1}^{N_t}\sum_{s=1}^{N_S} H_{is}' R_{is}^{-1}\left(\mathbf{z}_{is} - \mathbf{h}_{is}(\boldsymbol{\theta})\right) \tag{2.27}$$

which, when plugged into (2.25), gives

$$\begin{aligned} J &= \sum_{i=1}^{N_t} \sum_{s=1}^{N_S} H'_{is} \left(R_s^{-1}\right) H_{is}\big|_{\boldsymbol{\theta}=\boldsymbol{\theta}_{true}} \\ &= H' \left(R^{-1}\right) H\big|_{\boldsymbol{\theta}=\boldsymbol{\theta}_{true}} \end{aligned} \tag{2.28}$$

2.3 Simulations

2.3.1 Three-Sensor Case

We simulated three optical sensors at various fixed and known locations observing a target at three points in time at unknown locations (which is equivalent to viewing three different targets at unknown locations). Five scenarios of three sensors are examined for a set of target locations. They are shown in Figures 2.2–2.6. Each scenario is such that each target position can be observed by all sensors. As discussed in the previous section, the three sensor biases were roll, pitch and yaw angle offsets. The biases for each sensor were set to $1^\circ = 17.45\,\text{mrad}$. We made 100 Monte Carlo runs for each scenario. In order to establish a baseline for evaluating the performance of our algorithm, we also ran the simulations without biases and with biases, but without bias estimation. The horizontal and vertical fields-of-view of each sensor are assumed to be 60°. The measurement noise standard deviation σ_s (identical across sensors for both azimuth and elevation measurements) was assumed to be $0.34\,\text{mrad}$.

Description of the Scenarios

The sensors are assumed to provide LOS angle measurements. We denote by $\boldsymbol{\xi}_1, \boldsymbol{\xi}_2, \boldsymbol{\xi}_3$ the 3D Cartesian sensor positions, and $\mathbf{x}_1, \mathbf{x}_2, \mathbf{x}_3$ the 3D Cartesian target

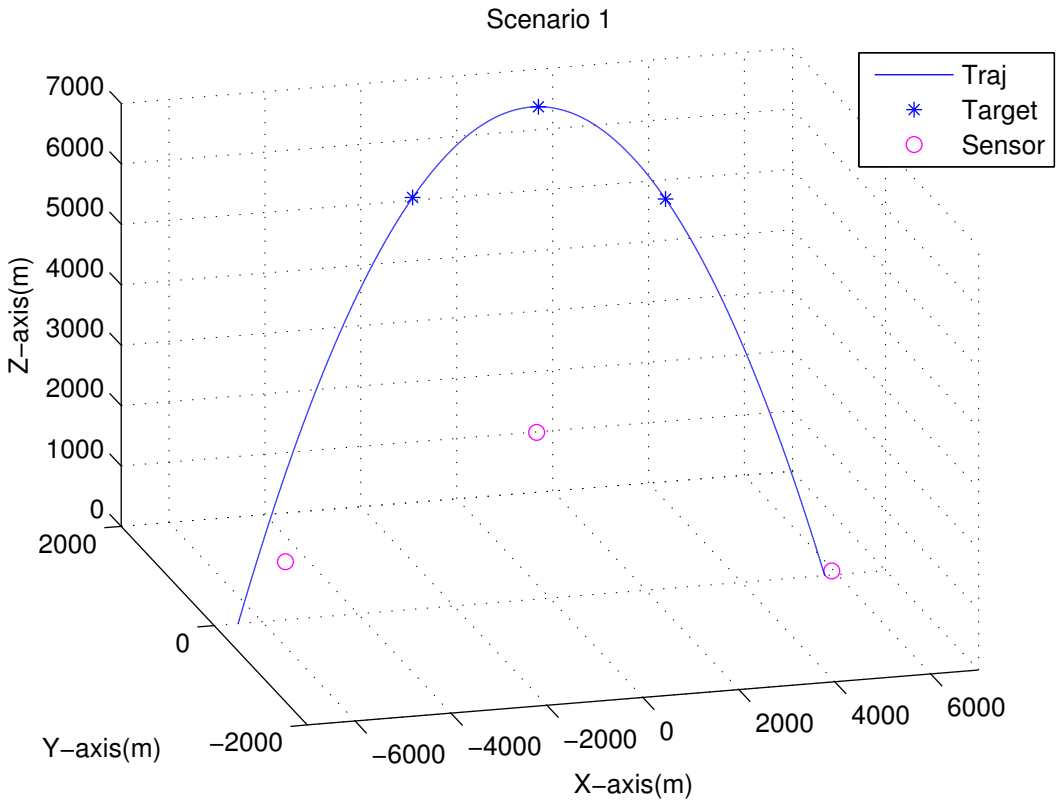

Fig. 2.2: Scenario 1

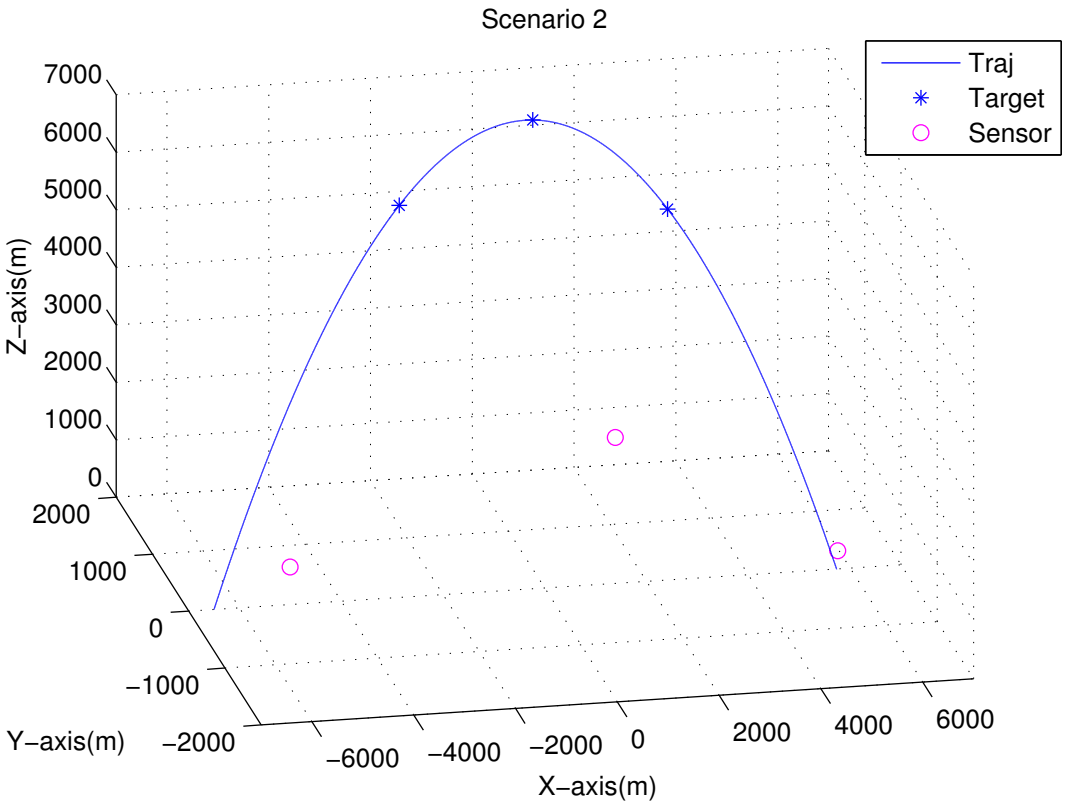

Fig. 2.3: Scenario 2

Table 2.1: Sensor positions (m) for the scenarios considered.

	First Sensor			Second Sensor			Third Sensor		
Scenario	ξ	η	ζ	ξ	η	ζ	ξ	η	ζ
1	-5500	15	950	-230	45	2720	5900	20	50
2	-4900	145	505	1230	-220	2765	5900	200	110
3	-4900	25	1050	1330	25	1585	4900	45	150
4	-5600	5	200	1230	10	1220	4900	20	50
5	-3500	1500	25	1230	-520	1265	4900	1350	20

positions (all in CCS). The three target positions are the same for all the scenarios, and they were chosen from a trajectory of a ballistic target as follows (in m)

$$\mathbf{x}_1 = [-2860\,, 0\,, 6820\,]' \tag{2.29}$$

$$\mathbf{x}_2 = [-235.9\,, 0\,, 8152\,]' \tag{2.30}$$

$$\mathbf{x}_3 = [2413\,, 0\,, 6451\,]' \tag{2.31}$$

Table 2.1 summarizes the sensor positions (in m) for the 5 scenarios considered.

Statistical efficiency of the estimates

In order to test for the statistical efficiency of the estimate (of the 18 dimensional vector (2.8)), the normalized estimation error squared (NEES) [2] is used, with the CRLB as the covariance matrix. The sample average NEES over 100 Monte Carlo runs is given in Table 2.2 for all the scenarios. The NEES is calculated using the FIM evaluated at both the true bias values and target positions, as well as at the estimated biases and target positions. According to the CRLB, the FIM has to be evaluated at the true parameter. Since this is not available in practice, however, it is useful to evaluate the FIM also at the estimated parameter, the only

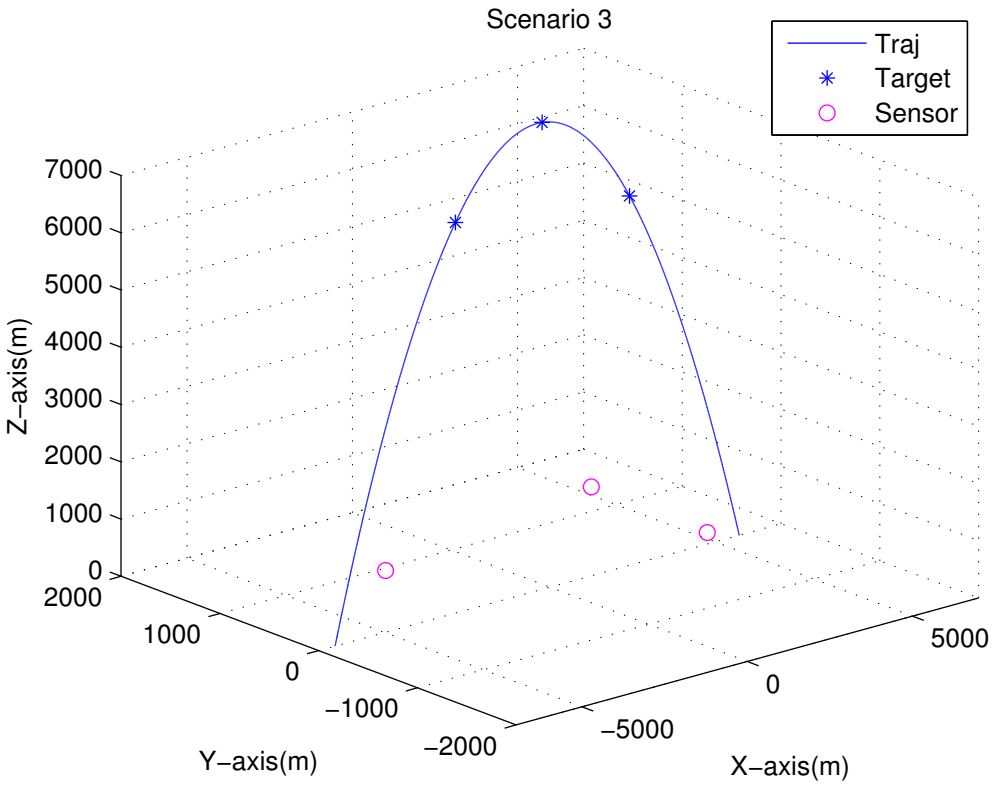

Fig. 2.4: Scenario 3

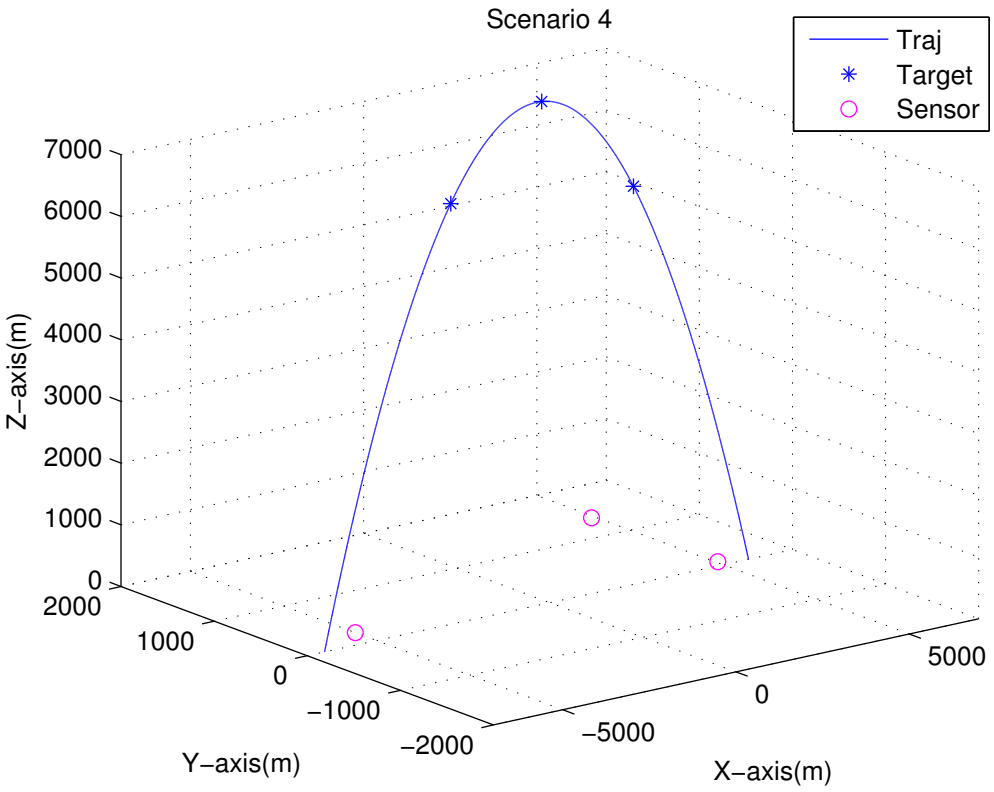

Fig. 2.5: Scenario 4

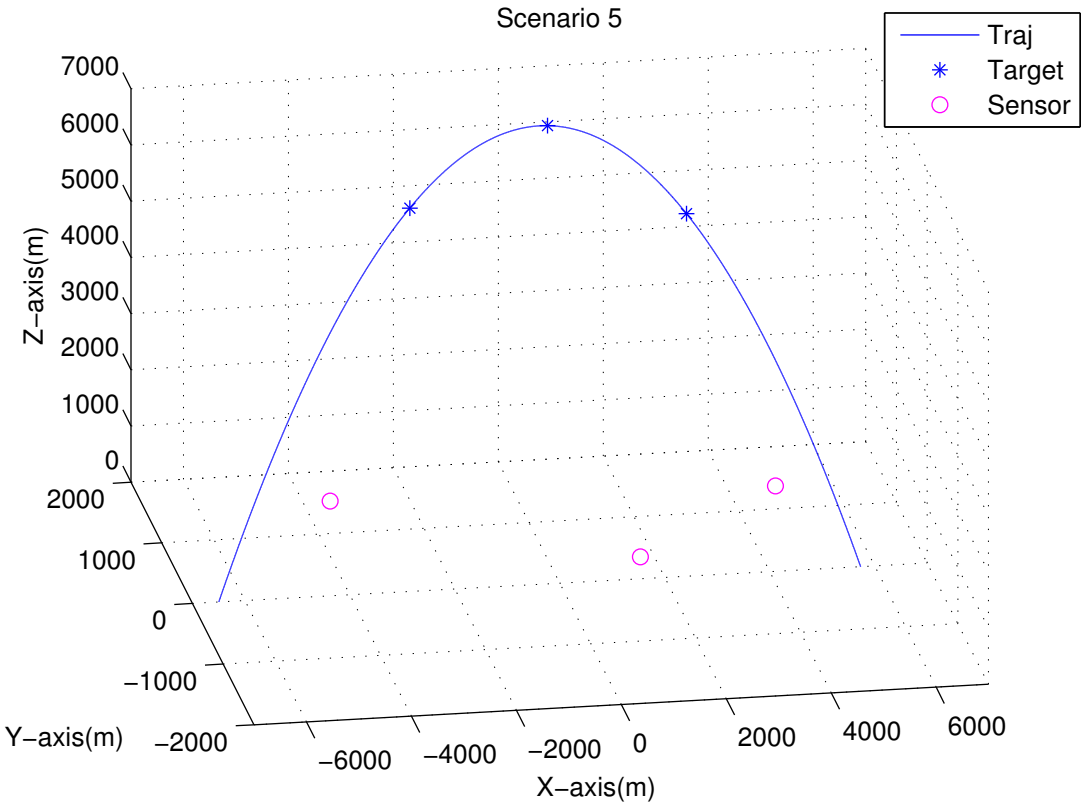

Fig. 2.6: Scenario 5

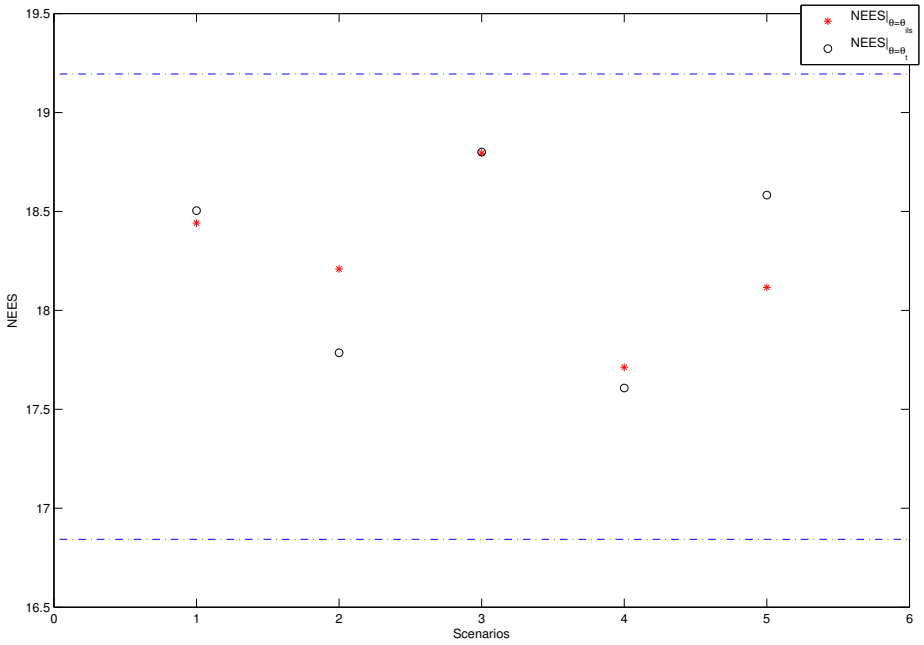

Fig. 2.7: Sample average NEES over 100 Monte Carlo runs for all 5 scenarios (Three-sensor case).

one available in real world implementations [24], [25]. The results are practically identical regardless of which values are chosen for evaluation of the FIM. The 95% probability region for the 100 sample average NEES of the 18 dimensional parameter vector is [16.84, 19.19]. For all 5 scenarios, the NEES is found to be within this interval and the MLE is therefore statistically efficient. Figure 2.7 shows the NEES for all scenarios, Figure 2.8 shows the individual bias component NEES for all scenarios, The 95% probability region for the 100 sample average single component NEES is [0.74, 1.29]. For all 5 scenarios these NEES are found to be within this interval.

The RMS position errors for the 3 targets are summarized in Table 2.3. In this table, the first estimation scheme was established as a baseline using bias-free

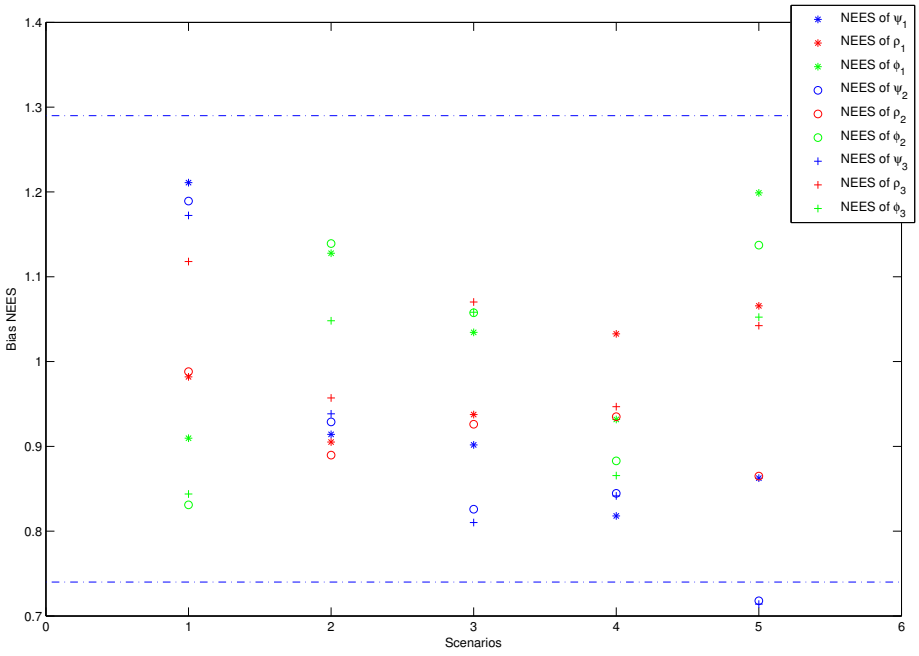

Fig. 2.8: Sample average bias NEES (CRLB evaluated at the estimate), for each of the 9 biases, over 100 Monte Carlo runs for all 5 scenarios (Three-sensor case).

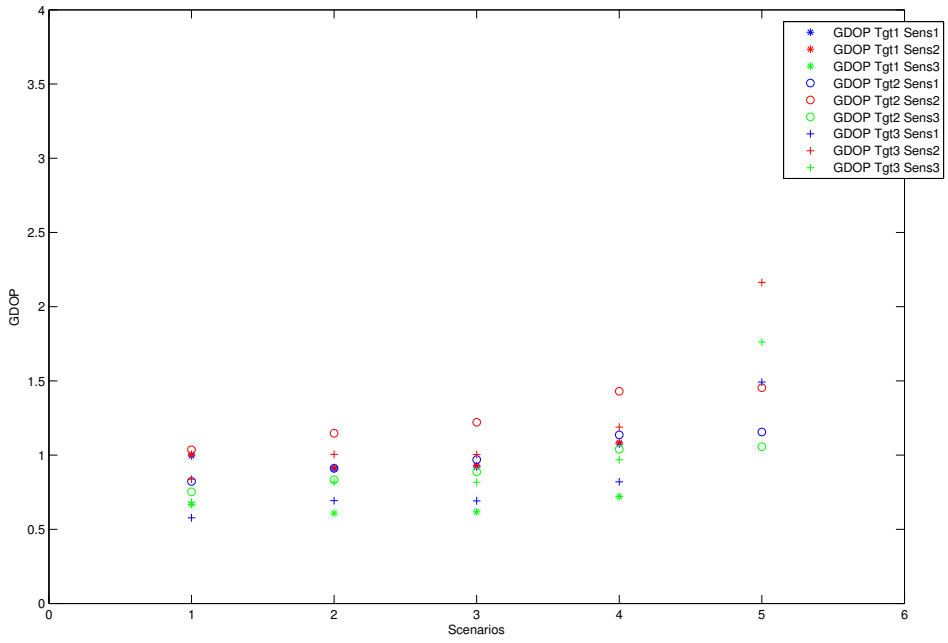

Fig. 2.9: GDOPs for the 5 scenarios considered (Three-sensor case).

LOS measurements to estimate the target positions.[2] For the second scheme, we used biased LOS measurements but we only estimated target positions. In the last scheme, we used biased LOS measurements and we simultaneously estimated the target positions and sensor biases. Bias estimation yields significantly improved target RMS position errors in the presence of biases.

Each component of $\boldsymbol{\theta}$ should also be individually consistent with its corresponding σ_{CRLB} (the square root of the corresponding diagonal element of the inverse of FIM). In this case, the sample average bias RMSE over 100 Monte Carlo runs should be within 15% of its corresponding bias standard deviation from the CRLB (σ_{CRLB}) with 95% probability. Table 2.4 demonstrates the consistency of the individual bias estimates. This complements the NEES evaluations from Figure 2.8.

To confirm that the bias estimates are unbiased, the average bias error $\bar{\bar{b}}$, from Table 2.5, over 100 Monte Carlo runs confirms that $|\bar{\bar{b}}|$ is less then $2\frac{\sigma_{\text{CRLB}}}{\sqrt{N}}$ (which it should be with 95% probability), i.e., these bias estimates are unbiased.

In order to examine the statistical efficiency for a variety of target-sensor geometries, the sensors' locations were varied from one scenario to another in order to vary the Geometric Dilution of Precision (GDOP), defined as

$$\text{GDOP} \triangleq \frac{\text{RMSE}}{r\sqrt{\sigma_\alpha^2 + \sigma_\epsilon^2}} \tag{2.32}$$

where "RMSE" is the RMS position error for a target location (in the absence of biases), r is the range to the target, and σ_α and σ_ϵ are the azimuth and elevation

[2] As shown in [24, 25] the unbiased LOS measurements yield composite measurements (full position MLEs) whose errors are zero-mean and their covariance is equal to the corresponding CRLB.

Table 2.2: Sample average NEES over 100 Monte Carlo runs for 5 scenarios (based on $18 \cdot 100 = 1800$ degrees of freedom chi-square distribution) (Three-sensor case).

Scenarios	1	2	3	4	5
$\text{NEES}\|_{\theta=\theta_t}$	18.5043	17.7856	18.8000	17.6076	18.5826
$\text{NEES}\|_{\theta=\hat{\theta}_{\text{ILS}}}$	18.4415	18.2095	18.7950	17.7124	18.1163

Table 2.3: Sample average position RMSE (m) for the 3 targets, over 100 Monte Carlo runs, for the 3 estimation schemes (Three-sensor case).

	First Target	Second Target	Third Target
Scheme	RMSE	RMSE	RMSE
1	3.33	3.51	2.82
2	146.61	167.43	134.80
3	38.93	43.82	37.68

measurement error standard deviations, respectively. Figure 2.9 shows the various GDOP levels in the 9 target-sensor combinations for each of the 5 scenarios for which statistical efficiency was confirmed.

2.3.2 Two-Sensor Case

We simulated two optical sensors at various fixed locations observing a target at six (unknown) locations (which is equivalent to viewing six different targets at unknown locations). In this case a 24-dimensional parameter vector is to be estimated.

It was observed that the rank of the FIM was 23 which implies incomplete observability. Even with more target points there was always a deficiency of 1 in the rank of the FIM. As shown in Figure 2.10, this can be explained as follows: a rotation of the sensors and all the targets around the axis defined by the line S_1S_2

Table 2.4: Sample average bias RMSE over 100 Monte Carlo runs and the corresponding bias standard deviation from the CRLB (σ_{CRLB}), for all configurations (mrad) (Three-sensor case).

Scenario		First Sensor			Second Sensor			Third Sensor		
		ψ	ρ	ϕ	ψ	ρ	ϕ	ψ	ρ	ϕ
1	RMSE	3.168	1.173	2.558	7.358	1.121	3.321	3.210	1.419	2.261
	σ_{CRLB}	2.872	1.183	2.679	6.721	1.129	3.639	2.954	1.341	2.459
2	RMSE	1.935	1.133	2.642	7.573	1.069	3.352	4.224	1.335	1.881
	σ_{CRLB}	2.028	1.190	2.485	7.855	1.129	3.138	4.355	1.362	1.835
3	RMSE	2.473	1.089	5.923	6.475	1.084	6.675	4.504	1.266	5.272
	σ_{CRLB}	2.600	1.124	5.780	7.054	1.140	6.455	4.969	1.239	5.105
4	RMSE	2.512	1.257	5.950	6.472	1.161	6.522	4.579	1.351	5.218
	σ_{CRLB}	2.801	1.243	6.198	7.094	1.201	6.976	5.024	1.388	5.634
5	RMSE	3.102	1.697	4.418	5.979	2.124	5.609	4.238	2.195	3.979
	σ_{CRLB}	3.334	1.646	4.034	7.078	2.295	5.253	5.011	2.150	3.869

Table 2.5: Sample average bias error $\bar{\tilde{b}}$ over N=100 Monte Carlo runs for all configurations (mrad) (to confirm that the bias estimates are unbiased) (Three-sensor case).

Scenario		First Sensor			Second Sensor			Third Sensor		
		ψ	ρ	ϕ	ψ	ρ	ϕ	ψ	ρ	ϕ
1	$\bar{\tilde{b}}$	0.336	-0.076	0.034	0.693	-0.127	0.128	0.240	-0.111	0.146
	$\frac{\sigma_{\text{CRLB}}}{\sqrt{N}}$	0.287	0.118	0.268	0.672	0.113	0.364	0.295	0.134	0.246
2	$\bar{\tilde{b}}$	-0.099	0.012	0.045	-0.356	0.002	0.017	-0.195	0.088	-0.038
	$\frac{\sigma_{\text{CRLB}}}{\sqrt{N}}$	0.203	0.119	0.248	0.785	0.113	0.314	0.436	0.136	0.184
3	$\bar{\tilde{b}}$	-0.191	0.125	0.039	-0.565	0.134	-0.076	-0.348	0.198	-0.162
	$\frac{\sigma_{\text{CRLB}}}{\sqrt{N}}$	0.260	0.112	0.578	0.705	0.114	0.645	0.497	0.124	0.510
4	$\bar{\tilde{b}}$	0.020	-0.153	-0.481	0.412	-0.094	-0.374	0.345	-0.180	-0.209
	$\frac{\sigma_{\text{CRLB}}}{\sqrt{N}}$	0.280	0.124	0.620	0.709	0.120	0.698	0.502	0.139	0.563
5	$\bar{\tilde{b}}$	0.522	-0.002	-0.058	0.823	0.038	0.034	0.576	-0.009	0.025
	$\frac{\sigma_{\text{CRLB}}}{\sqrt{N}}$	0.333	0.165	0.403	0.708	0.230	0.525	0.501	0.215	0.387

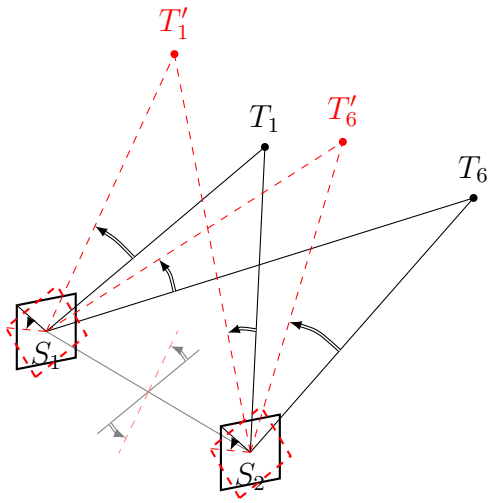

Fig. 2.10: Rotation around axis S_1S_2 of the sensors and all targets by the same angle leaves all the LOS angles from the sensors to the targets unchanged.

connecting the optical centers of the two sensors is not observable because this will yield the same measurements regardless of the magnitude of this rotation. Note that this rotation does not change the locations of the sensors, which are assumed known. Thus, with two sensors, one cannot estimate all 6 biases — we are limited to estimating 5 and this will be borne out by the FIM in the simulations. A similar observation was made in [10] for sensors that are facing each other. However the above discussion points out that the sensors do not have to face each other — there is an inherent lack of observability of any rotation around the above defined axis. This problem does not exist if there are 3 or more sensors[3] because there is no axis of rotation that does not change the location of at least one sensor.

Four scenarios of two sensors are examined for a set of target locations. They are shown in Figures 2.11–2.14. Each scenario is such that each target position can be observed by all sensors. As discussed in the previous section, the three

[3] Provided that the three sensors are not located in a straight line.

sensor biases were roll, pitch and yaw angle offsets. The second sensor roll bias is assumed to be known and null, this is in view of the above discussion about the inherent rank 1 deficiency of the FIM in the two sensors case which makes it impossible to estimate all the 6 sensor biases. Reducing the number of biases from 6 to 5 allows a full rank FIM. All the other biases for each sensor were set to $1^\circ = 17.45\,\text{mrad}$.

We made 100 Monte Carlo runs for each scenario. In order to establish a baseline for evaluating the performance of our algorithm, we also ran the simulations without bias, and with bias but without bias estimation. The measurement noise standard deviation σ_s (identical across sensors for both azimuth and elevation measurements) was assumed to be $0.34\,\text{mrad}$. As a fifth scenario we simulated two optical sensors observing two targets (two trajectories) at three points in time for each target, as shown in Figure 2.15.

Description of the Scenarios

The sensors are assumed to provide LOS angle measurements. We denote by $\boldsymbol{\xi}_1, \boldsymbol{\xi}_2$ the 3D Cartesian sensor positions, and $\mathbf{x}_1, \mathbf{x}_2, \mathbf{x}_3, \mathbf{x}_4, \mathbf{x}_5, \mathbf{x}_6$ the 3D Cartesian target positions (all in CCS). The six target positions are the same for the first four scenarios, and they were chosen from a trajectory of a ballistic target as follows (in m)

$$\mathbf{x}_1 = [-4931\,, 0\,, 3649\,]' \tag{2.33}$$

$$\mathbf{x}_2 = [-3731\,, 0\,, 5714\,]' \tag{2.34}$$

$$\mathbf{x}_3 = [-2400\,, 0\,, 7100\,]' \tag{2.35}$$

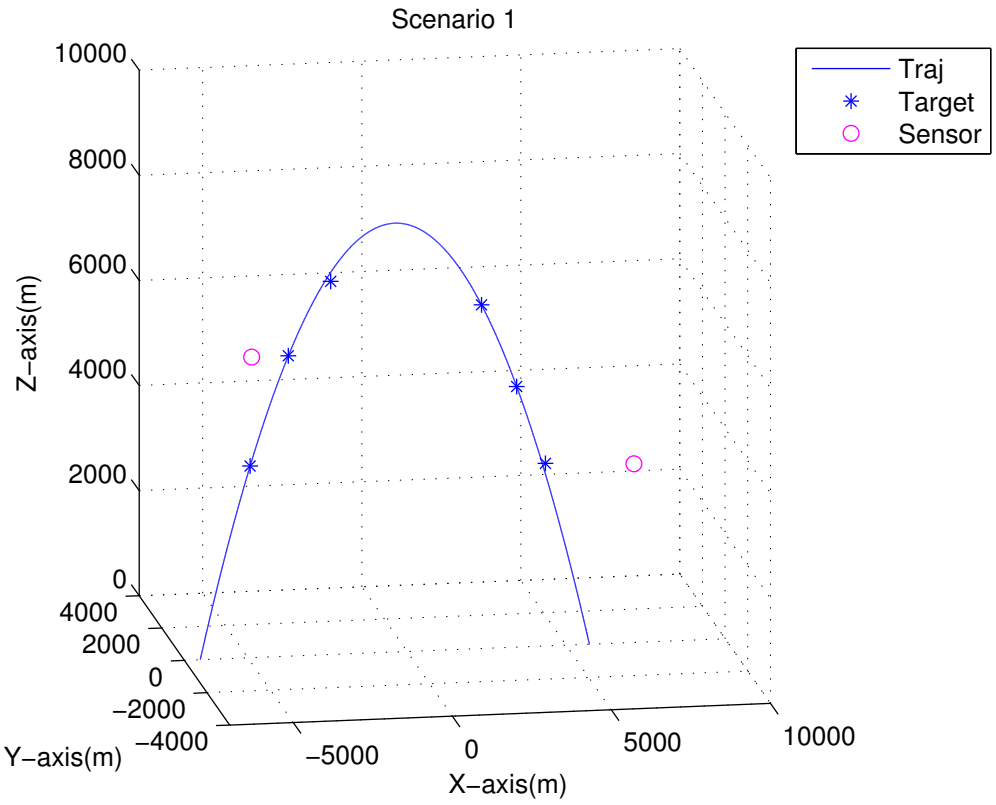

Fig. 2.11: Scenario 1 for the two-sensor case

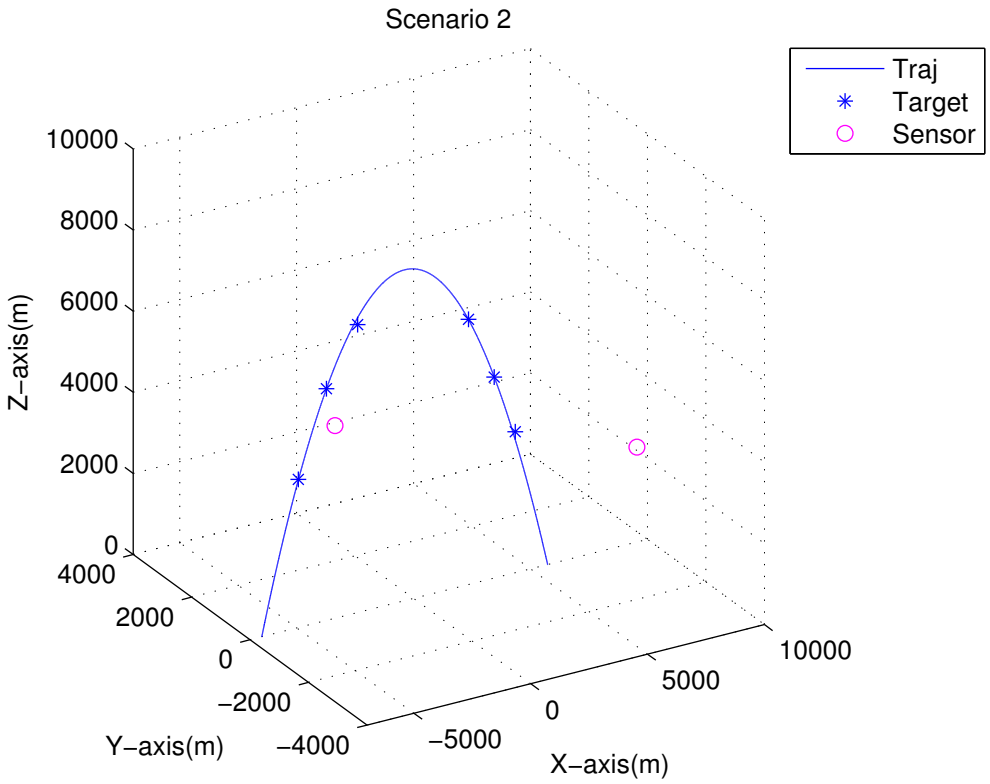

Fig. 2.12: Scenario 2 for the two-sensor case

Table 2.6: Sensor positions (m) for the scenarios considered.

	First Sensor			Second Sensor		
Scenario	ξ	η	ζ	ξ	η	ζ
1	-4550	5420	-945	6170	4250	-2700
2	-4550	5420	950	6170	4250	-2700
3	-4550	5420	950	6170	3250	-2700
4	-4550	5420	950	5170	4250	-2700
5	-1550	6120	-1445	6170	5250	-1400

$$\mathbf{x}_4 = [2341\,, 0\,, 6538\,]' \tag{2.36}$$

$$\mathbf{x}_5 = [3448\,, 0\,, 4956\,]' \tag{2.37}$$

$$\mathbf{x}_6 = [4351\,, 0\,, 3475\,]' \tag{2.38}$$

For the fifth scenario, the six target positions were chosen from two trajectories of two ballistic targets as follows (in m)

$$\mathbf{x}_1 = [-4931\,, 0\,, 3649\,]' \tag{2.39}$$

$$\mathbf{x}_2 = [2994\,, 0\,, 5670\,]' \tag{2.40}$$

$$\mathbf{x}_3 = [-2400\,, 0\,, 7100\,]' \tag{2.41}$$

$$\mathbf{x}_4 = [-1400\,, 0\,, 7932\,]' \tag{2.42}$$

$$\mathbf{x}_5 = [2376\,, 0\,, 6497\,]' \tag{2.43}$$

$$\mathbf{x}_6 = [4075\,, 0\,, 3823\,]' \tag{2.44}$$

Table 2.6 summarizes the sensor positions (in m) for the 5 scenarios considered.

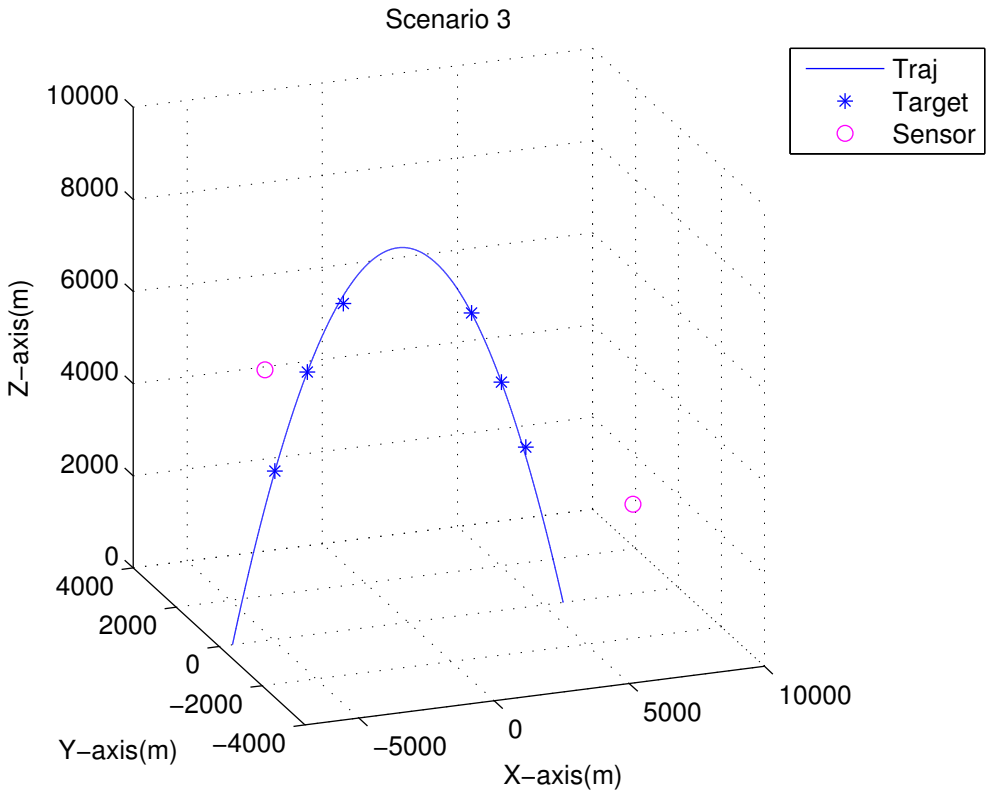

Fig. 2.13: Scenario 3 for the two-sensor case

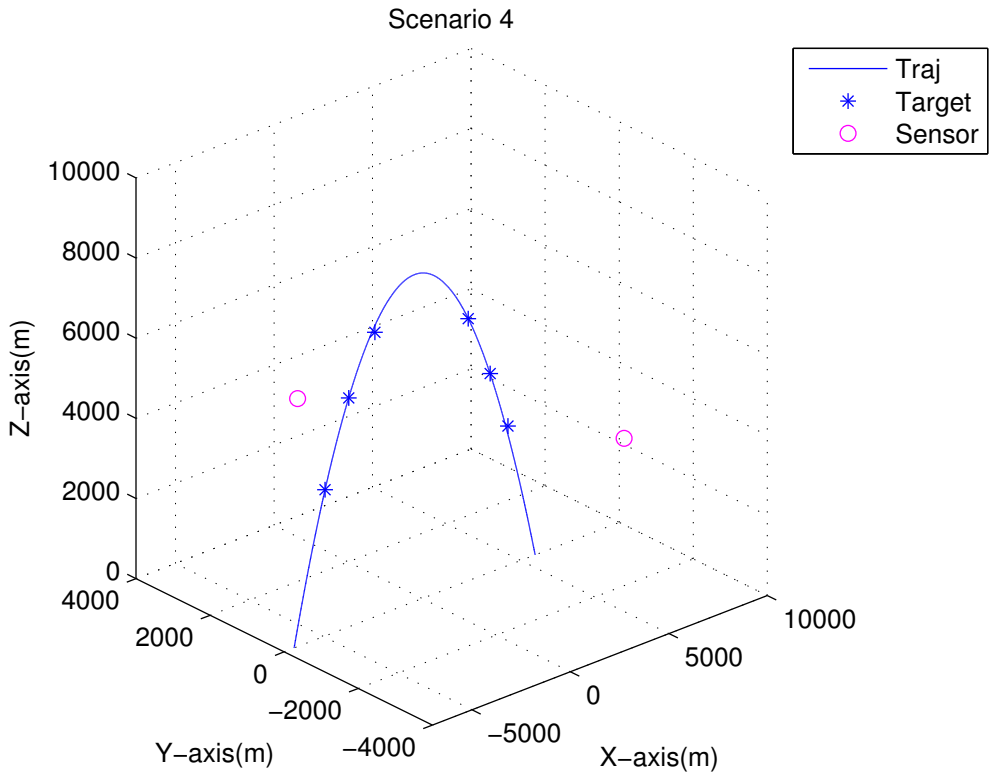

Fig. 2.14: Scenario 4 for the two-sensor case

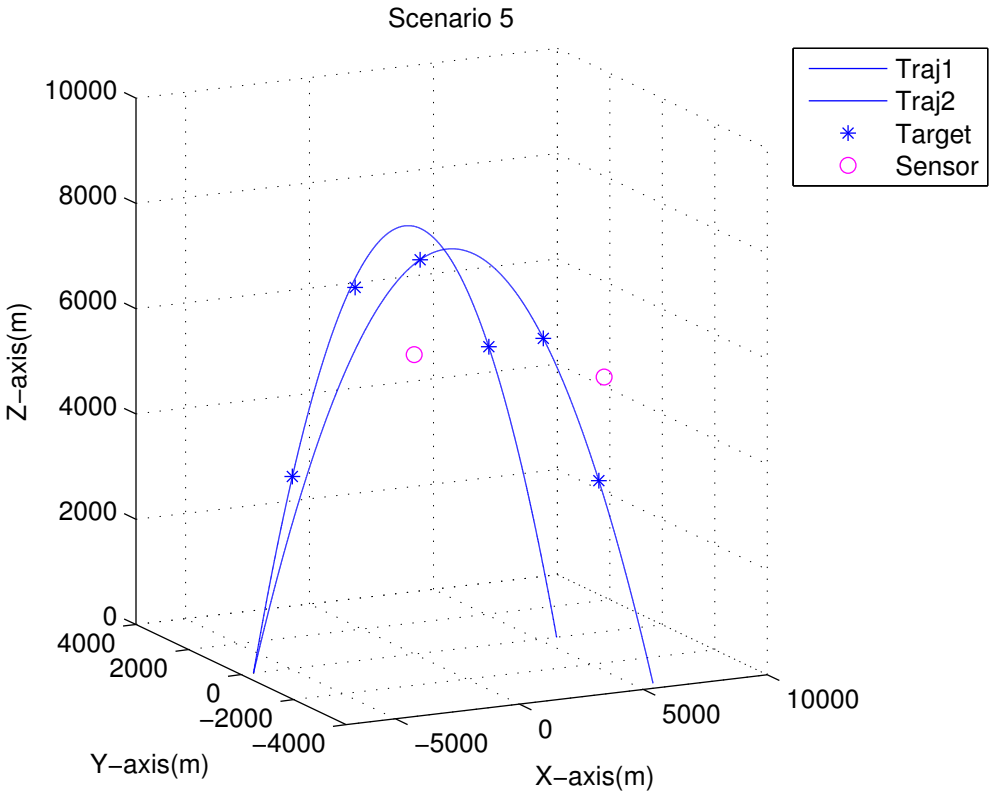

Fig. 2.15: Scenario 5 for the two-sensor case

Statistical efficiency of the estimates

In order to test for the statistical efficiency of the estimate (of the 23 dimensional vector), the NEES is used, with the CRLB as the covariance matrix. The sample average NEES over 100 Monte Carlo runs is given in Table 2.7 for all the scenarios. The NEES is calculated using the FIM evaluated at both the true bias values and target positions, as well as at the estimated biases and target positions. The results are practically identical regardless of which values are chosen for evaluation of the FIM. The 95% probability region for the 100 sample average NEES of the 23 dimensional parameter vector is [21.68, 24.34]. For all 5 scenarios these NEES are found to be within this interval and the MLE is therefore statistically efficient. Figure 2.16 shows the NEES for all scenarios, Figure 2.17 shows the individual bias component NEES for all scenarios, The 95% probability region for the 100 sample average single component NEES is [0.74, 1.29]. For all 5 scenarios these NEES are found to be within this interval.

The RMS position errors for the 6 targets are summarized in Table 2.8. In this table, the first estimation scheme was established as a baseline using bias-free LOS measurements to estimate the target positions. For the second scheme, we used biased LOS measurements but we only estimated target positions. In the last scheme, we used biased LOS measurements and we simultaneously estimated the target positions and sensor biases. For the second scheme, the estimation algorithm does not converge, while the third scheme shows satisfactory target RMS position errors in the presence of biases. The target position RMSE when the biases are also estimated, are close to the RMSE with no biases.

Each component of $\boldsymbol{\theta}$ should also be individually consistent with its cor-

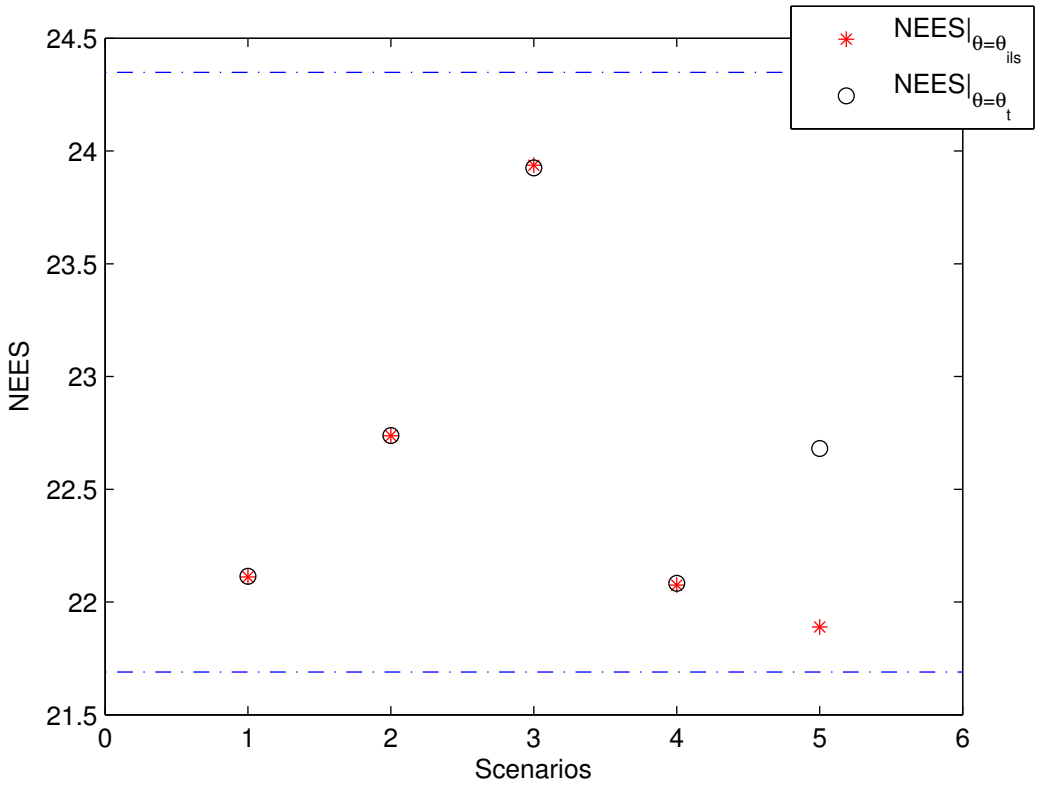

Fig. 2.16: Sample average NEES over 100 Monte Carlo runs for all 5 scenarios (Two-sensor case).

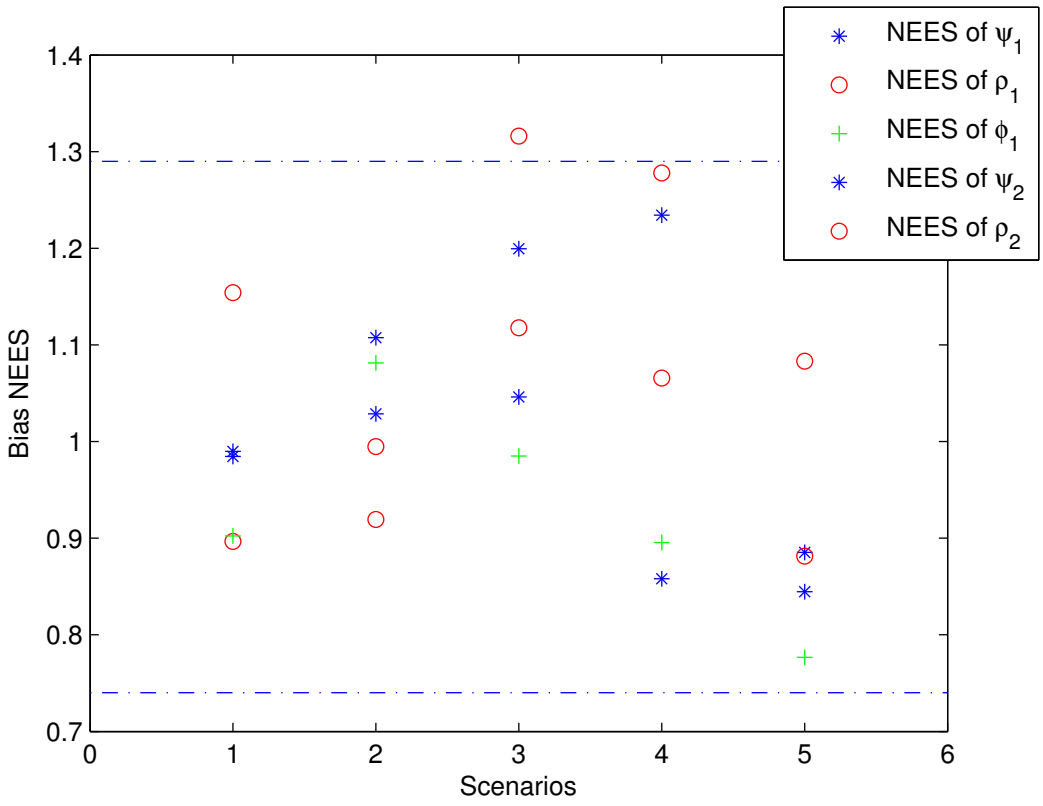

Fig. 2.17: Sample average bias NEES (CRLB evaluated at the estimate), for each of the 5 biases, over 100 Monte Carlo runs for all 5 scenarios (Two-sensor case).

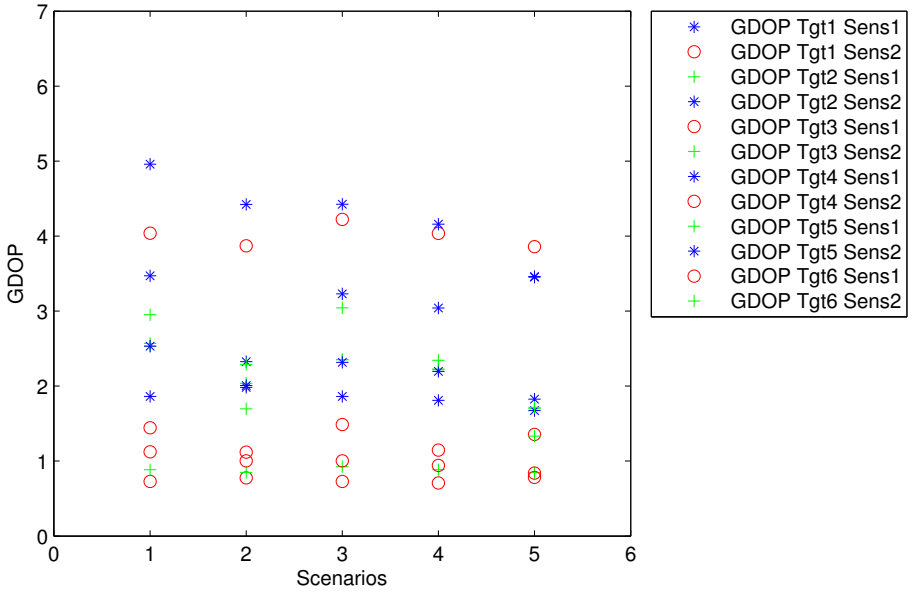

Fig. 2.18: GDOPs for the 5 scenarios considered (Two-sensor case).

responding σ_{CRLB} (the square root of the corresponding diagonal element of the inverse of FIM). In this case, the sample average bias RMSE over 100 Monte Carlo runs should be within 15% of its corresponding bias standard deviation from the CRLB (σ_{CRLB}) with 95% probability. Table 2.9 demonstrates the efficiency of the individual bias estimates.

To confirm that the bias estimates are unbiased, the average bias error $\bar{\tilde{b}}$, from Table 2.10, over 100 Monte Carlo runs confirms that $|\bar{\tilde{b}}|$ is less then $2\frac{\sigma_{\text{CRLB}}}{\sqrt{N}}$ (which it should be with 95% probability), i.e., these estimates are unbiased.

Figure 2.18 shows the various GDOP levels in the 12 target-sensor combinations for each of the 5 scenarios for which statistical efficiency was confirmed, in the case of the two sensors.

Table 2.7: Sample average NEES over 100 Monte Carlo runs for 5 scenarios (based on $23 \cdot 100 = 2300$ degrees of freedom chi-square distribution) (Two-sensor case).

Scenarios	1	2	3	4	5
$\text{NEES}\|_{\theta=\theta_t}$	22.1139	22.7382	23.9253	22.0830	22.6810
$\text{NEES}\|_{\theta=\hat{\theta}_{\text{ILS}}}$	22.1110	22.7369	23.9363	22.0750	21.8890

Table 2.8: Sample average position RMSE (m) for the 6 targets, over 100 Monte Carlo runs, for the 3 estimation schemes (Two-sensor case).

	First Target	Second Target	Third Target	Fourth Target	Fifth Target	Sixth Target
Scheme	RMSE	RMSE	RMSE	RMSE	RMSE	RMSE
1	3.68	4.84	3.42	4.06	4.64	3.63
3	7.08	7.65	6.49	7.91	7.70	7.76

Table 2.9: Sample average bias RMSE over 100 Monte Carlo runs and the corresponding bias standard deviation from the CRLB (σ_{CRLB}), for all configurations (mrad) (Two-sensor case).

		First Sensor			Second Sensor	
Scenario		ψ	ρ	ϕ	ψ	ρ
1	RMSE	0.195	0.271	0.254	0.186	0.314
	σ_{CRLB}	0.252	0.307	0.331	0.238	0.430
2	RMSE	0.437	0.442	0.500	0.428	0.348
	σ_{CRLB}	0.394	0.494	0.441	0.410	0.410
3	RMSE	1.675	1.668	1.634	1.646	0.4615
	σ_{CRLB}	1.279	1.572	1.305	1.207	0.536
4	RMSE	0.475	0.392	0.440	0.465	0.287
	σ_{CRLB}	0.467	0.440	0.510	0.483	0.384
5	RMSE	0.258	0.251	0.237	0.245	0.195
	σ_{CRLB}	0.345	0.246	0.357	0.347	0.168

Table 2.10: Sample average bias error $\bar{\bar{b}}$ over N=100 Monte Carlo runs for all configurations (mrad) (to confirm that the bias estimates are unbiased) (Two-sensor case).

Scenario		First Sensor			Second Sensor	
		ψ	ρ	ϕ	ψ	ρ
1	$\bar{\bar{b}}$	0.000	0.007	0.000	0.003	-0.045
	$\frac{\sigma_{\text{CRLB}}}{\sqrt{N}}$	0.025	0.030	0.033	0.023	0.043
2	$\bar{\bar{b}}$	-0.055	-0.058	-0.007	-0.016	-0.001
	$\frac{\sigma_{\text{CRLB}}}{\sqrt{N}}$	0.039	0.049	0.044	0.041	0.041
3	$\bar{\bar{b}}$	-0.351	-0.098	-0.254	0.275	0.056
	$\frac{\sigma_{\text{CRLB}}}{\sqrt{N}}$	0.128	0.157	0.130	0.120	0.053
4	$\bar{\bar{b}}$	-0.001	-0.069	0.042	-0.026	-0.013
	$\frac{\sigma_{\text{CRLB}}}{\sqrt{N}}$	0.046	0.044	0.051	0.048	0.038
5	$\bar{\bar{b}}$	0.037	0.028	0.006	0.040	-0.005
	$\frac{\sigma_{\text{CRLB}}}{\sqrt{N}}$	0.034	0.024	0.0358	0.034	0.016

2.4 Conclusions

In this chapter, we presented an algorithm that uses targets of opportunity for estimation of measurement biases. The first step was formulating a general bias model for synchronized optical sensors at fixed known locations. The association of measurements is assumed to be perfect. Based on this, we used a ML approach that led to a nonlinear least-squares estimation problem for simultaneous estimation of the 3D Cartesian positions of the targets of opportunity and the angle measurement biases of the sensors. The bias estimates, obtained via ILS, were shown to be unbiased and statistically efficient. In the three-sensor case it was shown that one has complete observability of the sensor biases. In the two-sensor case a rank deficiency of 1 in the FIM was observed. i,e., this allows estimation of only 5 out of 6 biases. A suitable geometric explanation was provided for this. For moving sensors this problem is expected to go away if the sensors move sufficiently.

Chapter 3

Bias Estimation for Moving Optical Sensor Measurements with Targets of Opportunity

3.1 Introduction

Integration of space based sensors into a Ballistic Missile Defense System (BMDS) allows for detection and tracking of threats over a larger area than ground based sensors. This paper examines the effect of sensor bias error on the tracking quality of a Space Tracking and Surveillance System (STSS) for the highly non-linear problem of tracking a ballistic missile. The STSS constellation consists of two or more satellites (on known trajectories) for tracking ballistic targets. Each satellite is equipped with an IR sensor that provides azimuth and elevation to the target. The tracking problem is made more difficult due to a constant or slowly varying bias error present in each sensor's line of sight measurements. The measurements provided by these sensors are assumed time-coincident (synchronous) and perfectly associated. The LOS measurements from the sensors are used to estimate simultaneously the Cartesian target of opportunity positions, and the sensor biases.

Space-based sensors can expand the range and effectiveness of the capabilities of a Ballistic Missile Defense System (BMDS) to counter future projected threats.

A space based tracking system utilizing an IR sensor will allow detection and tracking of targets outside of terrestrial radar coverage. This is possible because a sensitive IR sensor in relatively close proximity can detect and track a target against the cold background of space. Multisensor systems use fusion of data from multiple sensors to form accurate estimates of a target track. To fuse multiple sensor data the individual sensor data must be expressed in a common reference frame. A problem encountered in multisensor systems is the presence of errors due to sensor bias. Some sources of bias errors include: measurement biases due to the deterioration of initial sensor calibration over time; attitude errors caused by biases in the gyros of the inertial measurement units of (airborne, seaborne, or spaceborne) sensors; and timing errors due to the biases in the onboard clock of each sensor platform [20].

Sensor calibration using in-situ celestial observations to estimate bias in space-based missile tracking was discussed in [16]. In the present paper, bias estimation is investigated when only targets of opportunity are available. The tracking system consists of two or three satellites tracking a ballistic target. We assume the sensors are synchronized, their locations are known, and the data association is correct; and we estimate their orientation biases. We investigate the use of the minimum possible number of moving sensors and measurements. Two cases are considered. In the first case, we use three moving optical sensors to estimate 3 points on the (unknown) trajectory of a single target of opportunity simultaneously with the biases of the three optical sensors [6]. In the second case, we estimate the position of 6 points on the trajectory of a single target of opportunity simultaneously with the biases of two space-based optical sensors [5]. First, we discuss the observability requirement related to the bias estimation. We

evaluate the Cramér-Rao lower bound (CRLB) on the covariance of the bias estimates, which is the quantification of the available information on the sensor biases, and show via statistical tests that the estimation is statistically efficient — it meets the CRLB. Section II presents the problem formulation and solution in detail. Section III describes the simulations performed and gives the results. Finally, Section IV gives the conclusions.

3.2 Problem Formulation

The fundamental frame of reference used in this paper is the Earth Centered Inertial (ECI) Coordinate System. The ECI is defined by the orthogonal set of unit vectors $\{e_x, e_y, e_z\}$. The X-axis is directed toward the vernal Equinox, the Y-axis is in the equatorial plane and normal to the X-axis, and the Z-axis is directed along the rotation axis of the Earth (i.e., normal to the equatorial plane). In a multisensor scenario, sensor platform s will typically have a sensor reference frame associated with it (measurement frame of the sensor) defined by the orthogonal set of unit vectors $\{e_{\xi_s}, e_{\eta_s}, e_{\zeta_s}\}$. The origin of the measurement frame of the sensor is a translation of the ECI origin, and its axes are rotated with respect to the ECI axes. The rotation between these frames can be described by a set of Euler angles. We will refer to these angles $\phi_s + \phi_s^{\mathrm{n}}$, $\rho_s + \rho_s^{\mathrm{n}}$, $\psi_s + \psi_s^{\mathrm{n}}$ of sensor s as roll, pitch, and yaw respectively [20], where ϕ_s^{n} is the nominal roll angle, ϕ_s is the roll bias, etc.

Each angle defines a rotation about a prescribed axis, in order to align the sensor frame axes with the ECI axes. The xyz rotation sequence is chosen, which is accomplished by first rotating about the x axis by ϕ_s^{n}, then rotating about the

y axis by ρ_s^{n}, and finally rotating about the z axis by ψ_s^{n}. The rotations sequence can be expressed by the matrices

$$
\begin{aligned}
T_s(\psi_s^{\mathrm{n}}, \rho_s^{\mathrm{n}}, \phi_s^{\mathrm{n}}) =& T_z(\psi_s^{\mathrm{n}}) \cdot T_y(\rho_s^{\mathrm{n}}) \cdot T_x(\phi_s^{\mathrm{n}}) \\
=& \begin{bmatrix} \cos\psi_s^{\mathrm{n}} & \sin\psi_s^{\mathrm{n}} & 0 \\ -\sin\psi_s^{\mathrm{n}} & \cos\psi_s^{\mathrm{n}} & 0 \\ 0 & 0 & 1 \end{bmatrix} \\
\cdot& \begin{bmatrix} \cos\rho_s^{\mathrm{n}} & 0 & -\sin\rho_s^{\mathrm{n}} \\ 0 & 1 & 0 \\ \sin\rho_s^{\mathrm{n}} & 0 & \cos\rho_s^{\mathrm{n}} \end{bmatrix} \\
\cdot& \begin{bmatrix} 1 & 0 & 0 \\ 0 & \cos\phi_s^{\mathrm{n}} & \sin\phi_s^{\mathrm{n}} \\ 0 & -\sin\phi_s^{\mathrm{n}} & \cos\phi_s^{\mathrm{n}} \end{bmatrix}
\end{aligned} \tag{3.1}
$$

Assume there are N_S synchronized passive sensors, with known positions in ECI coordinates at times t_i,

$\boldsymbol{\xi}_s(t_i) = [\xi_s(t_i), \eta_s(t_i), \zeta_s(t_i)]'$, $\quad s = 1, 2, ..., N_S$, and N_t target locations at $\mathbf{x}(t_i) = [x(t_i), y(t_i), z(t_i)]'$, $i = 1, 2, ..., N_t$, also in ECI coordinates. We assume that each sensor sees all the target locations (same physical target at different times).[1] With the previous convention, the operations needed to transform the position of a given target location at t_i expressed in ECI coordinates into the sensor s coordinate system (based on its nominal orientation) is

$$\mathbf{x}_s^{\mathrm{n}}(t_i) = T(\boldsymbol{\omega}_s(t_i))(\mathbf{x}(t_i) - \boldsymbol{\xi}_s(t_i))$$

[1] This can also be different targets at a common time or at different times, as long as the sensors are synchronized.

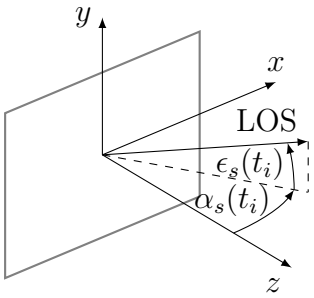

Fig. 3.1: Optical sensor coordinate system with the origin in the center of the focal plane.

$$i = 1, 2, ..., N_t, \quad s = 1, 2, ..., N_S \tag{3.2}$$

where $\boldsymbol{\omega}_s(t_i) = [\phi_s^{\mathrm{n}}(t_i), \rho_s^{\mathrm{n}}(t_i), \psi_s^{\mathrm{n}}(t_i)]'$ is the nominal orientation of sensor s at times t_i, $T(\boldsymbol{\omega}_s(t_i))$ is the appropriate rotation matrix, and the translation $(\mathbf{x}(t_i) - \boldsymbol{\xi}_s(t_i))$ is the difference between the vector position of the target i and the vector position of the sensor s, both expressed in ECI coordinates. The superscript "n" in (3.2) indicates that the rotation matrix is based on the nominal sensor orientation.

As shown in Figure 3.1, the azimuth angle $\alpha_s(t_i)$ is the angle in the sensor xz plane between the sensor z axis and the line of sight to the target, while the elevation angle $\epsilon_s(t_i)$ is the angle between the line of sight to the target and its projection onto the xz plane, i.e.,

$$\begin{bmatrix} \alpha_s(t_i) \\ \epsilon_s(t_i) \end{bmatrix} = \begin{bmatrix} \tan^{-1}\left(\frac{x_s(t_i)}{z_s(t_i)}\right) \\ \tan^{-1}\left(\frac{y_s(t_i)}{\sqrt{x_s^2(t_i)+z_s^2(t_i)}}\right) \end{bmatrix} \tag{3.3}$$

The model for the biased noise-free LOS measurements is then

$$\begin{bmatrix} \alpha_s^b(t_i) \\ \epsilon_s^b(t_i) \end{bmatrix} = \begin{bmatrix} g_1(\mathbf{x}(t_i), \boldsymbol{\xi}_s(t_i), \boldsymbol{\omega}_s(t_i), \mathbf{b}_s) \\ g_2(\mathbf{x}(t_i), \boldsymbol{\xi}_s(t_i), \boldsymbol{\omega}_s(t_i), \mathbf{b}_s) \end{bmatrix}$$
$$\stackrel{\Delta}{=} \boldsymbol{g}(\mathbf{x}(t_i), \boldsymbol{\xi}_s(t_i), \boldsymbol{\omega}_s(t_i), \mathbf{b}_s) \tag{3.4}$$

where g_1 and g_2 denote the sensor Cartesian coordinates-to-azimuth/elevation angle mapping that can be found by inserting (3.2) and (3.3) into (3.4), and the bias vector of sensor s is

$$\mathbf{b}_s = [\phi_s, \rho_s, \psi_s]' \tag{3.5}$$

For a given target, each sensor provides the noisy LOS measurements

$$\mathbf{z}_s(t_i) = \boldsymbol{g}(\mathbf{x}(t_i), \boldsymbol{\xi}_s(t_i), \boldsymbol{\omega}_s(t_i), \mathbf{b}_s) + \mathbf{w}_s(t_i) \tag{3.6}$$

where

$$\mathbf{w}_s(t_i) = [w_s^\alpha(t_i), w_s^\epsilon(t_i)]' \tag{3.7}$$

The measurement noises $\mathbf{w}_s(t_i)$ are zero-mean, white Gaussian with

$$R_s = \begin{bmatrix} (\sigma_s^\alpha)^2 & 0 \\ 0 & (\sigma_s^\epsilon)^2 \end{bmatrix} \tag{3.8}$$

and are assumed mutually independent. The problem is to estimate the bias vectors for all sensors and the locations of the targets of opportunity. We shall

obtain the maximum likelihood (ML) estimate of the augmented parameter vector

$$\boldsymbol{\theta} = [\mathbf{x}(t_1)', ..., \mathbf{x}(t_{N_t})', \mathbf{b}_1', ..., \mathbf{b}_{N_S}']' \tag{3.9}$$

consisting of the (unknown) target locations and sensor biases, by maximizing the likelihood function (LF) of $\boldsymbol{\theta}$

$$\Lambda(\boldsymbol{\theta}) = \prod_{i=1}^{N_t} \prod_{s=1}^{N_S} p\left(\mathbf{z}_s(t_i)|\boldsymbol{\theta}\right) \tag{3.10}$$

where

$$\begin{aligned} p\left(\mathbf{z}_s(t_i)|\boldsymbol{\theta}\right) &= |2\pi R_s|^{-1/2} \\ &\cdot \exp\left(-\frac{1}{2}\left[\mathbf{z}_s(t_i) - \mathbf{h}_{is}\left(\boldsymbol{\theta}\right)\right]' R_s^{-1}\left[\mathbf{z}_s(t_i) - \mathbf{h}_{is}\left(\boldsymbol{\theta}\right)\right]\right) \end{aligned} \tag{3.11}$$

and we use the compact notation

$$\mathbf{h}_{is}(\boldsymbol{\theta}) \stackrel{\Delta}{=} \boldsymbol{g}(\mathbf{x}(t_i), \boldsymbol{\xi}_s(t_i), \boldsymbol{\omega}_s(t_i), \mathbf{b}_s) \tag{3.12}$$

The ML estimate (MLE) is then

$$\hat{\boldsymbol{\theta}}^{ML} = \arg\max_{\boldsymbol{\theta}} \Lambda(\boldsymbol{\theta}) \tag{3.13}$$

In order to find the MLE, one has to solve a nonlinear least squares problem for the exponent in (3.11). This will be done using a numerical search via the Iterated Least Squares (ILS) technique [2].

3.2.1 Requirements for Bias Estimability

First requirement for bias estimability

For a given target location we have a two-dimensional measurement from each sensor (the two LOS angles to the target). We assume that each sensor sees all the target locations at a common time. Stacking together each measurement of N_t target locations seen by N_S sensors results in an overall measurement vector of dimension $2N_tN_S$. Given that the position and bias vectors of each target are three-dimensional, and knowing that the number of equations (size of the stacked measurement vector) has to be at least equal to the number of parameters to be estimated (target locations and biases), we must have

$$2N_tN_S \geq 3(N_t + N_S) \tag{3.14}$$

This is a necessary condition but not sufficient because (3.13) has to have a unique solution, i.e., the parameter vector has to be estimable. This is guaranteed by the second requirement.

Second requirement of bias estimability

This is the invertibility of the Fisher Information matrix (FIM). In order to have parameter observability, the FIM must be invertible. If the FIM is not invertible (i.e., it is singular), then the CRLB (the inverse of the FIM) will not exist — the FIM will have one or more infinite eigenvalues, which means total uncertainty in a subspace of the parameter space, i.e., ambiguity [2].

For the examples of bias estimability discussed in the sequel, to estimate the

biases of 3 sensors (9 bias components) we need 3 target locations (9 position components), i.e., the search is in an 18-dimensional space, while for 2 sensors (6 bias components) we need at least 6 target locations (18 position components) in order to meet the necessary requirement (3.14). As stated previously, the FIM must be invertible, so the rank of the FIM has to be equal to the number of parameters to be estimated (9+9=18, or 6+18=24, in the previous examples). The full rank of the FIM is a necessary and sufficient condition for estimability.

3.2.2 Iterated Least Squares

Given the estimate $\hat{\boldsymbol{\theta}}^j$ after j iterations, the ILS estimate after the $(j+1)$th iteration will be

$$\hat{\boldsymbol{\theta}}^{j+1} = \hat{\boldsymbol{\theta}}^j + \left[(H^j)' R^{-1} H^j\right]^{-1} (H^j)' R^{-1} [\mathbf{z} - \mathbf{h}(\hat{\boldsymbol{\theta}}^j)] \tag{3.15}$$

where

$$\mathbf{z} = [z_1(t_1)', ..., z_s(t_1)', ..., z_s(t_i)', ..., z_{N_S}(t_{N_t})']' \tag{3.16}$$

$$\mathbf{h}(\hat{\boldsymbol{\theta}}^j) = [h_{11}(\hat{\boldsymbol{\theta}}^j)', ..., h_{is}(\hat{\boldsymbol{\theta}}^j)', ..., h_{N_t N_S}(\hat{\boldsymbol{\theta}}^j)'] \tag{3.17}$$

$$R = \begin{bmatrix} R_1 & 0 & \cdots & 0 \\ 0 & R_2 & \cdots & 0 \\ \vdots & \vdots & \ddots & \vdots \\ 0 & \cdots & 0 & R_{N_S} \end{bmatrix} \tag{3.18}$$

where R_s is the measurement noise covariance matrix of sensor s, and

$$H^j = \left.\frac{\partial \mathbf{h}\left(\boldsymbol{\theta}^j\right)}{\partial \boldsymbol{\theta}}\right|_{\boldsymbol{\theta}=\hat{\boldsymbol{\theta}}^j} \tag{3.19}$$

is the Jacobian matrix of the vector consisting of the stacked measurement functions (3.17) w.r.t. (3.9) evaluated at the ILS estimate from the previous iteration j. In this case, the Jacobian matrix is, with the iteration index omitted for conciseness,

$$H = \begin{bmatrix} H_{11} & H_{21} & \cdots & H_{N_t 1} & H_{12} & \cdots & H_{N_t N_S} \end{bmatrix}' \tag{3.20}$$

where

$$H_{is} = \begin{bmatrix} \frac{\partial g_{1_s}(t_i)}{\partial x(t_1)} & \frac{\partial g_{2_s}(t_i)}{\partial x(t_1)} \\ \frac{\partial g_{1_s}(t_i)}{\partial y(t_1)} & \frac{\partial g_{2_s}(t_i)}{\partial y(t_1)} \\ \frac{\partial g_{1_s}(t_i)}{\partial z(t_1)} & \frac{\partial g_{2_s}(t_i)}{\partial z(t_1)} \\ \vdots & \vdots \\ \frac{\partial g_{1_s}(t_i)}{\partial x(t_{N_t})} & \frac{\partial g_{2_s}(t_i)}{\partial x(t_{N_t})} \\ \frac{\partial g_{1_s}(t_i)}{\partial y(t_{N_t})} & \frac{\partial g_{2_s}(t_i)}{\partial y(t_{N_t})} \\ \frac{\partial g_{1_s}(t_i)}{\partial z(t_{N_t})} & \frac{\partial g_{2_s}(t_i)}{\partial z(t_{N_t})} \\ \frac{\partial g_{1_s}(t_i)}{\partial \psi_1} & \frac{\partial g_{2_s}(t_i)}{\partial \psi_1} \\ \frac{\partial g_{1_s}(t_i)}{\partial \rho_1} & \frac{\partial g_{2_s}(t_i)}{\partial \rho_1} \\ \frac{\partial g_{1_s}(t_i)}{\partial \phi_1} & \frac{\partial g_{2_s}(t_i)}{\partial \phi_1} \\ \vdots & \vdots \\ \frac{\partial g_{1_s}(t_i)}{\partial \psi_{N_S}} & \frac{\partial g_{2_s}(t_i)}{\partial \psi_{N_S}} \\ \frac{\partial g_{1_s}(t_i)}{\partial \rho_{N_S}} & \frac{\partial g_{2_s}(t_i)}{\partial \rho_{N_S}} \\ \frac{\partial g_{1_s}(t_i)}{\partial \phi_{N_S}} & \frac{\partial g_{2_s}(t_i)}{\partial \phi_{N_S}} \end{bmatrix} \tag{3.21}$$

$$x(t_i)^0 = \frac{\xi_2(t_i) - \xi_1(t_i) + \zeta_1(t_i)\tan\alpha_1(t_i) - \zeta_2(t_i)\tan\alpha_2(t_i)}{\tan\alpha_1(t_i) - \tan\alpha_2(t_i)} \tag{3.22}$$

$$y(t_i)^0 = \frac{\tan\alpha_1(t_i)\left(\xi_2(t_i) + \tan\alpha_2(t_i)\left(\zeta_1(t_i) - \zeta_2(t_i)\right)\right) - \xi_1(t_i)\tan\alpha_2(t_i)}{\tan\alpha_1(t_i) - \tan\alpha_2(t_i)} \tag{3.23}$$

$$z(t_i)^0 = \eta_1(t_i) + \tan\epsilon_1(t_i)\left|\frac{(\xi_1(t_i) - \xi_2(t_i))\cos\alpha_2(t_i) + (\zeta_2(t_i) - \zeta_1(t_i))\sin\alpha_2(t_i)}{\sin\left(\alpha_1(t_i) - \alpha_2(t_i)\right)}\right| \tag{3.24}$$

The appropriate partial derivatives are given in appendix B.

3.2.3 Initialialization

In order to perform the numerical search via ILS, an initial estimate $\hat{\boldsymbol{\theta}}^0$ is required. Assuming that the biases are null, the LOS measurements from the first and the second sensor $\alpha_1(t_i)$, $\alpha_2(t_i)$, and $\epsilon_1(t_i)$ can be used to solve for each initial Cartesian target position, in ECI coordinates, using (3.22)–(3.24).

3.2.4 Cramér-Rao Lower Bound

In order to evaluate the efficiency of the estimator, the CRLB must be calculated. The CRLB provides a lower bound on the covariance matrix of an unbiased estimator as [1]

$$E\{(\boldsymbol{\theta} - \hat{\boldsymbol{\theta}})(\boldsymbol{\theta} - \hat{\boldsymbol{\theta}})'\} \geq J(\boldsymbol{\theta})^{-1} \tag{3.25}$$

where J is the Fisher Information Matrix (FIM), $\boldsymbol{\theta}$ is the true parameter vector to be estimated, and $\hat{\boldsymbol{\theta}}$ is the estimate. The FIM is

$$J(\boldsymbol{\theta}) = E\left\{\left[\nabla_{\boldsymbol{\theta}} \ln\Lambda(\boldsymbol{\theta})\right]\left[\nabla_{\boldsymbol{\theta}} \ln\Lambda(\boldsymbol{\theta})\right]'\right\}\Big|_{\boldsymbol{\theta}=\boldsymbol{\theta}_{\text{true}}} \tag{3.26}$$

where the gradient of the log-likelihood function is

$$\lambda(\boldsymbol{\theta}) \triangleq \ln \Lambda(\boldsymbol{\theta}) \tag{3.27}$$

$$\nabla_{\boldsymbol{\theta}} \lambda(\boldsymbol{\theta}) = \sum_{i=1}^{N_t} \sum_{s=1}^{N_S} H'_{is} R_s^{-1} \left(\mathbf{z}_s(t_i) - \mathbf{h}_{is}(\boldsymbol{\theta}) \right) \tag{3.28}$$

which, when plugged into (3.26), gives

$$\begin{aligned} J(\boldsymbol{\theta}) &= \sum_{i=1}^{N_t} \sum_{s=1}^{N_S} H'_{is} \left(R_s^{-1} \right) H_{is} \big|_{\boldsymbol{\theta}=\boldsymbol{\theta}_{\text{true}}} \\ &= H' \left(R^{-1} \right) H \big|_{\boldsymbol{\theta}=\boldsymbol{\theta}_{\text{true}}} \end{aligned} \tag{3.29}$$

Since $\boldsymbol{\theta}_{\text{true}}$ is not available in practice, J will be evaluated at the estimate, and, as it's pointed out later, the two results are practically the same.

3.2.5 Test for Efficiency with Monte Carlo Runs

The Normalized Estimation Error Squared (NEES) for the parameter θ (under the hypothesis of efficiency), defined as

$$\epsilon_\theta = (\theta - \hat{\theta})' P^{-1} (\theta - \hat{\theta}) = (\theta - \hat{\theta})' J(\theta) (\theta - \hat{\theta}) \tag{3.30}$$

is chi-square distributed with n_x (the dimension of θ) degrees of freedom, that is,

$$\epsilon_\theta \sim \chi^2_{n_x} \tag{3.31}$$

The hypothesis test for efficiency whether (3.31) can be accepted, i.e., that $P = J^{-1}$ is discussed in [2] and outlined next. The NEES is used in simulations

to check whether the estimator is efficient, that is, the errors are statistically consistent with the covariance given by the CRLB — this is the efficiency check. Thus the efficiency check of the estimator (in simulation — because this is the only situation where θ is available) consists of verifying whether (3.31) holds. The practical procedure to check the estimator efficiency is using the sample average NEES from N independent Monte Carlo runs defined as

$$\bar{\epsilon}_x = \frac{1}{N}\sum_{i=1}^{N} \epsilon_x^i \tag{3.32}$$

The quantity $N\bar{\epsilon}$ is chi-square distributed with Nn_x degrees of freedom.

Let the $1-Q$ (Q is the type I error probability of the test) two-sided probability region for $N\bar{\epsilon}$ be the interval $[\epsilon_1', \epsilon_2']$.

$$\epsilon_1' = \chi^2_{Nn_x}\left(\frac{Q}{2}\right) \tag{3.33}$$

$$\epsilon_2' = \chi^2_{Nn_x}\left(1-\frac{Q}{2}\right) \tag{3.34}$$

where in view of the division by N in (**??**), one has

$$\epsilon_i = \frac{\epsilon_i'}{N} \tag{3.35}$$

Thus, if the estimator is efficient, one has to have

$$P\left\{\bar{\epsilon}_x \in [\epsilon_1', \epsilon_2']\right\} = 1-Q \tag{3.36}$$

3.3 Simulations

We simulate a space based tracking system tracking a ballistic missile. The missile and satellite trajectories are generated using System Tool Kit (STK)[2]. The target modeled represents a ballistic missile with a flight time of about 20 minutes. STK provides the target and sensor positions in three dimensional Cartesian coordinates at 1 s intervals. The target launch time is chosen so that the satellite sensors were able to follow the missile trajectory throughout its flight path.

3.3.1 Three-Sensor Case

We simulated three space based optical sensors at various known orbits observing a target at three points in time at unknown locations. In this case, an 18-dimensional parameter vector is to be estimated. Figure 3.2 shows each target position observed by the sensors (Figure 3.3 gives an image of this). As discussed in the previous section, the three sensor biases are roll, pitch, and yaw angle offsets. The biases for each sensor were set to $0.5^\circ = 8.72$ mrad. We ran 100 Monte Carlo runs. In order to establish a baseline for evaluating the performance of our algorithm, we also ran the simulations without biases, and with biases but without bias estimation. The horizontal and vertical fields-of-view of each sensor are assumed to be 60°. The measurement noise standard deviation σ_s (identical across sensors for both azimuth and elevation measurements, $\sigma_s^\alpha = \sigma_s^\epsilon = \sigma_s$) was assumed to be 30 μrad.

[2] STK Systems Tool Kit are registered trademarks of Analytical Graphics, Inc.

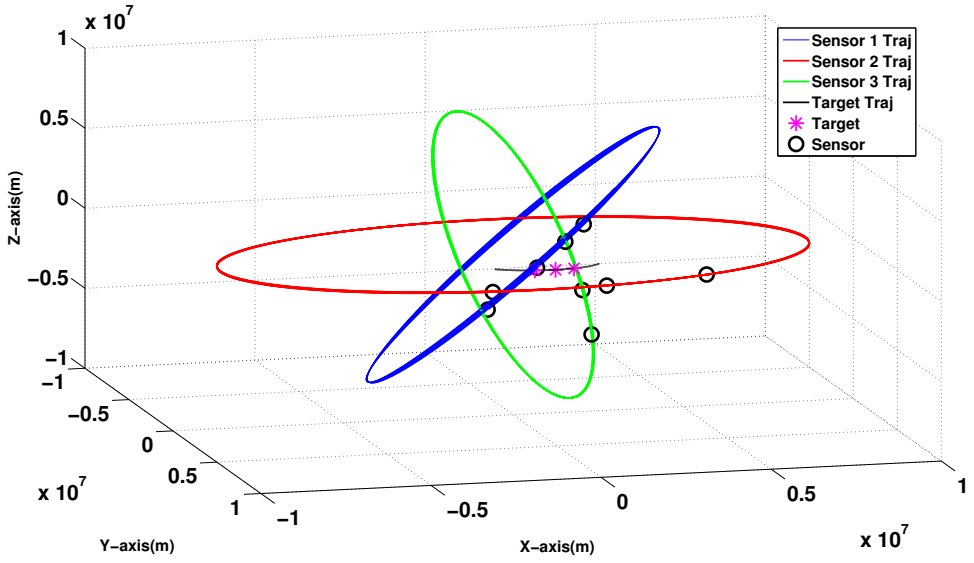

Fig. 3.2: Target and satellite trajectories for the three-sensor case.

Description of the scenarios

The sensors are assumed to provide LOS angle measurements. We denote by $\boldsymbol{\xi}_1, \boldsymbol{\xi}_2, \boldsymbol{\xi}_3$ the 3D Cartesian sensor locations, and $\mathbf{x}(t_1), \mathbf{x}(t_2), \mathbf{x}(t_3)$ the 3D Cartesian target locations (all in ECI). The three target locations were chosen from a trajectory of a ballistic target as follows (in km)

$$\mathbf{x}(t_1) = \begin{bmatrix} 7,518 & -1,311 & -1,673 \end{bmatrix}' \tag{3.37}$$

$$\mathbf{x}(t_2) = \begin{bmatrix} 7,942 & -509 & -1,375 \end{bmatrix}' \tag{3.38}$$

$$\mathbf{x}(t_3) = \begin{bmatrix} 7,988 & 317 & -1,012 \end{bmatrix}' \tag{3.39}$$

Table 3.1 summarizes the sensor positions (in km).

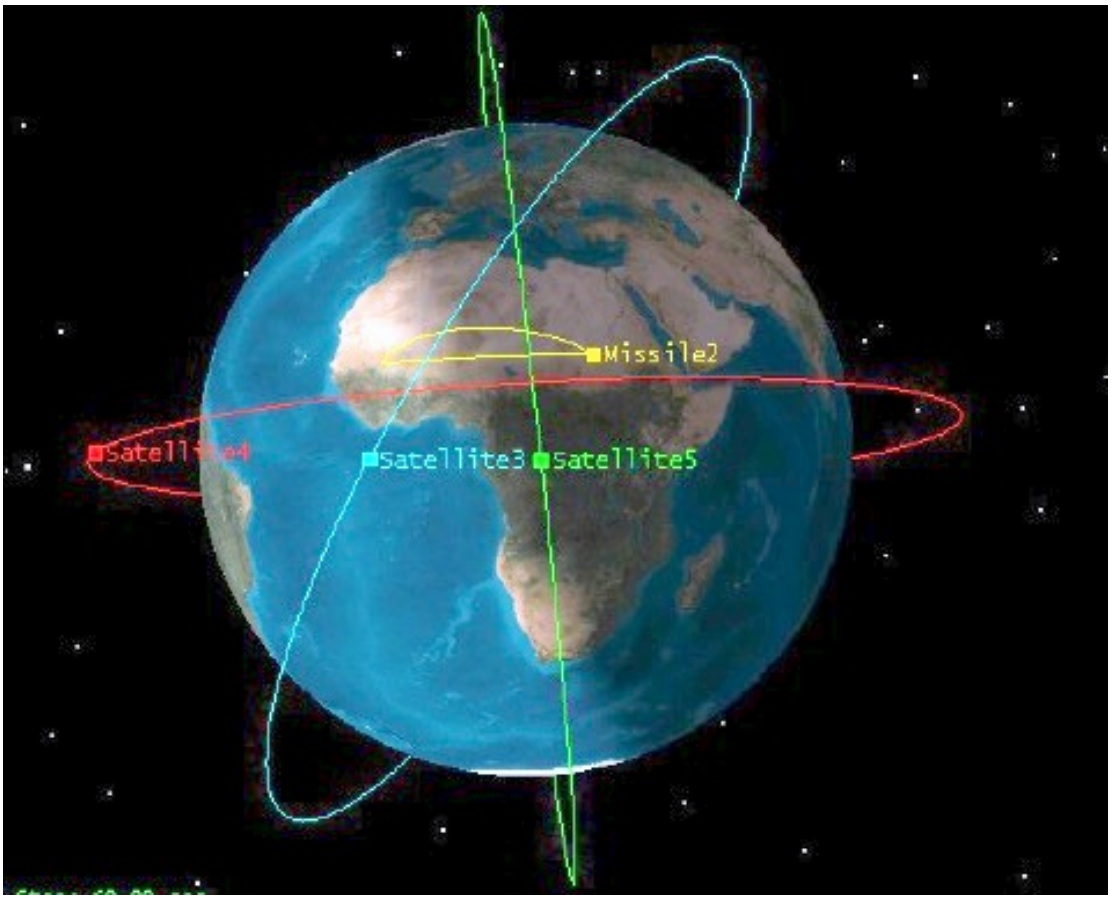

Fig. 3.3: Target and satellite trajectories for the three-sensor case.

Table 3.1: Sensor positions (km).

	t_1	t_2	t_3
ξ_1	1,235	1,062	887
η_1	158	-174	-507
ζ_1	6,927	6,955	6,963
ξ_2	5,549	3,061	112
η_2	1,116	2,993	4,418
ζ_2	6,285	7,295	7,212
ξ_3	6,499	7,897	8,389
η_3	-279	-719	-1,074
ζ_3	-5,407	-2,944	-143

Statistical efficiency of the estimates

In order to test for the statistical efficiency of the estimate (of the 18 dimensional vector (3.9)), the NEES [2] is used, with the CRLB as the covariance matrix. The sample average NEES over 100 Monte Carlo runs calculated using the FIM evaluated at the true bias values and target locations is approximately 17.3, and the sample average NEES calculated using the FIM evaluated at the estimated biases and target locations is approximately 17.6 and both fall in the interval given below. According to the CRLB, the FIM has to be evaluated at the true parameter. Since this is not available in practice, however, it is useful to evaluate the FIM also at the estimated parameter, the only one available in real world implementations [24], [25]. The results are very close regardless of which values are chosen for evaluation of the FIM. The 95% probability region for the 100 sample average NEES of the 18 dimensional parameter vector is $[16.84, 19.19]'$. This NEES is found to be within this interval and the MLE is therefore statistically efficient. Figure 3.4 shows the individual bias component NEES, The 95% probability region for the 100 sample average single component NEES is $[0.74, 1.29]'$. The NEES values are found to be within this interval.

The RMS position errors for the 3 target locations are summarized in Table 3.2. In this table, the first estimation scheme was established as a baseline using bias-free LOS measurements to estimate the target locations.[3] For the second scheme, we used biased LOS measurements but we only estimated target locations. In the last scheme, we used biased LOS measurements and we simulta-

[3] As shown in [24, 25] the unbiased LOS measurements yield composite measurements (full position MLEs) whose errors are zero-mean and their covariance is equal to the corresponding CRLB.

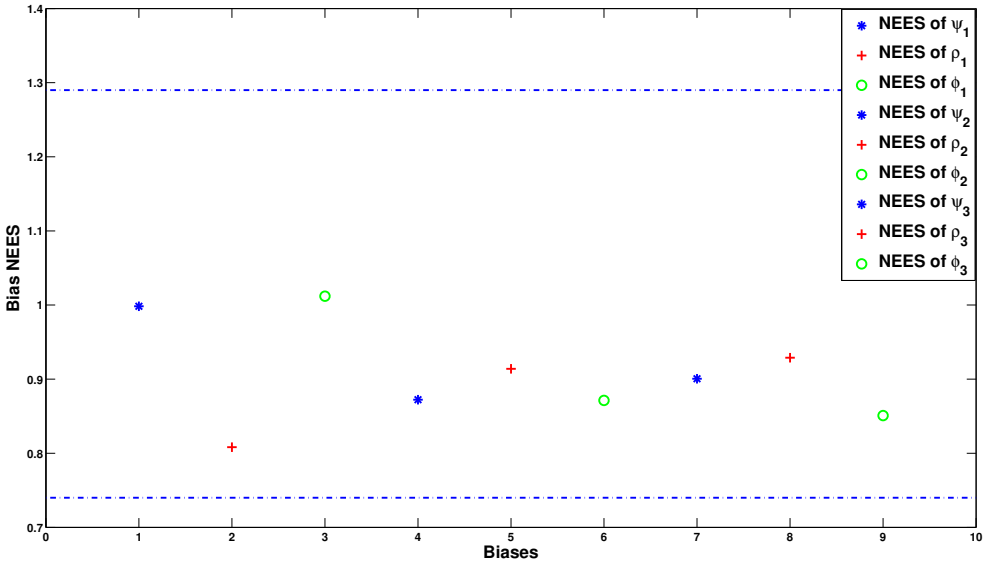

Fig. 3.4: Sample average bias NEES (CRLB evaluated at the estimate), for each of the 9 biases, over 100 Monte Carlo runs (Three-sensor case).

Table 3.2: Sample average position RMSE (m) for the 3 targets, over 100 Monte Carlo runs, for the 3 estimation schemes (Three-sensor case).

Scheme	1	2	3
First Target	127	69,391	673
Second Target	98	41,713	484
Third Target	82	16,271	343

neously estimated the target locations and sensor biases. Bias estimation yields significantly improved target RMS position errors in the presence of biases.

Each component of $\boldsymbol{\theta}$ should also be individually consistent with its corresponding σ_{CRLB} (the square root of the corresponding diagonal element of the inverse of the FIM). In this case, the sample average bias RMSE over 100 Monte Carlo runs should be within 15% of its corresponding bias standard deviation from the CRLB (σ_{CRLB}) with 95% probability. Table 3.3 demonstrates the consistency

Table 3.3: Sample average bias (μrad) RMSE over 100 Monte Carlo runs and the corresponding bias standard deviation from the CRLB (Three-sensor case).

	RMSE	σ_{CRLB}
ψ_1	138.009	138.211
ρ_1	176.073	195.808
ϕ_1	150.108	149.209
ψ_2	178.507	191.110
ρ_2	147.752	154.675
ϕ_2	230.009	246.231
ψ_3	229.131	241.389
ρ_3	134.680	139.726
ϕ_3	708.588	768.215

of the individual bias estimates. This complements the NEES evaluations from Figure 3.4.

To confirm that the bias estimates are unbiased, the average bias error $\bar{\tilde{b}}$, from Table 3.4 (over 100 Monte Carlo runs) confirms that $|\bar{\tilde{b}}|$ is less then $2\sigma_{\text{CRLB}}/\sqrt{N}$ (which it should hold with 95% probability), i.e., these estimates are unbiased.

3.3.2 Two-Sensor Case

We simulated two space-based optical sensors at various known orbits observing a target at six (unknown) locations (which is equivalent to viewing six different targets at unknown locations). In this case, a 24-dimensional parameter vector is to be estimated. As shown in Figure 3.5, each target position can be observed by all sensors. As discussed in the previous section, the three sensor biases were roll, pitch and yaw angle offsets. All the biases for each sensor were set to 50 μrad.

We made 100 Monte Carlo runs. In order to establish a baseline for evaluating the performance of our algorithm, we also ran the simulations without bias, and

Table 3.4: Sample average bias (μrad) error $\bar{\tilde{b}}$ over 100 Monte Carlo runs (Three-sensor case).

	$\bar{\tilde{b}}$	$2\frac{\sigma_{\text{CRLB}}}{\sqrt{N}}$
ψ_1	-1.728	27.642
ρ_1	16.945	39.161
ϕ_1	4.545	29.841
ψ_2	-17.323	38.222
ρ_2	5.262	30.935
ϕ_2	22.804	49.246
ψ_3	20.580	48.277
ρ_3	-7.454	27.945
ϕ_3	79.386	153.643

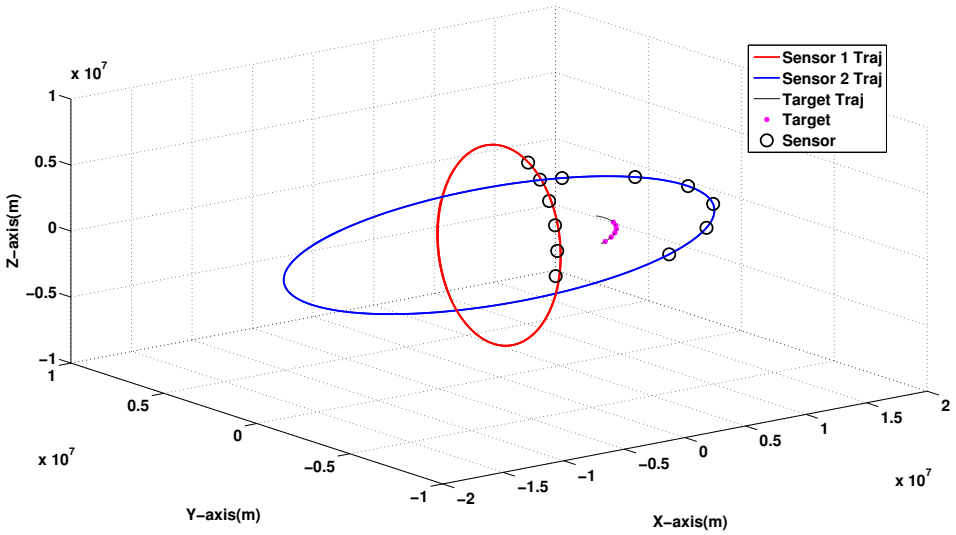

Fig. 3.5: Target and satellite trajectories for the two-sensor case

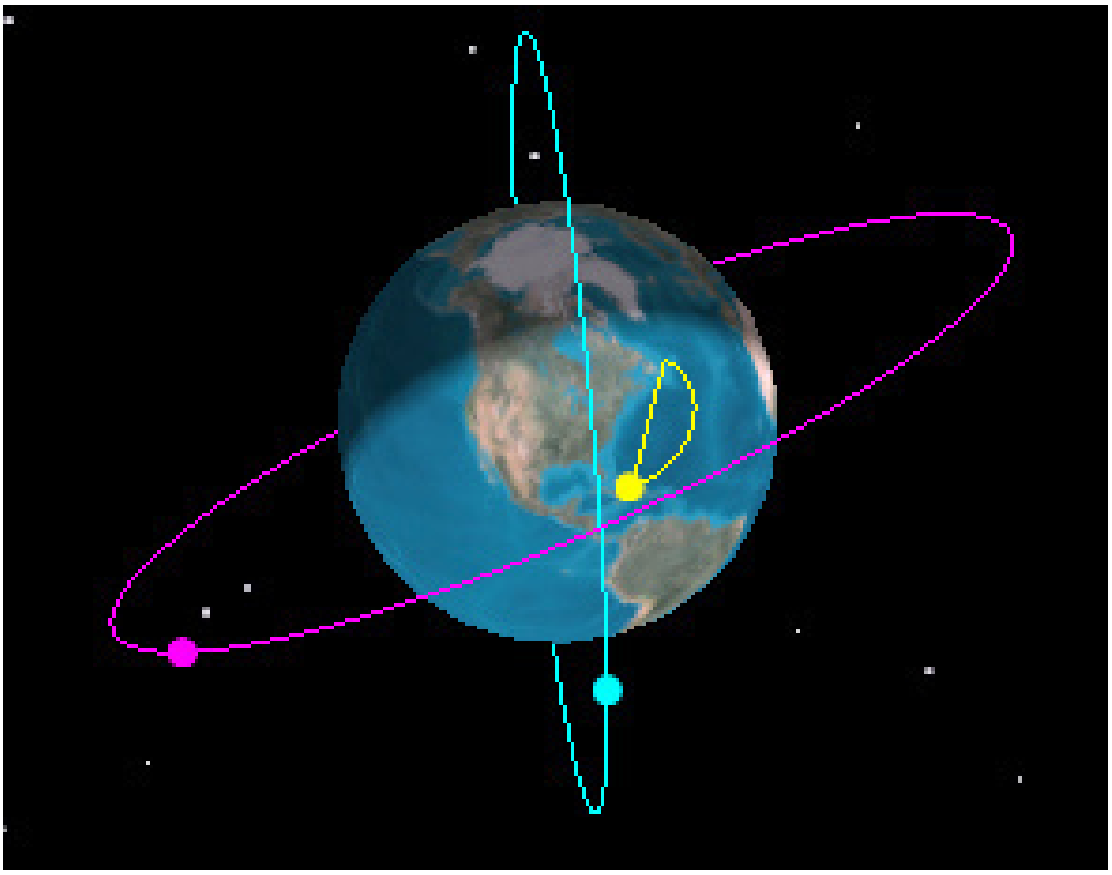

Fig. 3.6: Target and satellite trajectories for the two-sensor case

with bias but without bias estimation. The measurement noise standard deviation σ_s (identical across sensors for both azimuth and elevation measurements) was assumed to be $30\,\mu$rad.

Description of the scenarios

The sensors are assumed to provide LOS angle measurements. We denote by $\boldsymbol{\xi}_1, \boldsymbol{\xi}_2$ the 3D Cartesian sensor positions at six different times, and $\mathbf{x}(t_1), \mathbf{x}(t_2)$, $\mathbf{x}(t_3), \mathbf{x}(t_4)$,$\mathbf{x}(t_5), \mathbf{x}(t_6)$ the six 3D Cartesian target locations (all in ECI). The six target locations were chosen from a trajectory of a ballistic target as follows (in km)

$$\mathbf{x}(t_1) = \begin{bmatrix} -1,167 & -5,782 & 3,028 \end{bmatrix}' \tag{3.40}$$

$$\mathbf{x}(t_2) = \begin{bmatrix} -1,054 & -6,027 & 3,436 \end{bmatrix}' \tag{3.41}$$

$$\mathbf{x}(t_3) = \begin{bmatrix} -922 & -6,148 & 3,772 \end{bmatrix}' \tag{3.42}$$

$$\mathbf{x}(t_4) = \begin{bmatrix} -774 & -6,155 & 4,036 \end{bmatrix}' \tag{3.43}$$

$$\mathbf{x}(t_5) = \begin{bmatrix} -611 & -6,056 & 4,228 \end{bmatrix}' \tag{3.44}$$

$$\mathbf{x}(t_6) = \begin{bmatrix} -435 & -5,852 & 4,344 \end{bmatrix}' \tag{3.45}$$

Table 3.5 summarizes the sensor positions.

Statistical Efficiency of the Estimates

In order to test for the statistical efficiency of the estimate (of the 24 dimensional vector), the NEES is used, with the CRLB as the covariance matrix. The sample

Table 3.5: Sensor positions (km).

	t_1	t_2	t_3	t_4	t_5	t_6
ξ_1	187	-902	-1,934	-2,840	-3,559	-4,046
η_1	-1,439	-2,786	-3,951	-4,858	-5,447	-5,680
ζ_1	6,886	6,400	5,494	4,229	2,687	968
ξ_2	-3,966	123	4,195	7,646	9,965	10,810
η_2	-5,969	-7,238	-7,436	-6,533	-4,664	-2,105
ζ_2	8,519	8,458	7,145	4,774	1,698	-1,630

average NEES over 100 Monte Carlo runs calculated using the FIM evaluated at the true bias values and target locations is approximately 23.995, and the sample average NEES calculated using the FIM evaluated at the estimated biases and target locations is approximately 23.996 and both fall in the interval given below. The results are practically identical regardless of which values are chosen for evaluation of the FIM. The 95% probability region for the 100 sample average NEES of the 24 dimensional parameter vector is $[22.66, 25.37]'$. This NEES is found to be within this interval and the MLE is therefore statistically efficient. Figure 3.7 shows the individual bias component NEES. The 95% probability region for the 100 sample average single component NEES is $[0.74, 1.29]'$. These NEES are found to be within this interval, except for one component, which is slightly outside this region.

The RMS position errors for the 6 target locations are summarized in Table 3.6. In this table, the first estimation scheme was established as a baseline using bias-free LOS measurements to estimate the target locations. For the second scheme, we used biased LOS measurements but we only estimated target locations. In the last scheme, we used biased LOS measurements and we simultaneously estimated the target locations and sensor biases. Once again, bias estimation

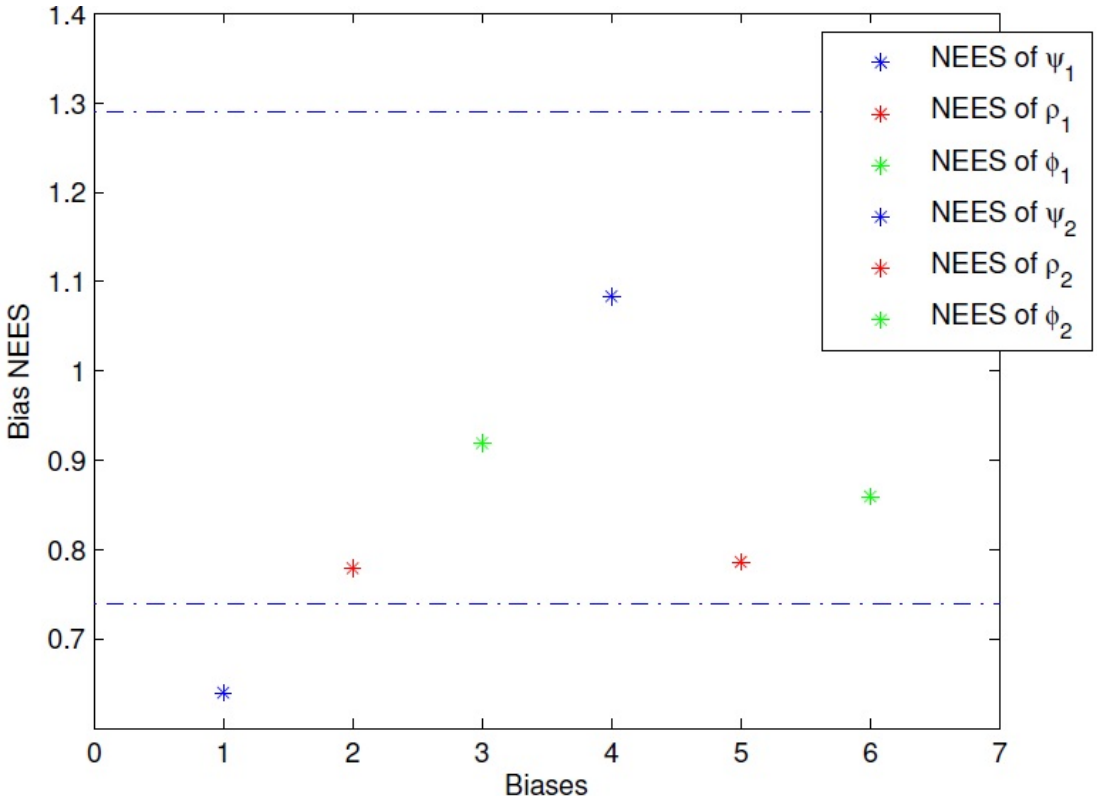

Fig. 3.7: Sample average bias NEES (CRLB evaluated at the estimate), for each of the 6 biases, over 100 Monte Carlo runs (Two-sensor case).

Table 3.6: Sample average position RMSE (m) for the 6 targets, over 100 Monte Carlo runs, for the 3 estimation schemes (Two-sensor case).

Scheme	1	2	3
First Target	234	93,123	521
Second Target	235	70,902	417
Third Target	212	60,840	403
Fourth Target	501	57,113	677
Fifth Target	637	262,712	754
Sixth Target	580	163,104	703

yields significantly improved target RMS position errors in the presence of biases.

Each component of $\boldsymbol{\theta}$ should also be individually consistent with its corresponding σ_{CRLB} (the square root of the corresponding diagonal element of the inverse of FIM). In this case, the sample average bias RMSE over 100 Monte Carlo runs should be within 15% of its corresponding bias standard deviation from the CRLB (σ_{CRLB}) with 95% probability. Table 3.7 demonstrates the efficiency of the individual bias estimates.

To confirm that the bias estimates are unbiased, the average bias error $\bar{\tilde{b}}$, from Table 3.8, over 100 Monte Carlo runs confirms that $|\bar{\tilde{b}}|$ is less then $2\sigma_{\text{CRLB}}/\sqrt{N}$ (which it should hold with 95% probability), i.e., these estimates are unbiased.

3.4 Conclusions

In this chapter we presented an algorithm that uses targets of opportunity for estimation of measurement biases. The first step was formulating a general bias model for synchronized space-based optical sensors at known locations. The association of measurements is assumed to be perfect. Based on this, we used a ML

Table 3.7: Sample average bias (μrad) RMSE over 100 Monte Carlo runs and the corresponding bias standard deviation from the CRLB (Two-sensor case).

	RMSE	σ_{CRLB}
ψ_1	74.945	72.334
ρ_1	108.100	99.322
ϕ_1	88.624	81.117
ψ_2	53.548	52.208
ρ_2	25.491	30.455
ϕ_2	140.719	98.743

Table 3.8: Sample average bias (mrad) error $\bar{\tilde{b}}$ over 100 Monte Carlo runs (Two-sensor case).

	$\bar{\tilde{b}}$	$\frac{\sigma_{\text{CRLB}}}{\sqrt{N}}$
ψ_1	-27.248	19.750
ρ_1	-13.943	21.213
ϕ_1	0.289	17.705
ψ_2	-9.677	12.289
ρ_2	5.167	0.654
ϕ_2	10.985	19.217

approach that led to a nonlinear least-squares estimation problem for simultaneous estimation of the 3D Cartesian locations of the targets of opportunity and the angle measurement biases of the sensors. The bias estimates, obtained via ILS, were shown to be unbiased and statistically efficient.

Chapter 4

Space Based Sensor Bias Estimation in the Presence of Data Association Uncertainty

4.1 Introduction

In this chapter, an approach to bias estimation in the presence of measurement association uncertainty using common targets of opportunity, is developed. Data association is carried out before the estimation of sensor angle measurement biases. Consequently, the quality of data association is critical to the overall tracking performance. Data association becomes especially challenging if the sensors are passive. Mathematically, the problem can be formulated as a multidimensional optimization problem, where the objective is to maximize the generalized likelihood that the associated measurements correspond to common targets, based on target locations and sensor bias estimates. Applying gating techniques significantly reduces the size of this problem. The association likelihoods are evaluated using an exhaustive search after which an acceptance test is applied to each solution in order to obtain the optimal (correct) solution.

We demonstrate the merits of this approach by applying it to a simulated tracking system, which consists of two or three satellites tracking a ballistic target. We assume the sensors are synchronized, their locations are known, and we esti-

mate their orientation biases together with the unknown target locations. Data association is a crucial task in many surveillance systems, and becomes especially challenging if the sensors are passive and measure Line of Sight (LOS) angles only for the targets. Measurements from multiple sensors have to be associated to determine the biases of the sensors and the positions of the targets from which the measurements originated. In general, the goal of data association is to partition the set of measurements across sensors into a number of subsets, in which the measurements are either from the same target (i.e., having the identical origin) or false alarms. For angle-only sensors, imperfect registration leads to LOS angle measurement errors in azimuth and elevation that can be much larger than those due to measurement noise. If uncorrected, registration errors can lead to large tracking errors and potentially to the formation of multiple tracks (ghosts) on the same target [8].

Mathematically, the problem can be formulated as a multidimensional optimization problem where the objective is to maximize the generalized likelihood, based on target locations and sensor bias estimates, that the associations correspond to real targets. Any feasible solution of this problem corresponds to a potential association hypothesis. In [26], the problem was formulated as a multidimensional assignment (S-D) problem where the objective was to maximize the likelihood that the associations correspond to targets. For $S \geq 3$, the multidimensional assignment problem is NP-hard. Many suboptimal algorithms have been proposed to find an approximate solution, such as Lagrangian relaxation [19], greedy rounding adaptive search (GRASP) [27], genetic algorithms [4] and linear relaxation and rounding techniques [29]. Moreover, in many cases, it is possible to resort to gating techniques [17] which drastically reduce the number of decisions

variables and make it possible to solve the problem optimally.

Even if a large part of the literature is devoted to this aspect, solving efficiently the multidimensional assignment problem is not the only challenge for data association problems. Indeed, the quality of near-optimal, or even optimal, solution may vary considerably depending on the context. In sparse configurations or with highly accurate sensors, the model behaves well and the optimal, or even an approximate solution, often has an acceptable percentage of correct associations. On the other hand, in medium or high density configurations or with sensors of low accuracy, the model behaves poorly, namely, there is ambiguity due to similarity of likelihoods. The optimal solution can have a poor association correctness while the correct solution can be suboptimal.

The optimal solution of the problem is supposed to be the most likely solution. As the complexity of the observed situations increases, the number of ambiguous elementary associations increases also. Since such associations get a high likelihood within the model, it usually happens that more than one solution can get an overall likelihood very close to the likelihood of the optimal solution. In such cases, any of these solutions, including the optimal one, could appear to be the correct association hypothesis. Therefore, it seems more reasonable to consider several candidate solutions rather than by selecting only one solution, even if it has a slightly better likelihood. The general scheme underlying our approach is based on the idea of selecting several good candidate solutions, by evaluating the likelihoods, and using a goodness of fit test to obtain the correct association hypothesis.

In the present chapter, bias estimation is investigated, in the presence of false alarms and missed detections, when only targets of opportunity are available. The

present problem is not amenable to the multidimensional assignment (S-D, [9]) because the number of measurements needed to obtain a solution for the sensor biases presents the sequential use of 2-D assignment and relaxation as in the S-D algorithm. By generating (enumerating) the set of all possible associations, which is guaranteed to contain the desired (correct association) solution, based on the association likelihoods using the target location estimates and the sensor bias estimates, an acceptance test can be applied to each solution in order to obtain the optimal (correct) solution. It appears, that through the use of gating techniques, the solution is obtained in a reasonable time.

We demonstrate the merits of this approach by applying it to a simulated tracking system, which consists of two or three satellites tracking a ballistic target. We assume the sensors are synchronized, their locations are known, and we estimate their orientation biases. We investigate the use of the minimum possible number of space-based sensors (which can not be less than two). Two cases are considered. In the first case, we use three optical sensors to estimate 3 points on the (unknown) trajectory of a single target of opportunity simultaneously with the biases of the three optical sensors [6]. In the second case, we estimate the position of 6 points on the trajectory of a single target of opportunity simultaneously with the biases of two space-based optical sensors [5].

Section II presents the problem formulation and solution in detail. Section III describes the simulations performed and gives the results. Finally, Section IV gives the conclusions.

4.2 Problem Formulation

Assume there are N_S synchronized passive sensors, with known positions in the Earth Centred Inertial (ECI) Coordinate System at times t_i,

$$\boldsymbol{\xi}_s(t_i) = [\xi_s(t_i), \eta_s(t_i), \zeta_s(t_i)]', \quad s = 1, 2, ..., N_S \tag{4.1}$$

and N_t target locations at

$$\mathbf{x}(t_i) = [x(t_i), y(t_i), z(t_i)]' \quad i = 1, 2, ..., N_t \tag{4.2}$$

also in ECI coordinates. We assume that each sensor sees all the target locations (same physical target at different times).[1] The operations needed to transform the position of a given target location at t_i expressed in ECI coordinates into the sensor s coordinate system (based on its nominal orientation) is

$$\begin{aligned} \mathbf{x}_s^{\mathrm{n}}(t_i) &= T(\boldsymbol{\omega}_s(t_i))(\mathbf{x}(t_i) - \boldsymbol{\xi}_s(t_i)) \\ i &= 1, 2, ..., N_t, \quad s = 1, 2, ..., N_S \end{aligned} \tag{4.3}$$

where $\boldsymbol{\omega}_s(t_i) = [\phi_s^{\mathrm{n}}(t_i), \rho_s^{\mathrm{n}}(t_i), \psi_s^{\mathrm{n}}(t_i)]'$ is the nominal orientation of sensor s at times t_i, $T(\boldsymbol{\omega}_s(t_i))$ is the appropriate rotation matrix, and the translation $(\mathbf{x}(t_i) - \boldsymbol{\xi}_s(t_i))$ is the difference between the vector position of the target at time t_i and the vector position of the sensor s at time t_i, both expressed in ECI coordinates. The superscript "n" in (4.3) indicates that the rotation matrix is based on the nominal sensor orientation.

[1] This can also be different targets at a common time or at different times, as long as the sensors are synchronized.

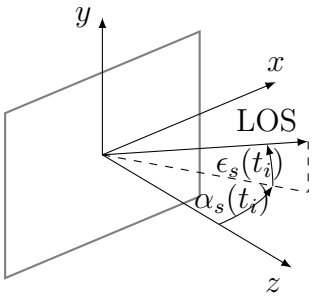

Fig. 4.1: Optical sensor coordinate system with the origin in the center of the focal plane.

As shown in Figure 1, the azimuth angle $\alpha_s(t_i)$ is the angle in the sensor's xz plane between the sensor's z axis and the projection of the line of sight to the target onto the xz plane, while the elevation angle $\epsilon_s(t_i)$ is the angle between the line of sight to the target and its projection onto the xz plane, i.e.,

$$\begin{bmatrix} \alpha_s(t_i) \\ \epsilon_s(t_i) \end{bmatrix} = \begin{bmatrix} \tan^{-1}\left(\frac{x_s(t_i)}{z_s(t_i)}\right) \\ \tan^{-1}\left(\frac{y_s(t_i)}{\sqrt{x_s^2(t_i)+z_s^2(t_i)}}\right) \end{bmatrix} \tag{4.4}$$

The model for the biased noise-free LOS measurements is then

$$\begin{aligned} \begin{bmatrix} \alpha_s^b(t_i) \\ \epsilon_s^b(t_i) \end{bmatrix} &= \begin{bmatrix} g_1(\mathbf{x}(t_i), \boldsymbol{\xi}_s(t_i), \boldsymbol{\omega}_s(t_i), \mathbf{b}_s) \\ g_2(\mathbf{x}(t_i), \boldsymbol{\xi}_s(t_i), \boldsymbol{\omega}_s(t_i), \mathbf{b}_s) \end{bmatrix} \\ &\triangleq \boldsymbol{g}[\mathbf{x}(t_i), \boldsymbol{\xi}_s(t_i), \boldsymbol{\omega}_s(t_i), \mathbf{b}_s] \end{aligned} \tag{4.5}$$

where g_1 and g_2 denote the sensor Cartesian coordinates-to-azimuth/elevation angle mapping that can be found by inserting (4.3) and (4.4) into (4.5), and the bias vector of sensor s is

$$\mathbf{b}_s = [\phi_s, \rho_s, \psi_s]' \tag{4.6}$$

For a given target, each sensor provides the noisy LOS measurements

$$\mathbf{z}_s(t_i) = \boldsymbol{g}[\mathbf{x}(t_i), \boldsymbol{\xi}_s(t_i), \boldsymbol{\omega}_s(t_i), \mathbf{b}_s] + \mathbf{w}_s(t_i) \tag{4.7}$$

where

$$\mathbf{w}_s(t_i) = [w_s^{\alpha}(t_i), w_s^{\epsilon}(t_i)]' \tag{4.8}$$

The measurement noises $\mathbf{w}_s(t_i)$ are zero-mean, white Gaussian with

$$R_s = \begin{bmatrix} (\sigma_s^{\alpha})^2 & 0 \\ 0 & (\sigma_s^{\epsilon})^2 \end{bmatrix} \tag{4.9}$$

and are assumed mutually independent. We shall assume, for simlicity, $\sigma_s^{\alpha} = \sigma_s^{\epsilon} = \sigma$.

The problem is to estimate the bias vectors for all sensors and the locations of the targets of opportunity. We shall obtain the maximum likelihood (ML) estimate of the augmented parameter vector

$$\boldsymbol{\theta} = [\mathbf{x}(t_1)', ..., \mathbf{x}(t_{N_t})', \mathbf{b}_1', ..., \mathbf{b}_{N_S}']' \tag{4.10}$$

consisting of the (unknown) target locations and sensor biases, by maximizing the likelihood function (LF) of $\boldsymbol{\theta}$.

It will be assumed that there is a single target at different (unknown) locations (4.2), observed at times t_i, $i = 1, .., N_t$. The set of measurements from sensor s at time t_i is

$$Z_s(t_i) = \{\mathbf{z}_s(l, t_i)\}_{l=1}^{n_{s,i}} \quad i = 1, 2, ..., N_t, \quad s = 1, 2, ..., N_S \tag{4.11}$$

and it contains the noisy measurement from the target and clutter points or false alarms (assumed to be spatially and temporally white). The problem consists of selecting the measurement $l_{s,i}$ deemed from the target, i.e., one from each of the $N_s N_t$ lists. Since a target may not be detected by every sensor, the probability of detection $P_D \leq 1$. The likelihood function (LF) of θ for a particular set of selected measurements (one from each sensor s and time t_i) assumed target-originated

$$\mathcal{L} = \{l_{s,i}\} \tag{4.12}$$

based on the entire set of measurements

$$Z = \{Z_s(t_i) \quad i = 1, 2, ..., N_t, \quad s = 1, 2, ..., N_S\} \tag{4.13}$$

is

$$\Lambda(\boldsymbol{\theta}; \mathcal{L}, Z_{\mathcal{L}}) = \prod_{i=1}^{N_t} \prod_{s=1}^{N_S} p\left(\mathbf{z}_s(l_{s,i}, t_i)|\boldsymbol{\theta}\right) \tag{4.14}$$

where $Z_{\mathcal{L}}$ is the set of selected measurements, and

$$p\left[\mathbf{z}_s(l_{s,i}, t_i)|\boldsymbol{\theta}\right] = \prod_{i=1}^{N_t} \prod_{s=1}^{N_S} \mathcal{N}\left(\mathbf{z}_s(l_{s,i}, t_i); \mathbf{h}_{is}\left(\boldsymbol{\theta}\right), R_s\right) \tag{4.15}$$

Note that each $\mathcal{L}$ consists of an $N_S N_t$-tuple. The ML estimate of $\boldsymbol{\theta}$ for a certain $\mathcal{L}$ is

$$\hat{\boldsymbol{\theta}}^{\mathrm{ML}}(\mathcal{L}) = \arg\max_{\boldsymbol{\theta}} \Lambda(\boldsymbol{\theta}; \mathcal{L}, Z_{\mathcal{L}}) \tag{4.16}$$

and

$$\hat{\boldsymbol{\theta}}^{\mathrm{ML}} = \hat{\boldsymbol{\theta}}(\mathcal{L}^{\mathrm{ML}}) \tag{4.17}$$

where

$$\mathcal{L}^{\mathrm{ML}} = \arg\max_{\mathcal{L}} \Lambda\big(\hat{\theta}^{\mathrm{ML}}(\mathcal{L}); \mathcal{L}, Z_{\mathcal{L}}\big) \tag{4.18}$$

i.e., the final estimate (4.17) of (4.10) is based on the most likely assignment (4.18). The final (generalized) likelihood to be used for acceptance testing is

$$\begin{aligned}\hat{\Lambda}(\mathcal{L}) &= \Lambda\big(\hat{\boldsymbol{\theta}}^{\mathrm{ML}}(\mathcal{L}^{\mathrm{ML}}); \mathcal{L}^{\mathrm{ML}}, Z_{\mathcal{L}^{\mathrm{ML}}}\big) \\ &= \prod_{i=1}^{N_t} \prod_{s=1}^{N_S} \mathcal{N}\left(\mathbf{z}_s(l_{s,i}, t_i); h_s[\,\hat{\theta}^{\mathrm{ML}}(\mathcal{L}^{\mathrm{ML}}), t_i\,], R_s\right)\end{aligned} \tag{4.19}$$

Solving (4.16) amounts to a nonlinear LS (NLS) problem. While there are many methods to obtain $\hat{\boldsymbol{\theta}}$, the iterated least squares (ILS) technique is preferred since it is easy to implement (no Hessian involved) and provides an (approximate) covariance matrix for its estimate at the same time. In order to find the MLE, one has to solve a nonlinear least squares problem for the exponent in (4.15). This will be done using a numerical search via the ILS technique [2].

4.2.1 Gating Region (Validation Region)

Validation gates are set up for selecting the candidate measurements originated from the target with high probability for each t_i. Measurements outside the validation regions can be ignored reasonably because the probabilities of them being

from the corresponding target are quite low according to the true measurement statistical characterization. After enumerating the set of all possible associations, i.e., generating all full tuples (of length N_S) with one measurement from each of the N_s lists, *the maximum cross range error* is used in gating to prune unlikely associations. If a candidate association fails in the gating test, there is no need to use it in the likelihood cost. The calculation of the gate is recursive. Beginning with the measurement $\mathbf{z}_1(l_{1,i}, t_i)$ from the first sensor (list), we take one measurement from each list at time t_i. If the measurement from the second list $\mathbf{z}_2(l_{2,i}t_i)$ falls inside the gate bounded by the cone with angle $4\sigma + max\ bias$, around the $\mathbf{z}_1(l_{1,i}t_i)$, this measurement is incorporated in the tuple for time t_i, which advances to the next list. Only full tuples (consisting of N_S LOS measurements), are to be considered. If no measurement of a particular sensor appears in any validated tuple at t_i, then none of these tuples carry information about the biases of this sensor. Consequently, none of these tuples (from t_i) will be used in the estimation of the N_S sensor biases. This is repeated for each t_i and then (16) can be carried out. Consequently, the CPU time spent in the cost computation can be reduced via the gating process.

4.2.2 Number of Hypotheses

The total number of hypotheses (combinations) for a scenario of N_t target locations and N_S sensors (assuming no missed detections) is

$$N_H = \prod_{i=1}^{N_t} \prod_{s=1}^{N_S} n_{s,i} \tag{4.20}$$

For example, in the case of the 2 sensors and 6 target locations, with medium clutter density, in a particular run, assume $n_{s,i}$ (number of clutter points plus the measurement from the target) as: $2, 1, 2, 1, 3, 3$ for $s = 1$ and $1, 5, 2, 2, 1, 2$ for $s = 2$; then the total number of hypotheses is 1440. The size of the search problem can be reduced considerably by applying gating in order to prevent implausible associations. In the previous example, only, 14% (201) passed the gating: then, this problem can be solved exactly by using an exhaustive search of modest size.

4.2.3 Requirements for bias estimability

First requirement for bias estimability

For a given target location we have a two-dimensional measurement from each sensor (the two LOS angles to the target). We assume that each sensor sees all the target locations at common times. Stacking together each measurement of N_t target locations seen by N_S sensors results in an overall measurement vector of dimension $2N_tN_S$. Given that the position and bias vectors of each target are three-dimensional, and knowing that the number of equations (size of the stacked measurement vector) has to be at least equal to the number of parameters to be estimated (target locations and biases), we must have

$$2N_tN_S \geq 3(N_t + N_S) \tag{4.21}$$

This is a necessary condition but not sufficient because (4.17) has to have a unique solution, i.e., the parameter vector has to be estimable. This is guaranteed by the second requirement.

Second requirement of bias estimability

This is the invertibility of the Fisher Information Matrix (FIM). In order to have parameter observability, the FIM must be invertible. If the FIM is not invertible (i.e., it is singular), then the CRLB (the inverse of the FIM) will not exist — the FIM will have one or more infinite eigenvalues, which means total uncertainty in a subspace of the parameter space, i.e., ambiguity [2].

For the examples of bias estimability discussed in the sequel, to estimate the biases of 3 sensors (9 bias components) we need 3 target locations (9 position components), i.e., the search is in an 18-dimensional space, while for 2 sensors (6 bias components) we need at least 6 target locations (18 position components) in order to meet the necessary requirement (4.21). As stated previously, the FIM must be invertible, so the rank of the FIM has to be equal to the number of parameters to be estimated (9+9=18, or 6+18=24, in the previous examples). The full rank of the FIM is a necessary and sufficient condition for estimability.

4.2.4 Iterated Least Squares for maximization

Given the estimate $\hat{\boldsymbol{\theta}}^j$ after j iterations, the ILS estimate after the $(j+1)$th iteration will be

$$\hat{\boldsymbol{\theta}}^{j+1} = \hat{\boldsymbol{\theta}}^j + \left[(H^j)' R^{-1} H^j\right]^{-1} (H^j)' R^{-1} [\mathbf{z} - \mathbf{h}(\hat{\boldsymbol{\theta}}^j)] \tag{4.22}$$

where

$$\mathbf{z} = [z_1(t_1)', ..., z_s(t_1)', ..., z_s(t_i)', ..., z_{N_S}(t_{N_t})']' \tag{4.23}$$

$$\mathbf{h}(\hat{\boldsymbol{\theta}}^j) = [h_{11}(\hat{\boldsymbol{\theta}}^j)', ..., h_{is}(\hat{\boldsymbol{\theta}}^j)', ..., h_{N_t N_S}(\hat{\boldsymbol{\theta}}^j)'] \tag{4.24}$$

$$R = \begin{bmatrix} R_1 & 0 & \cdots & 0 \\ 0 & R_2 & \cdots & 0 \\ \vdots & \vdots & \ddots & \vdots \\ 0 & \cdots & 0 & R_{N_S} \end{bmatrix} \tag{4.25}$$

where R_s is the measurement noise covariance matrix of sensor s, and

$$H^j = \left. \frac{\partial \mathbf{h}\left(\boldsymbol{\theta}^j\right)}{\partial \boldsymbol{\theta}} \right|_{\boldsymbol{\theta}=\hat{\boldsymbol{\theta}}^j} \tag{4.26}$$

is the Jacobian matrix of the vector consisting of the stacked measurement functions (2.16) w.r.t. (4.10) evaluated at the ILS estimate from the previous iteration j. In this case, the Jacobian matrix is, with the iteration index omitted for conciseness,

$$H = \begin{bmatrix} H_{11} & H_{21} & \cdots & H_{N_t 1} & H_{12} & \cdots & H_{N_t N_S} \end{bmatrix}' \tag{4.27}$$

where

$$H_{is} = \begin{bmatrix} \frac{\partial g_{1_s}(t_i)}{\partial x(t_1)} & \frac{\partial g_{2_s}(t_i)}{\partial x(t_1)} \\ \frac{\partial g_{1_s}(t_i)}{\partial y(t_1)} & \frac{\partial g_{2_s}(t_i)}{\partial y(t_1)} \\ \frac{\partial g_{1_s}(t_i)}{\partial z(t_1)} & \frac{\partial g_{2_s}(t_i)}{\partial z(t_1)} \\ \vdots & \vdots \\ \frac{\partial g_{1_s}(t_i)}{\partial x(t_{N_t})} & \frac{\partial g_{2_s}(t_i)}{\partial x(t_{N_t})} \\ \frac{\partial g_{1_s}(t_i)}{\partial y(t_{N_t})} & \frac{\partial g_{2_s}(t_i)}{\partial y(t_{N_t})} \\ \frac{\partial g_{1_s}(t_i)}{\partial z(t_{N_t})} & \frac{\partial g_{2_s}(t_i)}{\partial z(t_{N_t})} \\ \frac{\partial g_{1_s}(t_i)}{\partial \psi_1} & \frac{\partial g_{2_s}(t_i)}{\partial \psi_1} \\ \frac{\partial g_{1_s}(t_i)}{\partial \rho_1} & \frac{\partial g_{2_s}(t_i)}{\partial \rho_1} \\ \frac{\partial g_{1_s}(t_i)}{\partial \phi_1} & \frac{\partial g_{2_s}(t_i)}{\partial \phi_1} \\ \vdots & \vdots \\ \frac{\partial g_{1_s}(t_i)}{\partial \psi_{N_S}} & \frac{\partial g_{2_s}(t_i)}{\partial \psi_{N_S}} \\ \frac{\partial g_{1_s}(t_i)}{\partial \rho_{N_S}} & \frac{\partial g_{2_s}(t_i)}{\partial \rho_{N_S}} \\ \frac{\partial g_{1_s}(t_i)}{\partial \phi_{N_S}} & \frac{\partial g_{2_s}(t_i)}{\partial \phi_{N_S}} \end{bmatrix} \tag{4.28}$$

The appropriate partial derivatives are given in the appendix B.

4.2.5 Initialialization

In order to perform the numerical search via ILS, an initial estimate $\hat{\boldsymbol{\theta}}^0$ is required. Assuming that the biases are null, the LOS measurements from the first and the second sensor $\alpha_1(t_i)$, $\alpha_2(t_i)$ and $\epsilon_1(t_i)$ can be used to solve for each initial Cartesian

target position, in ECI coordinates, using (4.29)–(4.31).

$$x(t_i)^0 = \frac{\xi_2(t_i) - \xi_1(t_i) + \zeta_1(t_i)\tan\alpha_1(t_i) - \zeta_2(t_i)\tan\alpha_2(t_i)}{\tan\alpha_1(t_i) - \tan\alpha_2(t_i)} \tag{4.29}$$

$$y(t_i)^0 = \frac{\tan\alpha_1(t_i)\left(\xi_2(t_i) + \tan\alpha_2(t_i)\left(\zeta_1(t_i) - \zeta_2(t_i)\right)\right) - \xi_1(t_i)\tan\alpha_2(t_i)}{\tan\alpha_1(t_i) - \tan\alpha_2(t_i)} \tag{4.30}$$

$$z(t_i)^0 = \eta_1(t_i) + \tan\epsilon_1(t_i)\left|\frac{(\xi_1(t_i) - \xi_2(t_i))\cos\alpha_2(t_i) + (\zeta_2(t_i) - \zeta_1(t_i))\sin\alpha_2(t_i)}{\sin\left(\alpha_1(t_i) - \alpha_2(t_i)\right)}\right| \tag{4.31}$$

4.2.6 Cramér-Rao Lower Bound

In order to evaluate the efficiency of the estimator, the CRLB must be calculated. The CRLB provides a lower bound on the covariance matrix of an unbiased estimator as [2]

$$E\{(\boldsymbol{\theta} - \hat{\boldsymbol{\theta}})(\boldsymbol{\theta} - \hat{\boldsymbol{\theta}})'\} \geq J(\boldsymbol{\theta})^{-1} \tag{4.32}$$

where J is the Fisher Information Matrix (FIM), $\boldsymbol{\theta}$ is the true parameter vector to be estimated, and $\hat{\boldsymbol{\theta}}$ is the estimate. The FIM is

$$J(\boldsymbol{\theta}) = E\left\{\left[\nabla_{\boldsymbol{\theta}}\ln\Lambda(\boldsymbol{\theta})\right]\left[\nabla_{\boldsymbol{\theta}}\ln\Lambda(\boldsymbol{\theta})\right]'\right\}\Big|_{\boldsymbol{\theta}=\boldsymbol{\theta}_{\text{true}}} \tag{4.33}$$

where the gradient of the log-likelihood function is

$$\lambda(\boldsymbol{\theta}) \triangleq \ln\Lambda(\boldsymbol{\theta}) \tag{4.34}$$

$$\nabla_{\boldsymbol{\theta}}\lambda(\boldsymbol{\theta}) = \sum_{i=1}^{N_t}\sum_{s=1}^{N_S} H_{is}' R_s^{-1}\left(\mathbf{z}_s(t_i) - \mathbf{h}_{is}(\boldsymbol{\theta})\right) \tag{4.35}$$

which, when plugged into (4.33), gives

$$\begin{aligned} J(\boldsymbol{\theta}) &= \sum_{i=1}^{N_t} \sum_{s=1}^{N_S} H'_{is} \left(R_s^{-1}\right) H_{is}\big|_{\boldsymbol{\theta}=\boldsymbol{\theta}_{\text{true}}} \\ &= H' \left(R^{-1}\right) H\big|_{\boldsymbol{\theta}=\boldsymbol{\theta}_{\text{true}}} \end{aligned} \tag{4.36}$$

4.3 Simulations

We simulate a space based system tracking a ballistic missile. The missile and satellite trajectories are generated using System Tool Kit (STK)[2]. The target modeled represents a ballistic missile with a flight time of about 20 minutes. STK provides the target and sensor positions in three dimensional Cartesian coordinates at 1 s intervals. The target launch time is chosen so that the satellite based sensors were able to follow the missile trajectory throughout its flight path.

Any association $N_S N_t$-tuple that passes the gating test, falls into one of the following three categories:

- Completely correct (CC) association: The measurements in an association tuple have identical origin and there is no clutter measurement associated.
- Partially correct (PC) association: There are at least 2 measurements with common origin, and the rest may be from different origins or clutter measurements.
- Completely incorrect (CI) association: In an association tuple, there does not exist a pair of measurements that come from the same origin.

[2] STK Systems Tool Kit are registered trademarks of Analytical Graphics, Inc.

4.3.1 Statistical Acceptance test (Goodness of Fit)

In order to obtain the optimal (correct) association, the Sum of the Normalized Square Residuals (SNSR) is used as a measure of the goodness of fit, which is defined as the minimized value of the log likelihood function (4.19), multiplied by 2 for convenience

$$\lambda^{\star}(\hat{\theta}^{\mathrm{ML}}(\mathcal{L}^{\mathrm{ML}})) = \sum_{i=1}^{N_t}\sum_{s=1}^{N_S}\left(\left[\mathbf{z}_s(l_{s,i},t_i) - \mathbf{h}_{is}\left(\hat{\theta}^{\mathrm{ML}}(\mathcal{L}^{\mathrm{ML}})\right)\right]' R_s^{-1}\left[\mathbf{z}_s(l_{s,i},t_i) - \mathbf{h}_{is}\left(\hat{\theta}^{\mathrm{ML}}(\mathcal{L}^{\mathrm{ML}})\right)\right]\right) \tag{4.37}$$

This is similar to the linear least squares case (LS), under the Gaussian noise assumptions, where the fitting error was shown to be Chi-square distributed in [2].

In the present nonlinear LS problem, a Monte Carlo simulation is used to confirm the validity of this result, by summing up the fitting errors from N runs with independent random variables, with n_z being the number of measurements and n_x is the number of parameters, the total error obtained is Chi-square distributed with $N(n_z - n_x)$ degrees of freedom.

For the three sensor case ($n_x = 18$), the sample average SNSR over 100 Monte Carlo runs was evaluated using $n_z = 24$ LOS measurements yielding 5.71. The 99% upper limit of the probability region is, based on the $100(n_z - n_x) = 600$ degrees of freedom Chi-square distribution (divided by 100), approximately 6.83. Similar results were obtained for the two sensor case ($n_x = 24$): the sample average SNSR over 100 Monte Carlo runs was evaluated using $n_z = 28$ LOS measurements yielding 4.13. The 99% upper limit of the probability region is, based on the $100(n_z - n_x) = 400$ degrees of freedom Chi-square distribution (divided by 100), approximately 4.68.

The statistical acceptance test of an association, in a particular run, is based

on data from single run, which can be used with real data, and does not require knowledge of the true parameter. Then

$$\lambda^{\star}(\hat{\theta}^{\mathrm{ML}}(\mathcal{L}^{\mathrm{ML}})) \sim \chi^2_{n_z-n_x} \tag{4.38}$$

Namely, $\lambda^{\star}$ should be, with 99% probability, below the threshold $\chi^2_{n_z-n_x}(0.01)$ denoted as τ. Given an association tuple, if its SNSR (4.37) is less than the threshold τ, then this association is accepted, otherwise it is rejected.

For the three sensor case ($n_x = 18$), three scenarios are considered, in the first scenario, the SNSR is evaluated using $n_z = 30$ LOS measurements. The 99% upper limit of the probability region is 26.6, based on the $n_z - n_x = 12$ degrees of freedom Chi-square distribution ($\tau = 26.6$). In the second scenario, the SNSR is evaluated using $n_z = 24$ LOS measurements. The 99% upper limit of the probability region is 16.8, based on the $n_z - n_x = 6$ degrees of freedom Chi-square distribution ($\tau = 16.8$). In the third scenario, we evaluate the SNSR using an 18 LOS measurements, in this case ($\tau = 0$). Practically, in this case one has 18 unknowns and 18 nonlinear equations.

For the two sensor case ($n_x = 24$), three scenarios are considered, in the first scenario, the SNSR is evaluated using $n_z = 32$ LOS measurements. The 99% upper limit of the probability region is 20.1, based on the $n_z - n_x = 8$ degrees of freedom Chi-square distribution ($\tau = 20.1$). In the second scenario, the SNSR is evaluated using $n_z = 28$ LOS measurements. The 99% upper limit of the probability region is 13.3, based on the $n_z - n_x = 4$ degrees of freedom Chi-square distribution ($\tau = 13.3$). In the third scenario, we evaluate the SNSR using 24 LOS measurements ($\tau = 0$).

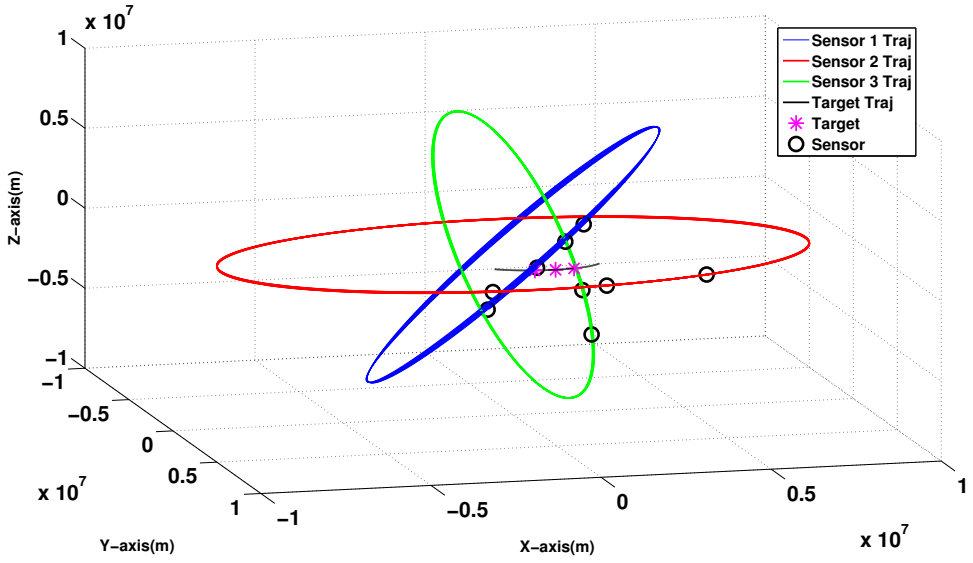

Fig. 4.2: Target and satellite trajectories for the three-sensor case

4.3.2 Three-Sensor Case

We simulated three space based optical sensors at various known orbits observing a target at three points in time at unknown locations. In this case, an 18-dimensional parameter vector is to be estimated. Figure 4.2 shows each target position observed by the sensors (Figure 4.3 gives an image of this). All the sensors are assumed to have the same accuracy, detection probability P_D and expected number of false measurements at each sensor at each time is assumed to be 3. As discussed in the previous section, the three sensor biases are roll, pitch and yaw angle offsets. The biases for each sensor were set to $0.5^\circ = 8.72$ mrad. We ran 100 Monte Carlo runs. The horizontal and vertical fields-of-view of each sensor are assumed to be 60°. The measurement noise standard deviation σ_s (identical across sensors for both azimuth and elevation measurements, $\sigma_s^\alpha = \sigma_s^\epsilon = \sigma$) was assumed to be 30 μrad.

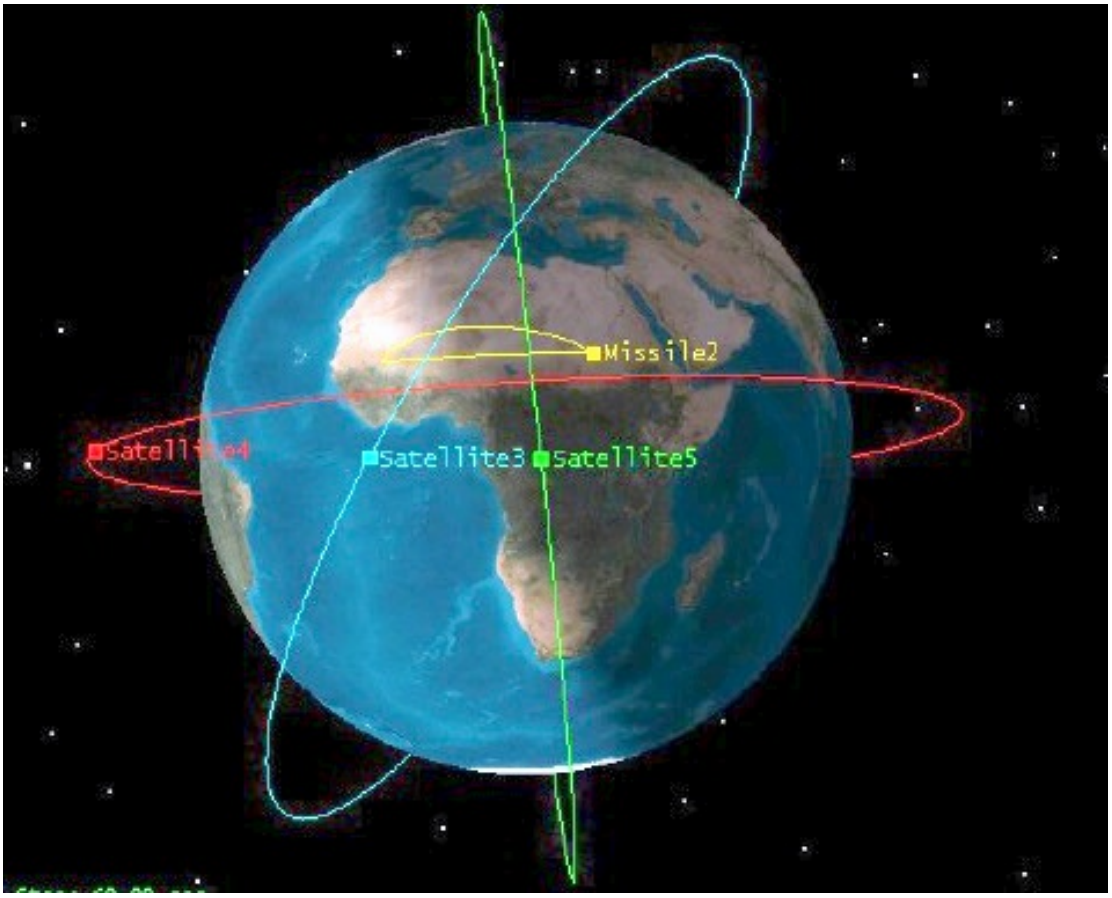

Fig. 4.3: Target and satellite trajectories for the three-sensor case

Table 4.1: Sensor positions (km).

	ξ_1	η_1	ζ_1	ξ_2	η_2	ζ_2	ξ_3	η_3	ζ_3
Time 1	1,235	158	6,927	5,549	1,116	6,285	6,499	-279	-5,407
Time 2	1,062	-174	6,955	3,061	2,993	7,295	7,897	-719	-2,944
Time 3	887	-507	6,963	112	4,418	7,212	8,389	-1,074	-143

Description of the Scenarios

The sensors are assumed to provide LOS angle measurements. We denote by $\boldsymbol{\xi}_1, \boldsymbol{\xi}_2, \boldsymbol{\xi}_3$ the 3D Cartesian sensor locations, and $\mathbf{x}(t_1), \mathbf{x}(t_2), \mathbf{x}(t_3)$ the 3D Cartesian target locations (all in ECI). The three target locations were chosen from a trajectory of a ballistic target as follows (in km)

$$\mathbf{x}(t_1) = \begin{bmatrix} 7,518 & -1,311 & -1,673 \end{bmatrix}' \tag{4.39}$$

$$\mathbf{x}(t_2) = \begin{bmatrix} 7,942 & -509 & -1,375 \end{bmatrix}' \tag{4.40}$$

$$\mathbf{x}(t_3) = \begin{bmatrix} 7,988 & 317 & -1,012 \end{bmatrix}' \tag{4.41}$$

Table 4.1 summarizes the sensor positions (in km).

The statistical acceptance of an association hypothesis is carried out as discussed in Sec. 4.3.1. The SNSR is evaluated for each validated association hypothesis. Three scenarios are considered, in the first scenario, $P_D = 0.8$, the SNSR is evaluated using $n_z = 30$ LOS measurements. The 99% upper limit of the probability region is 26.6, based on the $n_z - n_x = 12$ degrees of freedom Chi-square distribution ($\tau = 26.6$). In the second scenario, $P_D = 0.9$, the SNSR is evaluated using $n_z = 24$ LOS measurements. The 99% upper limit of the probability re-

Table 4.2: Sample average bias RMSE over 100 Monte Carlo runs and the corresponding bias standard deviation from the CRLB (σ_{CRLB})(μrad) (Three-sensor case).

Scenario		First Sensor			Second Sensor			Third Sensor		
		ψ	ρ	ϕ	ψ	ρ	ϕ	ψ	ρ	ϕ
1	RMSE	79.493	35.943	71.858	50.758	26.681	159.936	65.475	38.605	122.921
	σ_{CRLB}	78.365	39.332	85.466	50.407	25.728	152.354	69.317	38.452	133.942
2	RMSE	67.209	37.311	79.951	49.890	22.072	145.564	55.912	31.129	125.762
	σ_{CRLB}	68.909	36.620	82.351	48.584	24.235	143.217	62.641	34.364	126.637
3	RMSE	86.245	39.679	97.153	53.311	25.623	164.339	77.544	38.196	148.291
	σ_{CRLB}	78.349	39.337	85.473	50.401	25.729	152.355	69.320	38.459	133.963

gion is 16.8, based on the $n_z - n_x = 6$ degrees of freedom Chi-square distribution ($\tau = 16.8$). In the third scenario, $P_D = 1$, we evaluate the SNSR using an 18 LOS measurements, in this case ($\tau = 0$). Practically, in this case one has 18 unknowns and 18 nonlinear equations and the problem is not solvable unless $P_D = 1$, in this case, we set $\tau = 0.01$ to account for numerical imprecisions. For the first scenario, the SNRS of the completely correct (CC) association is 5.66. The SNSR of the partially correct (PC) associations and the completely incorrect (CI) associations are of the order of 10^9. For the second scenario, the SNSR of the completely correct (CC) association is 6.12. The SNSR of the partially correct (PC) associations and the completely incorrect (CI) associations are of the order of 10^9. For the last scenario, the SNSR of the completely correct (CC) association is $0.23 \cdot 10^{-24}$. The SNSR of the partially correct (PC) associations and the completely incorrect (CI) associations are of the order of 10^9.

The RMS bias errors for the optimal (correct) association, are summarized in Table 4.2, for the three scenarios in the three sensors case. The value of the σ_{CRLB} was calculated using (4.36) and they were provided by the ILS [7].

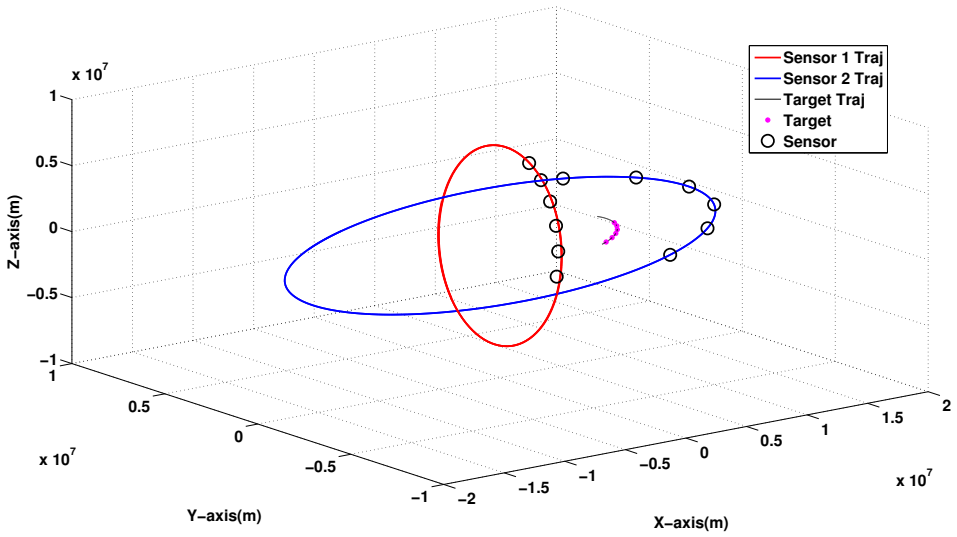

Fig. 4.4: Target and satellite trajectories for the two-sensor case

4.3.3 Two-Sensor Case

We simulated two space-based optical sensors at various known orbits observing a target at six (unknown) locations (which is equivalent to viewing six different targets at unknown locations). In this case, a 24-dimensional parameter vector is to be estimated. As shown in Figure 4.4, each target position can be observed by all sensors. All the sensors are assumed to have the same accuracy, detection probability P_D and expected number of false measurements at each sensor at each time is assumed to be 3. As discussed in the previous section, the three sensor biases were roll, pitch and yaw angle offsets. All the biases for each sensor were set to $0.5^\circ = 8.72$ mrad. The measurement noise standard deviation σ_s (identical across sensors for both azimuth and elevation measurements) was assumed to be $30\,\mu$rad.

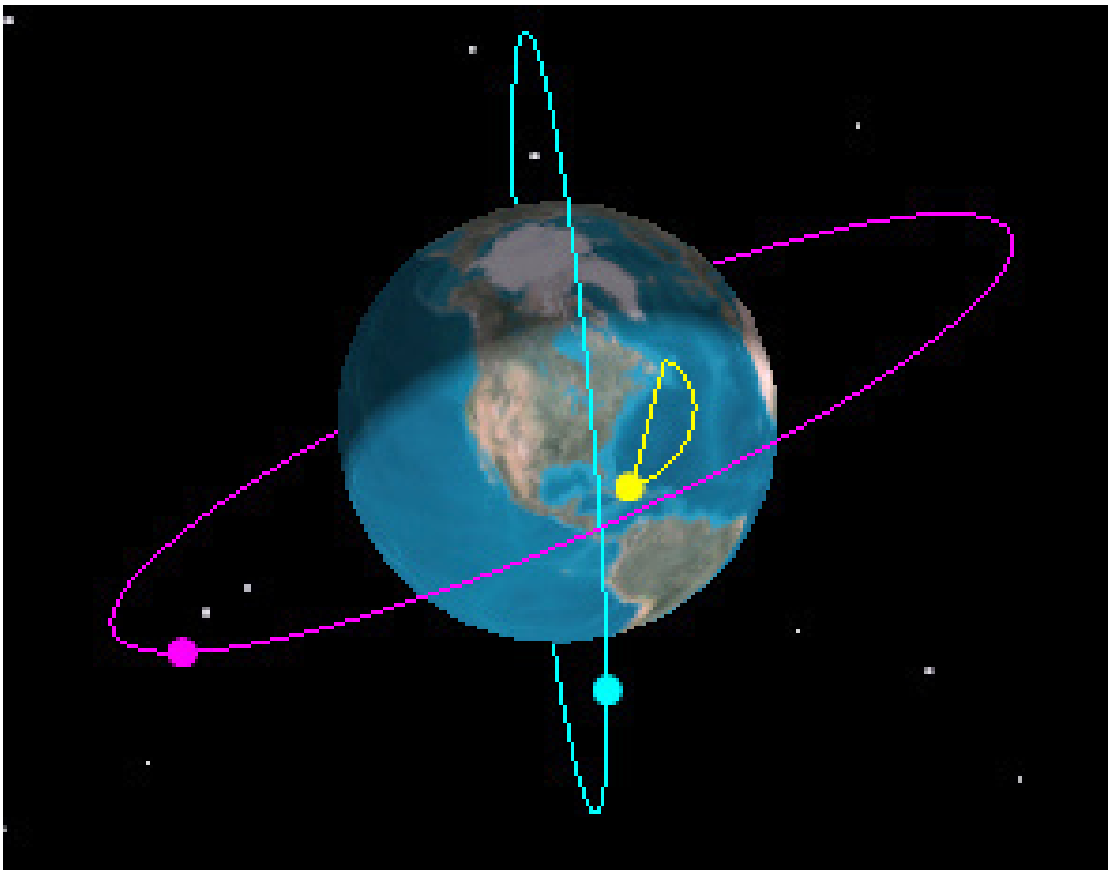

Fig. 4.5: Target and satellite trajectories for the two-sensor case

Table 4.3: Sensor positions (km).

	ξ_1	η_1	ζ_1	ξ_2	η_2	ζ_2
t_1	187	-1,439	6,886	-3,966	-5,969	8,519
t_2	-902	-2,786	6,400	123	-7,238	8,458
t_3	-1,934	-3,951	5,494	4,195	-7,436	7,145
t_4	-2,840	-4,858	4,229	7,646	-6,533	4,774
t_5	-3,559	-5,447	2,687	9,965	-4,664	1,698
t_6	-4,046	-5,680	968	10,810	-2,105	-1,630

Description of the Scenarios

The sensors are assumed to provide LOS angle measurements. We denote by $\boldsymbol{\xi}_1, \boldsymbol{\xi}_2$ the 3D Cartesian sensor positions at six different times, and $\mathbf{x}(t_1), \mathbf{x}(t_2)$, $\mathbf{x}(t_3), \mathbf{x}(t_4)$, $\mathbf{x}(t_5), \mathbf{x}(t_6)$ the six 3D Cartesian target locations (all in ECI). The six target locations were chosen from a trajectory of a ballistic target as follows (in km)

$$\mathbf{x}(t_1) = \begin{bmatrix} -1,167 & -5,782 & 3,028 \end{bmatrix}' \tag{4.42}$$

$$\mathbf{x}(t_2) = \begin{bmatrix} -1,054 & -6,027 & 3,436 \end{bmatrix}' \tag{4.43}$$

$$\mathbf{x}(t_3) = \begin{bmatrix} -922 & -6,148 & 3,772 \end{bmatrix}' \tag{4.44}$$

$$\mathbf{x}(t_4) = \begin{bmatrix} -774 & -6,155 & 4,036 \end{bmatrix}' \tag{4.45}$$

$$\mathbf{x}(t_5) = \begin{bmatrix} -611 & -6,056 & 4,228 \end{bmatrix}' \tag{4.46}$$

$$\mathbf{x}(t_6) = \begin{bmatrix} -435 & -5,852 & 4,344 \end{bmatrix}' \tag{4.47}$$

Table 4.3 summarizes the sensor positions.

The statistical acceptance is done as follows. The SNSR is evaluated for

each validated association hypothesis. Three scenarios were considered. In the first scenario, $P_D = 0.8$, the SNSR is evaluated using $n_z = 32$ LOS measurements. The 99% upper limit of the probability region is 20.8, based on the 8 degrees of freedom Chi-square distribution ($\tau = 20.8$). In the second scenario, $P_D = 0.9$, the SNSR is evaluated using $n_z = 28$ LOS measurements. The 99% upper limit of the probability region is 13.3, based on the 4 degrees of freedom Chi-square distribution ($\tau = 13.3$). In the third scenario, $P_D = 1$, we evaluate the SNSR using $n_z = 24$ LOS measurements, Practically, in this case one has 24 unknowns and 24 nonlinear equations and the problem is not solvable unless $P_D = 1$, in this case, we set $\tau = 0.01$ to account for numerical imprecisions. For the first scenario, the SNSR of the completely correct (CC) association is 6.47. The SNSR of the partially correct (PC) associations and the completely incorrect (CI) associations are of the order of 10^{10}. For the second scenario, the SNSR of the completely correct (CC) association is 7.12. The SNSR of the partially correct (PC) associations and the completely incorrect (CI) associations are of the order of 10^{10}. For the last scenario, the SNRS of the completely correct (CC) association is $0.42 \cdot 10^{-24}$. The SNSR of the partially correct (PC) associations and the completely incorrect (CI) associations are of the order of 10^{10}.

The RMS bias errors for the optimal (correct) association, are summarized in Table 4.4, for the three scenarios in the two sensors case.

4.4 Conclusions

In this chapter we presented an approach to bias estimation in the presence of measurement association uncertainty using common targets of opportunity. The

Table 4.4: Sample average bias RMSE over 100 Monte Carlo runs and the corresponding bias standard deviation from the CRLB (σ_{CRLB})(μrad) (Two-sensor case).

Scenario		First Sensor			Second Sensor		
		ψ	ρ	ϕ	ψ	ρ	ϕ
1	RMSE	128.469	139.761	164.244	74.097	43.693	166.525
	σ_{CRLB}	133.688	150.919	165.933	73.772	46.724	164.050
2	RMSE	143.732	148.461	173.969	80.755	49.571	173.860
	σ_{CRLB}	133.609	151.170	165.929	73.865	46.622	164.23
3	RMSE	149.383	168.707	180.788	82.082	52.476	181.479
	σ_{CRLB}	133.784	151.194	177.097	74.251	46.727	170.014

association likelihoods are evaluated, following gating, using an exhaustive search after which a statistical acceptance test is applied to each solution in order to discriminate the optimal (correct) solution from the incorrect associations. Using simulated space based tracking systems consisting of two or three satellites tracking a ballistic target, we showed that this approach performs well. Another significance of this work is the formulation of a measure of the goodness of fit (Sum of the Normalized Square Residuals — (SNSR)) for the nonlinear least squares case, under Gaussian noise assumptions. Similarly, to the linear least squares case, where the fitting error was shown to be Chi-square distributed [2], we showed that this can be used in the nonlinear LS, thus providing a statistical test that selects the correct associations.

Chapter 5

Statistical Efficiency of Simultaneous Target State and Sensor Bias Estimation

5.1 Introduction

In this chapter we provide a new methodology using an exoatmospheric target of opportunity seen in a satellites borne sensor's field of view to estimate the sensor's biases simultaneously with the state of the target. Each satellite is equipped with an IR sensor that provides the Line Of Sight (LOS) measurements azimuth and elevation to the target. The measurements provided by these sensors are assumed to be noisy but perfectly associated, i.e., it is known perfectly that they belong to the same target. The evaluation of the Cramér-Rao Lower Bound (CRLB) on the covariance of the bias estimates, and the statistical tests on the results of simulations show that this method is statistically efficient.

A space-based tracking system provides many advantages for missile defense as well as space situational awareness as a part of a system of systems that contribute to an overall picture. It can cover gaps in terrestrial radar coverage and expand the capabilities of a Ballistic Missile Defense System (BMDS), allow interceptors to engage enemy missiles earlier in their trajectories, discriminate between warheads and decoys, and provide warhead hit assessment. However, systemic

errors in sensing systems hinder accurate threat identification and target state estimation, and, in this way, the space-based tracking systems present some unique challenges [16].

For angle-only sensors, imperfect registration leads to LOS angle measurement biases in azimuth and elevation. If not corrected, the registration errors can seriously degrade the global surveillance system performance by increasing the tracking errors and even introducing ghost targets. In [15] the effect of sensor and timing bias error on the tracking quality of a space-based infrared (IR) tracking system that utilizes a Linearized Kalman Filter (LKF) for the highly non-linear problem of tracking a ballistic missile was presented. This was extended in [16] by proposing a method of using stars observed in the sensor background to reduce the sensor bias error. In [7] simultaneous sensors bias and targets position estimation using fixed passive sensors was proposed. A solution to the related observability issues discussed in [7] is proposed in [9] using space based sensors.

The new bias estimation algorithm developed in this paper, is validated using a hypothetical scenario created using System Tool Kit (STK) [28]. The tracking system consists of two optical sensors (space based) tracking a ballistic target. We assume the sensors are synchronized, their locations are known, and the data association is correct; and we estimate their orientation biases while simultaneously estimating the state of the target (position and velocity). We evaluate the Cramér-Rao lower bound (CRLB) on the covariance of the bias estimates, which is the quantification of the available information on the sensor biases, and show via statistical tests that the estimation is statistically efficient — it meets the CRLB.

Section II presents the problem formulation and solution in detail. Section

III describes the simulations performed and gives the results. Finally, Section IV gives the conclusions and future work.

5.2 Problem Formulation

An important prerequisite for successful multisensor integration (fusion) is that the data from the reporting sensors are transformed to a common reference frame free of systematic or registration errors (biases). The fundamental frame of reference used in this paper is the Earth Centered Inertial (ECI) Coordinate System.

In a multisensor scenario, sensor platform s has a sensor reference frame associated with it (measurement frame of the sensor) defined by the orthogonal set of unit vectors $(e_{\xi_s}, e_{\eta_s}, e_{\zeta_s})$. The origin of the measurement frame of the sensor is a translation of the (ECI) origin, and its axes are rotated with respect to the (ECI) axes. The rotation between these frames can be described by a set of Euler angles. We will refer to these angles $\phi_s + \phi_s^{\mathrm{n}}$, $\rho_s + \rho_s^{\mathrm{n}}$, $\psi_s + \psi_s^{\mathrm{n}}$ of sensor s, as roll, pitch and yaw respectively, where ϕ_s^{n} is the nominal roll angle, ϕ_s is the roll bias, etc.

Each angle defines a rotation about a prescribed axis, in order to align the sensor frame axes with the (ECI) axes. The xyz rotation sequence is chosen, which is accomplished by first rotating about the x axis by ϕ_s^{n}, then rotating about the y axis by ρ_s^{n}, and finally rotating about the z axis by ψ_s^{n}. The rotations sequence can be expressed by the matrices

$$T_s(\psi_s^{\mathrm{n}}, \rho_s^{\mathrm{n}}, \phi_s^{\mathrm{n}}) = T_z(\psi_s^{\mathrm{n}}) T_y(\rho_s^{\mathrm{n}}) T_x(\phi_s^{\mathrm{n}})$$

$$
\begin{aligned}
&= \begin{bmatrix} \cos\psi_s^{\mathrm{n}} & \sin\psi_s^{\mathrm{n}} & 0 \\ -\sin\psi_s^{\mathrm{n}} & \cos\psi_s^{\mathrm{n}} & 0 \\ 0 & 0 & 1 \end{bmatrix} \\
&\cdot \begin{bmatrix} \cos\rho_s^{\mathrm{n}} & 0 & -\sin\rho_s^{\mathrm{n}} \\ 0 & 1 & 0 \\ \sin\rho_s^{\mathrm{n}} & 0 & \cos\rho_s^{\mathrm{n}} \end{bmatrix} \\
&\cdot \begin{bmatrix} 1 & 0 & 0 \\ 0 & \cos\phi_s^{\mathrm{n}} & \sin\phi_s^{\mathrm{n}} \\ 0 & -\sin\phi_s^{\mathrm{n}} & \cos\phi_s^{\mathrm{n}} \end{bmatrix}
\end{aligned} \tag{5.1}
$$

Assume there are N_S synchronized passive sensors, with known positions in (ECI) coordinates,
$\boldsymbol{\xi}_s(k) = [\xi_s(k), \eta_s(k), \zeta_s(k)]', \quad s = 1, 2, ..., N_S, \quad k = 0, 1, 2, ..., K$, tracking a single target at unknown positions $\mathbf{x}(k) = [x(k), y(k), z(k)]'$, also in (ECI) coordinates.

With the previous convention, the operations needed to transform the position of the target location expressed in (ECI) coordinates into the sensor s coordinate system (based on its nominal orientation) is

$$
\mathbf{x}_s^{\mathrm{n}}(k) = T(\boldsymbol{\omega}_s(k))(\mathbf{x}(k) - \boldsymbol{\xi}_s(k)) \quad s = 1, 2, ..., N_S, \quad k = 0, 1, 2, ..., K \tag{5.2}
$$

where $\boldsymbol{\omega}_s(k) = [\phi_s^{\mathrm{n}}(k), \rho_s^{\mathrm{n}}(k), \psi_s^{\mathrm{n}}(k)]'$ is the nominal orientation of sensor s, $T(\boldsymbol{\omega}_s(k))$ is the appropriate rotation matrix, and the translation $(\mathbf{x}(k) - \boldsymbol{\xi}_s(k))$ is the difference between the vector position of the target and the vector position of the sensor s, both expressed in (ECI) coordinates. The superscript "n" in (5.2) indicates that

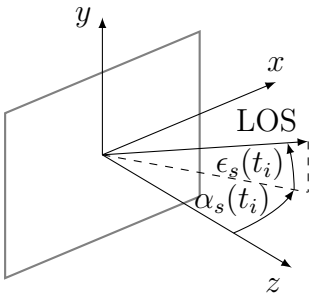

Fig. 5.1: Optical sensor coordinate system with the origin in the center of the focal plane.

the rotation matrix is based on the nominal sensor orientation.

Each passive sensor provides LOS measurements of the target position. As shown in Figure 1, the azimuth angle $\alpha_s(k)$ is the angle in the sensor xz plane between the sensor z axis and the line of sight to the target, while the elevation angle $\epsilon_s(k)$ is the angle between the line of sight to the target and its projection onto the xz plane, i.e.,

$$\begin{bmatrix} \alpha_s(k) \\ \epsilon_s(k) \end{bmatrix} = \begin{bmatrix} \tan^{-1}\left(\frac{x_s(k)}{z_s(k)}\right) \\ \tan^{-1}\left(\frac{y_s(k)}{\sqrt{x_s^2(k)+z_s^2(k)}}\right) \end{bmatrix} \tag{5.3}$$

The model for the biased noise-free LOS measurements is then

$$\begin{aligned} \begin{bmatrix} \alpha_s^b(k) \\ \epsilon_s^b(k) \end{bmatrix} &= \begin{bmatrix} h_1(\mathbf{x}(k), \boldsymbol{\xi}_s(k), \boldsymbol{\omega}_s(k), \mathbf{b}_s) \\ h_2(\mathbf{x}(k), \boldsymbol{\xi}_s(k), \boldsymbol{\omega}_s(k), \mathbf{b}_s) \end{bmatrix} \\ &\triangleq \boldsymbol{h}(\mathbf{x}(k), \boldsymbol{\xi}_s(k), \boldsymbol{\omega}_s(k), \mathbf{b}_s) \end{aligned} \tag{5.4}$$

where h_1 and h_2 denote the sensor Cartesian coordinates-to-azimuth/elevation angle mapping that can be found by inserting (5.2) and (5.3) into (5.4), and the

bias vector of sensor s is

$$\mathbf{b}_s = [\phi_s, \rho_s, \psi_s]' \tag{5.5}$$

At time k, each sensor provides the noisy LOS measurements

$$\mathbf{z}_s(k) = \boldsymbol{h}(\mathbf{x}(k), \boldsymbol{\xi}_s(k), \boldsymbol{\omega}_s(k), \mathbf{b}_s) + \mathbf{w}_s(k) \tag{5.6}$$

Let $\mathbf{z}$ be an augmented vector consisting of the batch stacked measurements from all the sensors up to time K

$$\mathbf{z} = [z_1(1), z_2(1), ..., z_{N_S}(1), ..., z_1(K), z_2(K), ..., z_{N_S}(K)] \tag{5.7}$$

and

$$\mathbf{w}_s(k) = [w_s^{\alpha}(k), w_s^{\epsilon}(k)]' \tag{5.8}$$

The measurement noises $\mathbf{w}_s(k)$ are zero-mean, white Gaussian with

$$R_s = \begin{bmatrix} (\sigma_s^{\alpha})^2 & 0 \\ 0 & (\sigma_s^{\epsilon})^2 \end{bmatrix} \quad s = 1, 2, ..., N_S \tag{5.9}$$

and are assumed mutually independent. The problem is to estimate the bias vectors for all sensors and the state vector (position and velocity) of the target of opportunity

$$\boldsymbol{\theta} = [x(K), y(K), z(K), \dot{x}(K), \dot{y}(K), \dot{z}(K), \mathbf{b}_1', ..., \mathbf{b}_{N_S}']' \tag{5.10}$$

from

$$\mathbf{z} = \mathbf{h}(\boldsymbol{\theta}) + \mathbf{w} \tag{5.11}$$

where

$$\mathbf{h}(\boldsymbol{\theta}) = [h_{11}(\boldsymbol{\theta})', h_{21}(\boldsymbol{\theta})', ..., h_{N_S1}(\boldsymbol{\theta})', ..., h_{1K}(\boldsymbol{\theta})', h_{2K}(\boldsymbol{\theta})', ..., h_{N_SK}(\boldsymbol{\theta})'] \tag{5.12}$$

$$\mathbf{w} = [\mathbf{w}_1(1)', \mathbf{w}_2(1)', ..., \mathbf{w}_{N_S}(1)', ..., \mathbf{w}_1(K)', \mathbf{w}_2(K)', ..., \mathbf{w}_{N_S}(K)'] \tag{5.13}$$

and the covariance of the stacked process noise (5.13) is the $(N_sK \times N_sK)$ block-diagonal matrix

$$R = \begin{bmatrix} R_1 & 0 & \cdots & 0 \\ 0 & R_2 & \cdots & 0 \\ \vdots & \vdots & \ddots & \vdots \\ 0 & \cdots & 0 & R_{N_S} \end{bmatrix} \tag{5.14}$$

5.2.1 Space target dynamics

The state space model for a discrete-time stochastic system is of the general form

$$\mathbf{x}(k+1) = f[\mathbf{x}(k), \mathbf{u}(k), \mathbf{v}(k)] \quad k = 0, 1, 2, ..., K \tag{5.15}$$

Although the motion of ballistic missiles in orbit about the Earth is nonlinear, with small time steps ($\leq 10s$) we can approximate the motion model with a discrete-time linear dynamic equation

$$\mathbf{x}(k+1) = F\mathbf{x}(k) + G\mathbf{u}(k) + G\mathbf{v}(k) \tag{5.16}$$

where $\mathbf{x}(\mathbf{k})$ is the 6 dimensional state vector at time k denoted as

$$\mathbf{x}(k) = [x(k), y(k), z(k), \dot{x}(k), \dot{y}(k), \dot{z}(k)]', \quad k = 0, 1, 2, ..., K \tag{5.17}$$

F is the state transition matrix, u is a known input representing the gravitational effects acting on the target, and $\mathbf{v}$ is the process noise (white noise acceleration) with covariance Q. The state transition matrix for a target with acceleration due to gravity is

$$F = \begin{bmatrix} 1 & 0 & 0 & \Delta t & 0 & 0 \\ 0 & 1 & 0 & 0 & \Delta t & 0 \\ 0 & 0 & 1 & 0 & 0 & \Delta t \\ 0 & 0 & 0 & 1 & 0 & 0 \\ 0 & 0 & 0 & 0 & 1 & 0 \\ 0 & 0 & 0 & 0 & 0 & 1 \end{bmatrix} \tag{5.18}$$

and the known input gain matrix (multiplying the appropriate components of the gravity vector) is

$$G = \begin{bmatrix} \Delta t^2/2 & 0 & 0 \\ 0 & \Delta t^2/2 & 0 \\ 0 & 0 & \Delta t^2/2 \\ \Delta t & 0 & 0 \\ 0 & \Delta t & 0 \\ 0 & 0 & \Delta t \end{bmatrix} \tag{5.19}$$

where Δt is the sampling interval. The gravity term is given by

$$u = g\mathbf{x}_p/a \tag{5.20}$$

where $\mathbf{x_p}$ is the position part pf the state $\mathbf{x}$ in (5.15), $g = 9.8$ m/s^2, and a is the distance from the target to the origin of the coordinates system. For simplicity we assume g to be constant. The ratio $\mathbf{x}_p/a$ yields the components of the gravity. of the target and provides the scaling factor for the gravity term. The process noise $\mathbf{v}$ accounts for the inaccurate modeling of the true system dynamics and is added to the state to model possible missile accelerations due to maneuvers with a covariance matrix Q,

$$Q = \begin{bmatrix} \sigma_x^2 & 0 & 0 \\ 0 & \sigma_y^2 & 0 \\ 0 & 0 & \sigma_z^2 \end{bmatrix} \tag{5.21}$$

We shall obtain the maximum likelihood (ML) estimate of the augmented parameter vector (5.10) consisting of the (unknown) target position, velocity and sensor biases (under the assumption $Q = 0$), by maximizing the likelihood function (LF) of $\boldsymbol{\theta}$ based on $\mathbf{z}$

$$\Lambda(\boldsymbol{\theta}; \mathbf{z}) = p\left(\mathbf{z}|\boldsymbol{\theta}\right) \tag{5.22}$$

The ML estimate (MLE) is then

$$\hat{\boldsymbol{\theta}}(\mathbf{z})^{ML} = \arg\max_{\boldsymbol{\theta}} \Lambda(\boldsymbol{\theta}; \mathbf{z}) \tag{5.23}$$

In order to find the MLE, one has to solve a nonlinear least squares problem. This will be done using a numerical search via the Batch Iterated Least Squares (ILS) technique.

5.2.2 Requirements for Bias Estimability

First requirement for bias estimability

Each sensor provides a two-dimensional measurement (the two LOS angles to the target) at time K. We assume that each sensor sees the target at all the times $0, 1, 2, ..., K$. Stacking together all the measurements results in an overall measurement vector of dimension $2KN_S$. Given that the position, velocity of the target and bias vectors of each sensor are three-dimensional, and knowing that the number of equations (size of the stacked measurement vector) has to be at least equal to the number of parameters to be estimated (target state and biases), we must have

$$2KN_S \geq \ 3N_S + 6 \tag{5.24}$$

This is a necessary condition but not sufficient because (5.23) has to have a unique solution, i.e., the parameter vector has to be estimable. This is guaranteed by the second requirement.

Second requirement of bias estimability

This is the invertibility of the Fisher Information matrix (FIM). In order to have parameter observability, the FIM must be invertible. If the FIM is not invertible (i.e., it is singular), then the CRLB (the inverse of the FIM) will not exist — the FIM will have one or more infinite eigenvalues, which means total uncertainty in

a subspace of the parameter space, i.e., ambiguity [2].

For the example of bias estimability discussed in the sequel, to estimate the biases of 2 sensors (6 bias components) and 6 target components (3 position and 3 velocity components), i.e., the search is in an 12-dimensional space in order to meet the necessary requirement (5.24). As stated previously, the FIM must be invertible, so the rank of the FIM has to be equal to the number of parameters to be estimated (6+6=12, in the previous example). The full rank of the FIM is a necessary and sufficient condition for estimability. There exists, however, a subtle unobservability for this example that will necessitate the use of more measurements than the strict minimum number of measurements given by (5.24).

5.2.3 Iterated Least Squares

Given the estimate $\hat{\boldsymbol{\theta}}^j$ after j iterations, the batch ILS estimate after the $(j+1)$th iteration will be

$$\hat{\boldsymbol{\theta}}^{j+1} = \hat{\boldsymbol{\theta}}^j + \left[(H^j)' R^{-1} H^j\right]^{-1} (H^j)' R^{-1} [\mathbf{z} - \mathbf{h}(\hat{\boldsymbol{\theta}}^j)] \tag{5.25}$$

where

$$\mathbf{h}(\hat{\boldsymbol{\theta}}^j) = [h_{11}(\hat{\boldsymbol{\theta}}^j)', h_{21}(\hat{\boldsymbol{\theta}}^j)', ..., h_{N_S 1}(\hat{\boldsymbol{\theta}}^j)', ..., h_{1K}(\hat{\boldsymbol{\theta}}^j)', h_{2K}(\hat{\boldsymbol{\theta}}^j)', ..., h_{N_S K}(\hat{\boldsymbol{\theta}}^j)'] \tag{5.26}$$

where

$$H^j = \left.\frac{\partial \mathbf{h}\left(\boldsymbol{\theta}^j\right)}{\partial \boldsymbol{\theta}}\right|_{\boldsymbol{\theta}=\hat{\boldsymbol{\theta}}^j} \tag{5.27}$$

is the Jacobian matrix of the vector consisting of the stacked measurement functions (5.26) w.r.t. (5.10) evaluated at the ILS estimate from the previous iteration

j. In this case, the Jacobian matrix is, with the iteration index omitted for conciseness,

$$H = \begin{bmatrix} H_{11} & H_{21} & H_{N_S 1} & \cdots & H_{1K} & H_{2K} & H_{N_S K} \end{bmatrix}' \tag{5.28}$$

where

$$H_{sk} = \begin{bmatrix} \frac{h_{1s}(k)}{\partial x(k)} & \frac{h_{1s}(k)}{\partial y(k)} & \frac{h_{1s}(k)}{\partial z(k)} & \frac{h_{1s}(k)}{\partial \dot{x}(k)} & \frac{h_{1s}(k)}{\partial \dot{y}(k)} & \frac{h_{1s}(k)}{\partial \dot{z}(k)} & \frac{h_{1s}(k)}{\partial b_{\alpha_1}} & \frac{h_{1s}(k)}{\partial b_{\epsilon_1}} & \frac{h_{1s}(k)}{\partial b_{\rho_1}} & \cdots & \frac{h_{1s}(k)}{\partial b_{\alpha_{N_S}}} & \frac{h_{1s}(k)}{\partial b_{\epsilon_{N_S}}} & \frac{h_{1s}(k)}{\partial b_{\rho_{N_S}}} \\ \frac{h_{2s}(k)}{\partial x(k)} & \frac{h_{2s}(k)}{\partial y(k)} & \frac{h_{2s}(k)}{\partial z(k)} & \frac{h_{2s}(k)}{\partial \dot{x}(k)} & \frac{h_{2s}(k)}{\partial \dot{y}(k)} & \frac{h_{2s}(k)}{\partial \dot{z}(k)} & \frac{h_{2s}(k)}{\partial b_{\epsilon_1}} & \frac{h_{2s}(k)}{\partial b_{\epsilon_1}} & \frac{h_{2s}(k)}{\partial b_{\rho_1}} & \cdots & \frac{h_{2s}(k)}{\partial b_{\epsilon_{N_S}}} & \frac{h_{2s}(k)}{\partial b_{\epsilon_{N_S}}} & \frac{h_{2s}(k)}{\partial b_{\rho_{N_S}}} \end{bmatrix} \tag{5.29}$$

The appropriate partial derivatives are given in the Appendix C.

5.2.4 Initialialization

In order to perform the numerical search via ILS, an initial estimate $\hat{\boldsymbol{\theta}}^0$ is required. Assuming that the biases are null, the LOS measurements from the first and the second sensor $\alpha_1(k)$, $\alpha_2(k)$ and $\epsilon_1(k)$ can be used to solve for each initial Cartesian target position, in ECI coordinates, using (5.30)–(5.32). The two Cartesian positions formed from (5.30)–(5.32) can then be differenced to provide an approximate velocity. This procedure is analogous to two-point differencing [2] and will provide a full six-dimensional state to initialize the ILS algorithm.

$$x(k)^0 = \frac{\xi_2(k) - \xi_1(k) + \zeta_1(k)\tan\alpha_1(k) - \zeta_2(k)\tan\alpha_2(k)}{\tan\alpha_1(k) - \tan\alpha_2(k)} \tag{5.30}$$

$$y(k)^0 = \frac{\tan\alpha_1(k)\left(\xi_2(k) + \tan\alpha_2(k)\left(\zeta_1(k) - \zeta_2(k)\right)\right) - \xi_1(k)\tan\alpha_2(k)}{\tan\alpha_1(k) - \tan\alpha_2(k)} \tag{5.31}$$

$$z(k)^0 = \eta_1(k) + \tan\epsilon_1(k) \left| \frac{(\xi_1(k) - \xi_2(k))\cos\alpha_2(k) + (\zeta_2(k) - \zeta_1(k))\sin\alpha_2(k)}{\sin(\alpha_1(k) - \alpha_2(k))} \right| \tag{5.32}$$

5.2.5 Cramér-Rao Lower Bound

In order to evaluate the efficiency of the estimator, the CRLB must be calculated. The CRLB provides a lower bound on the covariance matrix of an unbiased estimator as [2]

$$E\{(\boldsymbol{\theta} - \hat{\boldsymbol{\theta}})(\boldsymbol{\theta} - \hat{\boldsymbol{\theta}})'\} \geq J(\boldsymbol{\theta})^{-1} \tag{5.33}$$

where J is the Fisher Information Matrix (FIM), $\boldsymbol{\theta}$ is the true parameter vector to be estimated, and $\hat{\boldsymbol{\theta}}$ is the estimate. The FIM is

$$J(\boldsymbol{\theta}) = E\left\{ [\nabla_{\boldsymbol{\theta}} \ln\Lambda(\boldsymbol{\theta})] [\nabla_{\boldsymbol{\theta}} \ln\Lambda(\boldsymbol{\theta})]' \right\}\Big|_{\boldsymbol{\theta}=\boldsymbol{\theta}_{\text{true}}} \tag{5.34}$$

where the gradient of the log-likelihood function is

$$\lambda(\boldsymbol{\theta}) \triangleq \ln\Lambda(\boldsymbol{\theta}) \tag{5.35}$$

$$J(\boldsymbol{\theta}) = H'\left(R^{-1}\right) H\Big|_{\boldsymbol{\theta}=\boldsymbol{\theta}_{\text{true}}} \tag{5.36}$$

Since $\boldsymbol{\theta}_{\text{true}}$ is not available in practice, J will be evaluated at the estimate, and, as it is shown later, the two results are practically the same.

5.2.6 Statistical Test for Efficiency with Monte Carlo Runs

Another measure of performance involves weighting the estimate error by the inverse of the covariance matrix. The normalized estimation error squared (NEES) for the parameter θ (under the hypothesis of efficiency), defined as

$$\epsilon_\theta = (\theta - \hat{\theta})' P^{-1} (\theta - \hat{\theta}) = (\theta - \hat{\theta})' J(\theta) (\theta - \hat{\theta}) \tag{5.37}$$

is chi-square distributed with n_x (the dimension of θ) degrees of freedom, that is,

$$\epsilon_\theta \sim \chi^2_{n_x} \tag{5.38}$$

The hypothesis test for efficiency whether (5.38) can be accepted, i.e., that $P = J^{-1}$ is discussed in [2] and outlined next. The NEES is used in simulations to check whether the estimator is efficient, that is, the errors are statistically consistent with the covariance given by the CRLB — this is the efficiency check. Thus the efficiency check of the estimator (in simulation — because this is the only situation where θ is available) consists of verifying whether (5.38) holds. The practical procedure to check the estimator efficiency is using the sample average NEES from N independent Monte Carlo runs defined as

$$\bar{\epsilon}_\theta = \frac{1}{N} \sum_{i=1}^{N} \epsilon_\theta^i \tag{5.39}$$

The quantity $N\bar{\epsilon}$ is chi-square distributed with Nn_x degrees of freedom.

Let Q be the type I error probability of the test. The $1 - Q$ two-sided

probability region for $N\bar{\epsilon}$ is the interval $[\epsilon_1', \epsilon_2']$.

$$\epsilon_1' = \chi^2_{Nn_x}\left(\frac{Q}{2}\right) \tag{5.40}$$

$$\epsilon_2' = \chi^2_{Nn_x}\left(1 - \frac{Q}{2}\right) \tag{5.41}$$

where in view of the division by N in (5.39), one has

$$\epsilon_i = \frac{\epsilon_i'}{N} \tag{5.42}$$

Thus, if the estimator is efficient, one has to have

$$P\left\{\bar{\epsilon}_\theta \in [\epsilon_1', \epsilon_2']\right\} = 1 - Q \tag{5.43}$$

5.3 Simulations

In this paper we used a hypothetical scenario to test our new methodology. The missile and satellite trajectories are generated using System Tool Kit (STK). The sensor satellites are in a circular orbits of 600 km and 700 km altitude with 0°, 60° degrees inclination, respectively. The target modeled represents a long range ballistic missile with a flight time of about 20 minutes. STK provides the target and sensor positions in three dimensional Cartesian coordinates at 1 s intervals. The measurement noise standard deviation σ_s (identical across sensors for both azimuth and elevation measurements, $\sigma_s^\alpha = \sigma_s^\epsilon = \sigma_s$) was assumed to be 30 μrad. The target launch time was chosen so that the satellite sensors were able to follow the missile trajectory throughout its flight path. As shown in Figure 5.3, these satellite orbits enabled maximum visibility of the missile trajectory

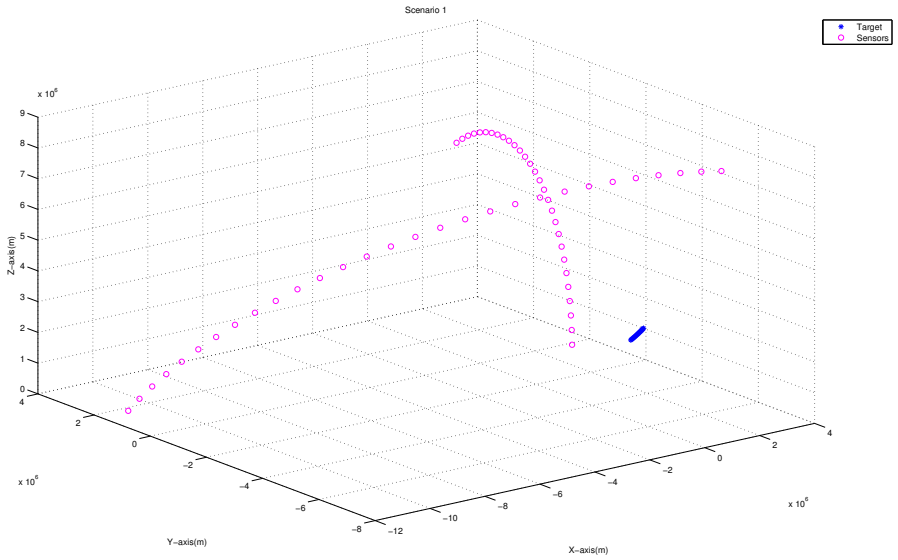

Fig. 5.2: Target and satellite trajectories for the two-sensor case

Table 5.1: Sensor Biases (mrad).

	ψ	ρ	ϕ
Sensor 1	5.7596	4.3633	-3.8397
Sensor 2	4.8869	5.4105	-5.0615

from multiple angles. The missile and satellite trajectories displayed in Figure 5.3 represent 5 minutes of flight time. In order to establish a baseline for evaluating the performance of our method, we also ran the simulations without biases and with biases, but without bias estimation. As discussed in the previous section, the three sensor biases were roll, pitch and yaw angle offsets. Table 5.1 summarizes the bias values (in mrad).

Statistical Efficiency of the Estimates

In order to test for the statistical efficiency of the estimate (of the 12 dimensional vector (5.10)), the NEES is used, with the CRLB as the covariance matrix.

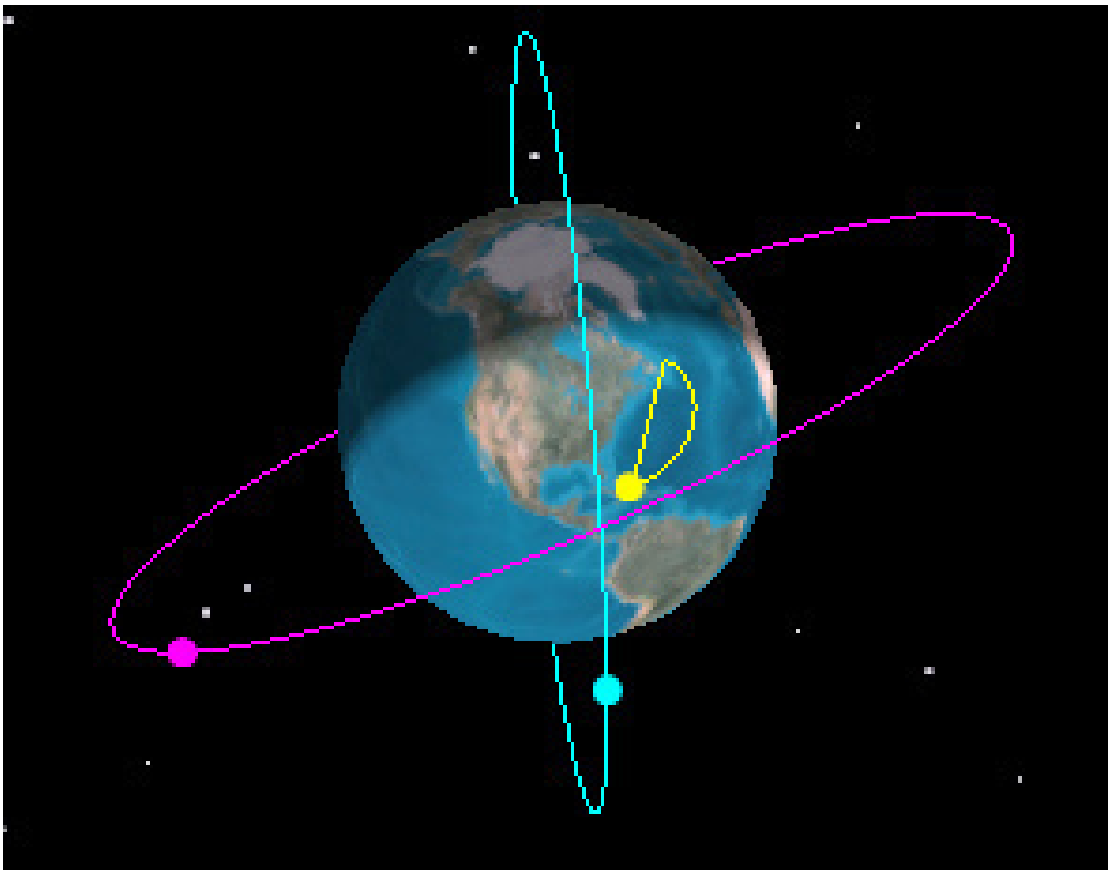

Fig. 5.3: Target and satellite trajectories for the two-sensor case

The sample average NEES over 100 Monte Carlo runs calculated using the FIM evaluated at the true bias values, target position, and velocity is approximately 11.52, and the sample average NEES calculated using the FIM evaluated at the estimated biases, target position and velocity is approximately 11.63 and both fall in the interval given below. According to the CRLB, the FIM has to be evaluated at the true parameter. Since this is not available in practice, however, it is useful to evaluate the FIM also at the estimated parameter, the only one available in real world implementations [25]. The results are practically identical regardless of which values are chosen for evaluation of the FIM. The 95% probability region for the 100 sample average NEES of the 12 dimensional parameter vector is [11.20, 12.81]. This NEES is found to be within this interval and the MLE is therefore statistically efficient. Figure 5.4 shows the individual bias component NEES. The 95% probability region for the 100 sample average single component NEES is [0.74, 1.29]. These NEES are found to be within this interval.

The RMS errors for the target position and velocity are summarized in Table 5.2. In this table, the first estimation scheme was established as a baseline using bias-free LOS measurements to estimate the target position and velocity. For the second scheme, we used biased LOS measurements but we only estimated target position and velocity. In the last scheme, we used biased LOS measurements and we simultaneously estimated the target position, velocity, and sensor biases. Once again, bias estimation yields significantly improved target RMS position and velocity errors in the presence of biases.

Each component of $\boldsymbol{\theta}$ should also be individually consistent with its corresponding σ_{CRLB} (the square root of the corresponding diagonal element of the inverse of FIM). In this case, the sample average bias RMSE over 100 Monte

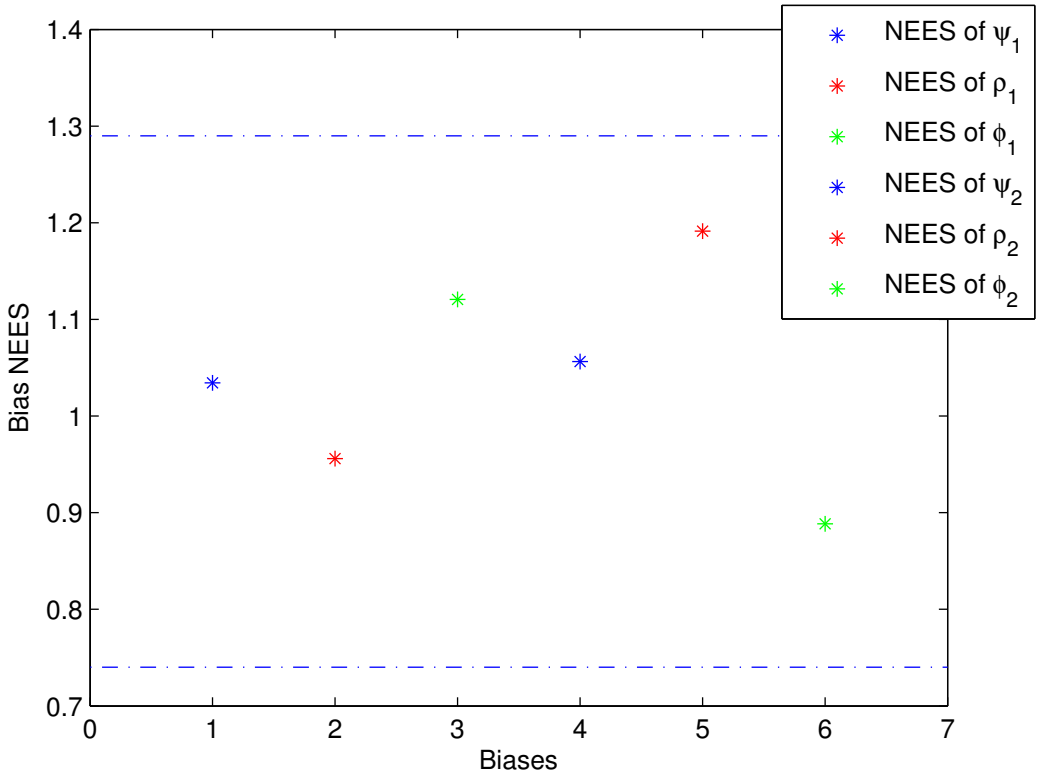

Fig. 5.4: Sample average bias NEES (CRLB evaluated at the estimate), for each of the 6 biases, over 100 Monte Carlo runs (Two-sensor case).

Table 5.2: Sample average RMSE (m) for the target position and velocity, over 100 Monte Carlo runs, for the 3 estimation schemes.

Scheme	Position RMSE	Velocity RMSE
1	107.44	5.16
2	47,161.10	25,149.32
3	494.49	19.55

Table 5.3: Sample average bias (mrad) RMSE over 100 Monte Carlo runs and the corresponding bias standard deviation from the CRLB.

	RMSE	σ_{CRLB}
ψ_1	0.0326	0.0334
ρ_1	0.0239	0.0211
ϕ_1	0.0239	0.0261
ψ_2	0.0248	0.0252
ρ_2	0.0099	0.0096
ϕ_2	0.0122	0.0122

Carlo runs should be within 15% of its corresponding bias standard deviation from the CRLB (σ_{CRLB}) with 95% probability. The utmost limit ("existing information") for the scenario considered is around 15-45 μrad standard deviation for the bias errors, i,e., of the order of σ_s. Table 5.3 demonstrates the efficiency of the individual bias estimates.

5.4 Conclusions

In this chapter we presented a new algorithm that uses a target of opportunity for estimation of measurement biases together with target state. The first step was formulating a general bias model for synchronized space-based optical sensors at known locations. The association of measurements is assumed to be perfect. Based on this, we used an ML approach that led to a batch nonlinear least-squares estimation problem for simultaneous estimation of the 3D Cartesian position and velocity components of the target of opportunity and the angle measurement biases of the sensors. The bias estimates, obtained via ILS, were shown to be unbiased and statistically efficient. For future work we plan to relax the no process noise assumption, reformulate the problem and again evaluate the statistical

efficiency of the algorithm.

Chapter 6

Conclusions and Future Work

In this study we set out to improve target tracking using a passive sensor tracking system through bias estimation when only targets of opportunity are available. The main focus was solving bias issues in a space-based infrared tracking system based on the Missile Defense Agency's Space Tracking and Surveillance System. The first step was formulating a general bias model for optical sensors at known locations. Based on this, we used an ML approach that led to a nonlinear least-squares estimation problem for simultaneous estimation of the Cartesian location, or position and velocity components of the target of opportunity and the angle measurement biases of the sensors. We ran simulations against a number of different scenarios involving two or three optical sensors at various fixed or moving known locations using a target of opportunity at six or three points in time at unknown locations. In all cases, the bias estimates, obtained via ILS, were shown to be unbiased and statistically efficient.

The results of this dissertation point the way to an important area of future work. For future work we plan to relax the no process noise assumption, reformulate the problem and again evaluate the statistical efficiency of the algorithm; we also plan to use one optical moving sensor to estimate the state of a target of

opportunity and the pointing biases of the sensors. Lastly, although not directly related to bias correction, since the STSS is only one of the systems in the missile defense and space tracking architecture, fusing the space based sensor tracking results with other sensor measurements is an area of interest worth pursuing. This could take the form of other sensors providing observations to help refine the space sensor track estimates, especially if there are missing observations. With only a few sensors in orbit, the STSS may not be present during the entire flight of a ballistic threat. Being able to receive a cuing from other sensors is an important capability.

Working on passive sensors bias estimation over the past four years has been quite an experience. We hope that we have added in some meaningful way to the overall body of work in the area of multisensor-multitarget tracking. We would like to think that this dissertation does not represent the conclusion of work on bias estimation, but rather, a milestone in a process of continuous exploration.

A Chapter II Partial Derivatives

The appropriate partial derivatives of (2.20) are

$$\frac{\partial g_{1is}}{\partial x_k} = \frac{\partial g_{1is}}{\partial x_{is}}\frac{\partial x_{is}}{\partial x_k} + \frac{\partial g_{1is}}{\partial y_{is}}\frac{\partial y_{is}}{\partial x_k} + \frac{\partial g_{1is}}{\partial z_{is}}\frac{\partial z_{is}}{\partial x_k} \tag{.1}$$

$$\frac{\partial g_{1is}}{\partial y_k} = \frac{\partial g_{1is}}{\partial x_{is}}\frac{\partial x_{is}}{\partial y_k} + \frac{\partial g_{1is}}{\partial y_{is}}\frac{\partial y_{is}}{\partial y_k} + \frac{\partial g_{1is}}{\partial z_{is}}\frac{\partial z_{is}}{\partial y_k} \tag{.2}$$

$$\frac{\partial g_{1is}}{\partial z_k} = \frac{\partial g_{1is}}{\partial x_{is}}\frac{\partial x_{is}}{\partial z_k} + \frac{\partial g_{1is}}{\partial y_{is}}\frac{\partial y_{is}}{\partial z_k} + \frac{\partial g_{1is}}{\partial z_{is}}\frac{\partial z_{is}}{\partial z_k} \tag{.3}$$

$$\frac{\partial g_{1is}}{\partial \psi_k} = \frac{\partial g_{1is}}{\partial x_{is}}\frac{\partial x_{is}}{\partial \psi_k} + \frac{\partial g_{1is}}{\partial y_{is}}\frac{\partial y_{is}}{\partial \psi_k} + \frac{\partial g_{1is}}{\partial z_{is}}\frac{\partial z_{is}}{\partial \psi_k} \tag{.4}$$

$$\frac{\partial g_{1is}}{\partial \rho_k} = \frac{\partial g_{1is}}{\partial x_{is}}\frac{\partial x_{is}}{\partial \rho_k} + \frac{\partial g_{1is}}{\partial y_{is}}\frac{\partial y_{is}}{\partial \rho_k} + \frac{\partial g_{1is}}{\partial z_{is}}\frac{\partial z_{is}}{\partial \rho_k} \tag{.5}$$

$$\frac{\partial g_{1is}}{\partial \phi_k} = \frac{\partial g_{1is}}{\partial x_{is}}\frac{\partial x_{is}}{\partial \phi_k} + \frac{\partial g_{1is}}{\partial y_{is}}\frac{\partial y_{is}}{\partial \phi_k} + \frac{\partial g_{1is}}{\partial z_{is}}\frac{\partial z_{is}}{\partial \phi_k} \tag{.6}$$

$$\frac{\partial g_{2is}}{\partial x_k} = \frac{\partial g_{2is}}{\partial x_{is}}\frac{\partial x_{is}}{\partial x_k} + \frac{\partial g_{2is}}{\partial y_{is}}\frac{\partial y_{is}}{\partial x_k} + \frac{\partial g_{2is}}{\partial z_{is}}\frac{\partial z_{is}}{\partial x_k} \tag{.7}$$

$$\frac{\partial g_{2is}}{\partial y_k} = \frac{\partial g_{2is}}{\partial x_{is}}\frac{\partial x_{is}}{\partial y_k} + \frac{\partial g_{2is}}{\partial y_{is}}\frac{\partial y_{is}}{\partial y_k} + \frac{\partial g_{2is}}{\partial z_{is}}\frac{\partial z_{is}}{\partial y_k} \tag{.8}$$

$$\frac{\partial g_{2is}}{\partial z_k} = \frac{\partial g_{2is}}{\partial x_{is}}\frac{\partial x_{is}}{\partial z_k} + \frac{\partial g_{2is}}{\partial y_{is}}\frac{\partial y_{is}}{\partial z_k} + \frac{\partial g_{2is}}{\partial z_{is}}\frac{\partial z_{is}}{\partial z_k} \tag{.9}$$

$$\frac{\partial g_{2is}}{\partial \psi_k} = \frac{\partial g_{2is}}{\partial x_{is}}\frac{\partial x_{is}}{\partial \psi_k} + \frac{\partial g_{2is}}{\partial y_{is}}\frac{\partial y_{is}}{\partial \psi_k} + \frac{\partial g_{2is}}{\partial z_{is}}\frac{\partial z_{is}}{\partial \psi_k} \tag{.10}$$

$$\frac{\partial g_{2is}}{\partial \rho_k} = \frac{\partial g_{2is}}{\partial x_{is}}\frac{\partial x_{is}}{\partial \rho_k} + \frac{\partial g_{2is}}{\partial y_{is}}\frac{\partial y_{is}}{\partial \rho_k} + \frac{\partial g_{2is}}{\partial z_{is}}\frac{\partial z_{is}}{\partial \rho_k} \tag{.11}$$

$$\frac{\partial g_{2is}}{\partial \phi_k} = \frac{\partial g_{2is}}{\partial x_{is}}\frac{\partial x_{is}}{\partial \phi_k} + \frac{\partial g_{2is}}{\partial y_{is}}\frac{\partial y_{is}}{\partial \phi_k} + \frac{\partial g_{2is}}{\partial z_{is}}\frac{\partial z_{is}}{\partial \phi_k} \tag{.12}$$

Given that (2.2) can be written as

$$\mathbf{x}_{is} = \begin{bmatrix} x_{is} \\ y_{is} \\ z_{is} \end{bmatrix} = T_s(\mathbf{x}_i - \boldsymbol{\xi}_s)$$

$$= \begin{bmatrix} T_{s_{11}} & T_{s_{12}} & T_{s_{13}} \\ T_{s_{21}} & T_{s_{22}} & T_{s_{23}} \\ T_{s_{31}} & T_{s_{32}} & T_{s_{33}} \end{bmatrix} \begin{bmatrix} x_i - \xi_s \\ y_i - \eta_s \\ z_i - \zeta_s \end{bmatrix} \tag{.13}$$

therefore

$$x_{is} = T_{s_{11}}(x_i - \xi_s) + T_{s_{12}}(y_i - \eta_s) + T_{s_{13}}(z_i - \zeta_s) \tag{.14}$$

$$y_{is} = T_{s_{21}}(x_i - \xi_s) + T_{s_{22}}(y_i - \eta_s) + T_{s_{23}}(z_i - \zeta_s) \tag{.15}$$

$$z_{is} = T_{s_{31}}(x_i - \xi_s) + T_{s_{32}}(y_i - \eta_s) + T_{s_{33}}(z_i - \zeta_s) \tag{.16}$$

and

$$\begin{aligned} \tfrac{\partial x_{is}}{\partial x_k} &= T_{s_{11}}, \quad \tfrac{\partial x_{is}}{\partial y_k} = T_{s_{12}}, \quad \tfrac{\partial x_{is}}{\partial y_k} = T_{s_{13}} \\ \tfrac{\partial y_{is}}{\partial x_k} &= T_{s_{21}}, \quad \tfrac{\partial y_{is}}{\partial y_k} = T_{s_{22}}, \quad \tfrac{\partial y_{is}}{\partial y_k} = T_{s_{23}} \\ \tfrac{\partial z_{is}}{\partial x_k} &= T_{s_{31}}, \quad \tfrac{\partial z_{is}}{\partial y_k} = T_{s_{32}}, \quad \tfrac{\partial z_{is}}{\partial y_k} = T_{s_{33}} \end{aligned} \tag{.17}$$

$$\frac{\partial x_{is}}{\partial \psi_k} = \frac{\partial T_{s_{11}}}{\partial \psi_k}(x_i - \xi_s) + \frac{\partial T_{s_{12}}}{\partial \psi_k}(y_i - \eta_s) + \frac{\partial T_{s_{13}}}{\partial \psi_k}(z_i - \zeta_s) \tag{.18}$$

$$\frac{\partial x_{is}}{\partial \rho_k} = \frac{\partial T_{s_{11}}}{\partial \rho_k}(x_i - \xi_s) + \frac{\partial T_{s_{12}}}{\partial \rho_k}(y_i - \eta_s) + \frac{\partial T_{s_{13}}}{\partial \rho_k}(z_i - \zeta_s) \tag{.19}$$

$$\frac{\partial x_{is}}{\partial \phi_k} = \frac{\partial T_{s_{11}}}{\partial \phi_k}(x_i - \xi_s) + \frac{\partial T_{s_{12}}}{\partial \phi_k}(y_i - \eta_s) + \frac{\partial T_{s_{13}}}{\partial \phi_k}(z_i - \zeta_s) \tag{.20}$$

$$\frac{\partial y_{is}}{\partial \psi_k} = \frac{\partial T_{s_{21}}}{\partial \psi_k}(x_i - \xi_s) + \frac{\partial T_{s_{22}}}{\partial \psi_k}(y_i - \eta_s) + \frac{\partial T_{s_{23}}}{\partial \psi_k}(z_i - \zeta_s) \tag{.21}$$

$$\frac{\partial y_{is}}{\partial \rho_k} = \frac{\partial T_{s21}}{\partial \rho_k}(x_i - \xi_s) + \frac{\partial T_{s22}}{\partial \rho_k}(y_i - \eta_s) + \frac{\partial T_{s23}}{\partial \rho_k}(z_i - \zeta_s) \tag{.22}$$

$$\frac{\partial y_{is}}{\partial \phi_k} = \frac{\partial T_{s11}}{\partial \phi_k}(x_i - \xi_s) + \frac{\partial T_{s22}}{\partial \phi_k}(y_i - \eta_s) + \frac{\partial T_{s23}}{\partial \phi_k}(z_i - \zeta_s) \tag{.23}$$

$$\frac{\partial z_{is}}{\partial \psi_k} = \frac{\partial T_{s31}}{\partial \psi_k}(x_i - \xi_s) + \frac{\partial T_{s32}}{\partial \psi_k}(y_i - \eta_s) + \frac{\partial T_{s33}}{\partial \psi_k}(z_i - \zeta_s) \tag{.24}$$

$$\frac{\partial z_{is}}{\partial \rho_k} = \frac{\partial T_{s31}}{\partial \rho_k}(x_i - \xi_s) + \frac{\partial T_{s32}}{\partial \rho_k}(y_i - \eta_s) + \frac{\partial T_{s33}}{\partial \rho_k}(z_i - \zeta_s) \tag{.25}$$

$$\frac{\partial z_{is}}{\partial \phi_k} = \frac{\partial T_{s31}}{\partial \phi_k}(x_i - \xi_s) + \frac{\partial T_{s32}}{\partial \phi_k}(y_i - \eta_s) + \frac{\partial T_{s33}}{\partial \phi_k}(z_i - \zeta_s) \tag{.26}$$

$$\frac{\partial g_{1is}}{\partial x_{is}} = \frac{z_{is}}{z_{is}^2 + x_{is}^2} \tag{.27}$$

$$\frac{\partial g_{1is}}{\partial y_{is}} = 0 \tag{.28}$$

$$\frac{\partial g_{1is}}{\partial z_{is}} = -\frac{x_{is}}{x_{is}^2 + z_{is}^2} \tag{.29}$$

$$\frac{\partial g_{2is}}{\partial x_{is}} = -\frac{x_{is} y_{is}}{\sqrt{(x_{is}^2 + z_{is}^2)}(x_{is}^2 + y_{is}^2 + z_{is}^2)} \tag{.30}$$

$$\frac{\partial g_{2is}}{\partial y_{is}} = \frac{\sqrt{x_{is}^2 + z_{is}^2}}{x_{is}^2 + y_{is}^2 + z_{is}^2} \tag{.31}$$

$$\frac{\partial g_{2is}}{\partial z_{is}} = -\frac{z_{is} y_{is}}{(x_{is}^2 + y_{is}^2 + z_{is}^2)(\sqrt{x_{is}^2 + z_{is}^2})} \tag{.32}$$

$$\frac{\partial T_{s11}}{\partial \psi_k} = -\sin\psi_k \cos\rho_k \tag{.33}$$

$$\frac{\partial T_{s12}}{\partial \psi_k} = -\sin\psi_k \sin\rho_k \sin\phi_k - \cos\psi_k \cos\phi_k \tag{.34}$$

$$\frac{\partial T_{s13}}{\partial \psi_k} = -\sin\psi_k \sin\rho_k \cos\phi_k + \cos\psi_k \sin\phi_k \tag{.35}$$

$$\frac{\partial T_{s21}}{\partial \psi_k} = \cos\psi_k \cos\rho_k \tag{.36}$$

$$\frac{\partial T_{s22}}{\partial \psi_k} = \cos\psi_k \sin\rho_k \sin\phi_k - \sin\psi_k \cos\phi_k \tag{.37}$$

$$\frac{\partial T_{s23}}{\partial \psi_k} = \cos\psi_k \sin\rho_k \cos\phi_k + \sin\psi_k \sin\phi_k \tag{.38}$$

$$\frac{\partial T_{s_{31}}}{\partial \psi_k} = 0 \tag{.39}$$
$$\frac{\partial T_{s_{32}}}{\partial \psi_k} = 0 \tag{.40}$$
$$\frac{\partial T_{s_{33}}}{\partial \psi_k} = 0 \tag{.41}$$
$$\frac{\partial T_{s_{11}}}{\partial \rho_k} = -\cos\psi_k \sin\rho_k \tag{.42}$$
$$\frac{\partial T_{s_{12}}}{\partial \rho_k} = \cos\psi_k \cos\rho_k \sin\phi_k \tag{.43}$$
$$\frac{\partial T_{s_{13}}}{\partial \rho_k} = \cos\psi_k \cos\rho_k \cos\phi_k \tag{.44}$$
$$\frac{\partial T_{s_{21}}}{\partial \rho_k} = -\sin\psi_k \sin\phi_k \tag{.45}$$
$$\frac{\partial T_{s_{22}}}{\partial \rho_k} = \sin\psi_k \cos\rho_k \sin\phi_k \tag{.46}$$
$$\frac{\partial T_{s_{23}}}{\partial \rho_k} = \sin\psi_k \cos\rho_k \cos\phi_k \tag{.47}$$
$$\frac{\partial T_{s_{31}}}{\partial \rho_k} = -\cos\phi_k \tag{.48}$$
$$\frac{\partial T_{s_{32}}}{\partial \rho_k} = -\sin\rho_k \sin\phi_k \tag{.49}$$
$$\frac{\partial T_{s_{33}}}{\partial \rho_k} = -\sin\rho_k \cos\phi_k \tag{.50}$$
$$\frac{\partial T_{s_{11}}}{\partial \phi_k} = 0 \tag{.51}$$
$$\frac{\partial T_{s_{12}}}{\partial \phi_k} = \cos\psi_k \sin\rho_k \cos\phi_k + \sin\psi_k \sin\phi_k \tag{.52}$$
$$\frac{\partial T_{s_{13}}}{\partial \phi_k} = -\cos\psi_k \sin\rho_k \sin\phi_k + \sin\psi_k \cos\phi_k \tag{.53}$$
$$\frac{\partial T_{s_{21}}}{\partial \phi_k} = 0 \tag{.54}$$
$$\frac{\partial T_{s_{22}}}{\partial \phi_k} = \sin\psi_k \sin\rho_k \cos\phi_k - \cos\psi_k \sin\phi_k \tag{.55}$$
$$\frac{\partial T_{s_{23}}}{\partial \phi_k} = -\sin\psi_k \sin\rho_k \sin\phi_k - \cos\psi_k \cos\phi_k \tag{.56}$$
$$\frac{\partial T_{s_{31}}}{\partial \phi_k} = 0 \tag{.57}$$

$$\frac{\partial T_{s32}}{\partial \phi_k} = \cos\psi_k \cos\phi_k \tag{.58}$$

$$\frac{\partial T_{s33}}{\partial \phi_k} = -\cos\rho_k \sin\phi_k \tag{.59}$$

B Chapter III Partial Derivatives

The appropriate partial derivatives of (3.21) are

$$\frac{\partial g_{1_s}(t_i)}{\partial x(t_k)} = \frac{\partial g_{1_s}(t_i)}{\partial x_s(t_i)}\frac{\partial x_s(t_i)}{\partial x(t_k)} + \frac{\partial g_{1_s}(t_i)}{\partial y_s(t_i)}\frac{\partial y_s(t_i)}{\partial x(t_k)} + \frac{\partial g_{1_s}(t_i)}{\partial z_s(t_i)}\frac{\partial z_s(t_i)}{\partial x(t_k)} \tag{.60}$$

$$\frac{\partial g_{1_s}(t_i)}{\partial y(t_k)} = \frac{\partial g_{1_s}(t_i)}{\partial x_s(t_i)}\frac{\partial x_s(t_i)}{\partial y(t_k)} + \frac{\partial g_{1_s}(t_i)}{\partial y_s(t_i)}\frac{\partial y_s(t_i)}{\partial y(t_k)} + \frac{\partial g_{1_s}(t_i)}{\partial z_s(t_i)}\frac{\partial z_s(t_i)}{\partial y(t_k)} \tag{.61}$$

$$\frac{\partial g_{1_s}(t_i)}{\partial z(t_k)} = \frac{\partial g_{1_s}(t_i)}{\partial x_s(t_i)}\frac{\partial x_s(t_i)}{\partial z(t_k)} + \frac{\partial g_{1_s}(t_i)}{\partial y_s(t_i)}\frac{\partial y_s(t_i)}{\partial z(t_k)} + \frac{\partial g_{1_s}(t_i)}{\partial z_s(t_i)}\frac{\partial z_s(t_i)}{\partial z(t_k)} \tag{.62}$$

$$\frac{\partial g_{1_s}(t_i)}{\partial \psi_k} = \frac{\partial g_{1_s}(t_i)}{\partial x_s(t_i)}\frac{\partial x_s(t_i)}{\partial \psi_k} + \frac{\partial g_{1_s}(t_i)}{\partial y_s(t_i)}\frac{\partial y_s(t_i)}{\partial \psi_k} + \frac{\partial g_{1_s}(t_i)}{\partial z_s(t_i)}\frac{\partial z_s(t_i)}{\partial \psi_k} \tag{.63}$$

$$\frac{\partial g_{1_s}(t_i)}{\partial \rho_k} = \frac{\partial g_{1_s}(t_i)}{\partial x_s(t_i)}\frac{\partial x_s(t_i)}{\partial \rho_k} + \frac{\partial g_{1_s}(t_i)}{\partial y_s(t_i)}\frac{\partial y_s(t_i)}{\partial \rho_k} + \frac{\partial g_{1_s}(t_i)}{\partial z_s(t_i)}\frac{\partial z_s(t_i)}{\partial \rho_k} \tag{.64}$$

$$\frac{\partial g_{1_s}(t_i)}{\partial \phi_k} = \frac{\partial g_{1_s}(t_i)}{\partial x_s(t_i)}\frac{\partial x_s(t_i)}{\partial \phi_k} + \frac{\partial g_{1_s}(t_i)}{\partial y_s(t_i)}\frac{\partial y_s(t_i)}{\partial \phi_k} + \frac{\partial g_{1_s}(t_i)}{\partial z_s(t_i)}\frac{\partial z_s(t_i)}{\partial \phi_k} \tag{.65}$$

$$\frac{\partial g_{2_s}(t_i)}{\partial x(t_k)} = \frac{\partial g_{2_s}(t_i)}{\partial x_s(t_i)}\frac{\partial x_s(t_i)}{\partial x(t_k)} + \frac{\partial g_{2_s}(t_i)}{\partial y_s(t_i)}\frac{\partial y_s(t_i)}{\partial x(t_k)} + \frac{\partial g_{2_s}(t_i)}{\partial z_s(t_i)}\frac{\partial z_s(t_i)}{\partial x(t_k)} \tag{.66}$$

$$\frac{\partial g_{2_s}(t_i)}{\partial y(t_k)} = \frac{\partial g_{2_s}(t_i)}{\partial x_s(t_i)}\frac{\partial x_s(t_i)}{\partial y(t_k)} + \frac{\partial g_{2_s}(t_i)}{\partial y_s(t_i)}\frac{\partial y_s(t_i)}{\partial y(t_k)} + \frac{\partial g_{2_s}(t_i)}{\partial z_s(t_i)}\frac{\partial z_s(t_i)}{\partial y(t_k)} \tag{.67}$$

$$\frac{\partial g_{2_s}(t_i)}{\partial z(t_k)} = \frac{\partial g_{2_s}(t_i)}{\partial x_s(t_i)}\frac{\partial x_s(t_i)}{\partial z(t_k)} + \frac{\partial g_{2_s}(t_i)}{\partial y_s(t_i)}\frac{\partial y_s(t_i)}{\partial z(t_k)} + \frac{\partial g_{2_s}(t_i)}{\partial z_s(t_i)}\frac{\partial z_s(t_i)}{\partial z(t_k)} \tag{.68}$$

$$\frac{\partial g_{2_s}(t_i)}{\partial \psi_k} = \frac{\partial g_{2_s}(t_i)}{\partial x_s(t_i)}\frac{\partial x_s(t_i)}{\partial \psi_k} + \frac{\partial g_{2_s}(t_i)}{\partial y_s(t_i)}\frac{\partial y_s(t_i)}{\partial \psi_k} + \frac{\partial g_{2_s}(t_i)}{\partial z_s(t_i)}\frac{\partial z_s(t_i)}{\partial \psi_k} \tag{.69}$$

$$\frac{\partial g_{2_s}(t_i)}{\partial \rho_k} = \frac{\partial g_{2_s}(t_i)}{\partial x_s(t_i)}\frac{\partial x_s(t_i)}{\partial \rho_k} + \frac{\partial g_{2_s}(t_i)}{\partial y_s(t_i)}\frac{\partial y_s(t_i)}{\partial \rho_k} + \frac{\partial g_{2_s}(t_i)}{\partial z_s(t_i)}\frac{\partial z_s(t_i)}{\partial \rho_k} \tag{.70}$$

$$\frac{\partial g_{2_s}(t_i)}{\partial \phi_k} = \frac{\partial g_{2_s}(t_i)}{\partial x_s(t_i)}\frac{\partial x_s(t_i)}{\partial \phi_k} + \frac{\partial g_{2_s}(t_i)}{\partial y_s(t_i)}\frac{\partial y_s(t_i)}{\partial \phi_k} + \frac{\partial g_{2_s}(t_i)}{\partial z_s(t_i)}\frac{\partial z_s(t_i)}{\partial \phi_k} \tag{.71}$$

Given that (3.2) can be written as

$$\mathbf{x}_s(t_i) = \begin{bmatrix} x_s(t_i) \\ y_s(t_i) \\ z_s(t_i) \end{bmatrix} = T_s(\mathbf{x}(t_i) - \boldsymbol{\xi}_s)$$

$$= \begin{bmatrix} T_{s_{11}} & T_{s_{12}} & T_{s_{13}} \\ T_{s_{21}} & T_{s_{22}} & T_{s_{23}} \\ T_{s_{31}} & T_{s_{32}} & T_{s_{33}} \end{bmatrix} \begin{bmatrix} x(t_i) - \xi_s \\ y(t_i) - \eta_s \\ z(t_i) - \zeta_s \end{bmatrix} \tag{.72}$$

therefore

$$x_s(t_i) = T_{s_{11}}(x(t_i) - \xi_s) + T_{s_{12}}(y(t_i) - \eta_s) + T_{s_{13}}(z(t_i) - \zeta_s) \tag{.73}$$

$$y_s(t_i) = T_{s_{21}}(x(t_i) - \xi_s) + T_{s_{22}}(y(t_i) - \eta_s) + T_{s_{23}}(z(t_i) - \zeta_s) \tag{.74}$$

$$z_s(t_i) = T_{s_{31}}(x(t_i) - \xi_s) + T_{s_{32}}(y(t_i) - \eta_s) + T_{s_{33}}(z(t_i) - \zeta_s) \tag{.75}$$

and

$$\begin{array}{lll} \frac{\partial x_s(t_i)}{\partial x(t_k)} = T_{s_{11}}, & \frac{\partial x_s(t_i)}{\partial y(t_k)} = T_{s_{12}}, & \frac{\partial x_s(t_i)}{\partial y(t_k)} = T_{s_{13}} \\ \frac{\partial y_s(t_i)}{\partial x(t_k)} = T_{s_{21}}, & \frac{\partial y_s(t_i)}{\partial y(t_k)} = T_{s_{22}}, & \frac{\partial y_s(t_i)}{\partial y(t_k)} = T_{s_{23}} \\ \frac{\partial z_s(t_i)}{\partial x(t_k)} = T_{s_{31}}, & \frac{\partial z_s(t_i)}{\partial y(t_k)} = T_{s_{32}}, & \frac{\partial z_s(t_i)}{\partial y(t_k)} = T_{s_{33}} \end{array} \tag{.76}$$

$$\frac{\partial x_s(t_i)}{\partial \psi_k} = \frac{\partial T_{s_{11}}}{\partial \psi_k}(x(t_i) - \xi_s) + \frac{\partial T_{s_{12}}}{\partial \psi_k}(y(t_i) - \eta_s) + \frac{\partial T_{s_{13}}}{\partial \psi_k}(z(t_i) - \zeta_s) \tag{.77}$$

$$\frac{\partial x_s(t_i)}{\partial \rho_k} = \frac{\partial T_{s_{11}}}{\partial \rho_k}(x(t_i) - \xi_s) + \frac{\partial T_{s_{12}}}{\partial \rho_k}(y(t_i) - \eta_s) + \frac{\partial T_{s_{13}}}{\partial \rho_k}(z(t_i) - \zeta_s) \tag{.78}$$

$$\frac{\partial x_s(t_i)}{\partial \phi_k} = \frac{\partial T_{s_{11}}}{\partial \phi_k}(x(t_i) - \xi_s) + \frac{\partial T_{s_{12}}}{\partial \phi_k}(y(t_i) - \eta_s) + \frac{\partial T_{s_{13}}}{\partial \phi_k}(z(t_i) - \zeta_s) \tag{.79}$$

$$\frac{\partial y_s(t_i)}{\partial \psi_k} = \frac{\partial T_{s21}}{\partial \psi_k}(x(t_i) - \xi_s) + \frac{\partial T_{s22}}{\partial \psi_k}(y(t_i) - \eta_s) + \frac{\partial T_{s23}}{\partial \psi_k}(z(t_i) - \zeta_s) \tag{.80}$$

$$\frac{\partial y_s(t_i)}{\partial \rho_k} = \frac{\partial T_{s21}}{\partial \rho_k}(x(t_i) - \xi_s) + \frac{\partial T_{s22}}{\partial \rho_k}(y(t_i) - \eta_s) + \frac{\partial T_{s23}}{\partial \rho_k}(z(t_i) - \zeta_s) \tag{.81}$$

$$\frac{\partial y_s(t_i)}{\partial \phi_k} = \frac{\partial T_{s11}}{\partial \phi_k}(x(t_i) - \xi_s) + \frac{\partial T_{s22}}{\partial \phi_k}(y(t_i) - \eta_s) + \frac{\partial T_{s23}}{\partial \phi_k}(z(t_i) - \zeta_s) \tag{.82}$$

$$\frac{\partial z_s(t_i)}{\partial \psi_k} = \frac{\partial T_{s31}}{\partial \psi_k}(x(t_i) - \xi_s) + \frac{\partial T_{s32}}{\partial \psi_k}(y(t_i) - \eta_s) + \frac{\partial T_{s33}}{\partial \psi_k}(z(t_i) - \zeta_s) \tag{.83}$$

$$\frac{\partial z_s(t_i)}{\partial \rho_k} = \frac{\partial T_{s31}}{\partial \rho_k}(x(t_i) - \xi_s) + \frac{\partial T_{s32}}{\partial \rho_k}(y(t_i) - \eta_s) + \frac{\partial T_{s33}}{\partial \rho_k}(z(t_i) - \zeta_s) \tag{.84}$$

$$\frac{\partial z_s(t_i)}{\partial \phi_k} = \frac{\partial T_{s31}}{\partial \phi_k}(x(t_i) - \xi_s) + \frac{\partial T_{s32}}{\partial \phi_k}(y(t_i) - \eta_s) + \frac{\partial T_{s33}}{\partial \phi_k}(z(t_i) - \zeta_s) \tag{.85}$$

$$\frac{\partial g_{1_s}(t_i)}{\partial x_s(t_i)} = \frac{z_s(t_i)}{z_s(t_i)^2 + x_s(t_i)^2} \tag{.86}$$

$$\frac{\partial g_{1_s}(t_i)}{\partial y_s(t_i)} = 0 \tag{.87}$$

$$\frac{\partial g_{1_s}(t_i)}{\partial z_s(t_i)} = -\frac{x_s(t_i)}{x_s(t_i)^2 + z_s(t_i)^2} \tag{.88}$$

$$\frac{\partial g_{2_s}(t_i)}{\partial x_s(t_i)} = -\frac{x_s(t_i)y_s(t_i)}{\sqrt{(x_s(t_i)^2 + z_s(t_i)^2)}(x_s(t_i)^2 + y_s(t_i)^2 + z_s(t_i)^2)} \tag{.89}$$

$$\frac{\partial g_{2_s}(t_i)}{\partial y_s(t_i)} = \frac{\sqrt{x_s(t_i)^2 + z_s(t_i)^2}}{x_s(t_i)^2 + y_s(t_i)^2 + z_s(t_i)^2} \tag{.90}$$

$$\frac{\partial g_{2_s}(t_i)}{\partial z_s(t_i)} = -\frac{z_s(t_i)y_s(t_i)}{(x_s(t_i)^2 + y_s(t_i)^2 + z_s(t_i)^2)(\sqrt{x_s(t_i)^2 + z_s(t_i)^2})} \tag{.91}$$

$$\frac{\partial T_{s_{11}}}{\partial \psi_k} = -\sin\psi_k \cos\rho_k \tag{.92}$$
$$\frac{\partial T_{s_{12}}}{\partial \psi_k} = -\sin\psi_k \sin\rho_k \sin\phi_k - \cos\psi_k \cos\phi_k \tag{.93}$$
$$\frac{\partial T_{s_{13}}}{\partial \psi_k} = -\sin\psi_k \sin\rho_k \cos\phi_k + \cos\psi_k \sin\phi_k \tag{.94}$$
$$\frac{\partial T_{s_{21}}}{\partial \psi_k} = \cos\psi_k \cos\rho_k \tag{.95}$$
$$\frac{\partial T_{s_{22}}}{\partial \psi_k} = \cos\psi_k \sin\rho_k \sin\phi_k - \sin\psi_k \cos\phi_k \tag{.96}$$
$$\frac{\partial T_{s_{23}}}{\partial \psi_k} = \cos\psi_k \sin\rho_k \cos\phi_k + \sin\psi_k \sin\phi_k \tag{.97}$$
$$\frac{\partial T_{s_{31}}}{\partial \psi_k} = 0 \tag{.98}$$
$$\frac{\partial T_{s_{32}}}{\partial \psi_k} = 0 \tag{.99}$$
$$\frac{\partial T_{s_{33}}}{\partial \psi_k} = 0 \tag{.100}$$

$$\frac{\partial T_{s_{11}}}{\partial \rho_k} = -\cos\psi_k \sin\rho_k \tag{.101}$$
$$\frac{\partial T_{s_{12}}}{\partial \rho_k} = \cos\psi_k \cos\rho_k \sin\phi_k \tag{.102}$$
$$\frac{\partial T_{s_{13}}}{\partial \rho_k} = \cos\psi_k \cos\rho_k \cos\phi_k \tag{.103}$$
$$\frac{\partial T_{s_{21}}}{\partial \rho_k} = -\sin\psi_k \sin\phi_k \tag{.104}$$
$$\frac{\partial T_{s_{22}}}{\partial \rho_k} = \sin\psi_k \cos\rho_k \sin\phi_k \tag{.105}$$
$$\frac{\partial T_{s_{23}}}{\partial \rho_k} = \sin\psi_k \cos\rho_k \cos\phi_k \tag{.106}$$
$$\frac{\partial T_{s_{31}}}{\partial \rho_k} = -\cos\phi_k \tag{.107}$$

$$\frac{\partial T_{s_{32}}}{\partial \rho_k} = -\sin\rho_k \sin\phi_k \tag{.108}$$

$$\frac{\partial T_{s_{33}}}{\partial \rho_k} = -\sin\rho_k \cos\phi_k \tag{.109}$$

$$\frac{\partial T_{s_{11}}}{\partial \phi_k} = 0 \tag{.110}$$

$$\frac{\partial T_{s_{12}}}{\partial \phi_k} = \cos\psi_k \sin\rho_k \cos\phi_k + \sin\psi_k \sin\phi_k \tag{.111}$$

$$\frac{\partial T_{s_{13}}}{\partial \phi_k} = -\cos\psi_k \sin\rho_k \sin\phi_k + \sin\psi_k \cos\phi_k \tag{.112}$$

$$\frac{\partial T_{s_{21}}}{\partial \phi_k} = 0 \tag{.113}$$

$$\frac{\partial T_{s_{22}}}{\partial \phi_k} = \sin\psi_k \sin\rho_k \cos\phi_k - \cos\psi_k \sin\phi_k \tag{.114}$$

$$\frac{\partial T_{s_{23}}}{\partial \phi_k} = -\sin\psi_k \sin\rho_k \sin\phi_k - \cos\psi_k \cos\phi_k \tag{.115}$$

$$\frac{\partial T_{s_{31}}}{\partial \phi_k} = 0 \tag{.116}$$

$$\frac{\partial T_{s_{32}}}{\partial \phi_k} = \cos\psi_k \cos\phi_k \tag{.117}$$

$$\frac{\partial T_{s_{33}}}{\partial \phi_k} = -\cos\rho_k \sin\phi_k \tag{.118}$$

C Chapter V Partial Derivatives

The appropriate partial derivatives of (5.29) are

$$\frac{\partial h_{1s}(k)}{\partial x(k)} = \frac{\partial h_{1s}(k)}{\partial x_s(k)}\frac{\partial x_s(k)}{\partial x(k)} + \frac{\partial h_{1s}(k)}{\partial y_s(k)}\frac{\partial y_s(k)}{\partial x(k)} + \frac{\partial h_{1s}(k)}{\partial z_s(k)}\frac{\partial z_s(k)}{\partial x(k)} \tag{.119}$$

$$\frac{\partial h_{1s}(k)}{\partial y(k)} = \frac{\partial h_{1s}(k)}{\partial x_s(k)}\frac{\partial x_s(k)}{\partial y(k)} + \frac{\partial h_{1s}(k)}{\partial y_s(k)}\frac{\partial y_s(k)}{\partial y(k)} + \frac{\partial h_{1s}(k)}{\partial z_s(k)}\frac{\partial z_s(k)}{\partial y(k)} \tag{.120}$$

$$\frac{\partial h_{1s}(k)}{\partial z(k)} = \frac{\partial h_{1s}(k)}{\partial x_s(k)}\frac{\partial x_s(k)}{\partial z(k)} + \frac{\partial h_{1s}(k)}{\partial y_s(k)}\frac{\partial y_s(k)}{\partial z(k)} + \frac{\partial h_{1s}(k)}{\partial z_s(k)}\frac{\partial z_s(k)}{\partial z(k)} \tag{.121}$$

$$\frac{\partial h_{1s}(k)}{\partial \psi_k} = \frac{\partial h_{1s}(k)}{\partial x_s(k)}\frac{\partial x_s(k)}{\partial \psi_k} + \frac{\partial h_{1s}(k)}{\partial y_s(k)}\frac{\partial y_s(k)}{\partial \psi_k} + \frac{\partial h_{1s}(k)}{\partial z_s(k)}\frac{\partial z_s(k)}{\partial \psi_k} \tag{.122}$$

$$\frac{\partial h_{1s}(k)}{\partial \rho_k} = \frac{\partial h_{1s}(k)}{\partial x_s(k)}\frac{\partial x_s(k)}{\partial \rho_k} + \frac{\partial h_{1s}(k)}{\partial y_s(k)}\frac{\partial y_s(k)}{\partial \rho_k} + \frac{\partial h_{1s}(k)}{\partial z_s(k)}\frac{\partial z_s(k)}{\partial \rho_k} \tag{.123}$$

$$\frac{\partial h_{1s}(k)}{\partial \phi_k} = \frac{\partial h_{1s}(k)}{\partial x_s(k)}\frac{\partial x_s(k)}{\partial \phi_k} + \frac{\partial h_{1s}(k)}{\partial y_s(k)}\frac{\partial y_s(k)}{\partial \phi_k} + \frac{\partial h_{1s}(k)}{\partial z_s(k)}\frac{\partial z_s(k)}{\partial \phi_k} \tag{.124}$$

$$\frac{\partial h_{2s}(k)}{\partial x(k)} = \frac{\partial h_{2s}(k)}{\partial x_s(k)}\frac{\partial x_s(k)}{\partial x(k)} + \frac{\partial h_{2s}(k)}{\partial y_s(k)}\frac{\partial y_s(k)}{\partial x(k)} + \frac{\partial h_{2s}(k)}{\partial z_s(k)}\frac{\partial z_s(k)}{\partial x(k)} \tag{.125}$$

$$\frac{\partial h_{2s}(k)}{\partial y(k)} = \frac{\partial h_{2s}(k)}{\partial x_s(k)}\frac{\partial x_s(k)}{\partial y(k)} + \frac{\partial h_{2s}(k)}{\partial y_s(k)}\frac{\partial y_s(k)}{\partial y(k)} + \frac{\partial h_{2s}(k)}{\partial z_s(k)}\frac{\partial z_s(k)}{\partial y(k)} \tag{.126}$$

$$\frac{\partial h_{2s}(k)}{\partial z(k)} = \frac{\partial h_{2s}(k)}{\partial x_s(k)}\frac{\partial x_s(k)}{\partial z(k)} + \frac{\partial h_{2s}(k)}{\partial y_s(k)}\frac{\partial y_s(k)}{\partial z(k)} + \frac{\partial h_{2s}(k)}{\partial z_s(k)}\frac{\partial z_s(k)}{\partial z(k)} \tag{.127}$$

$$\frac{\partial h_{2s}(k)}{\partial \psi_k} = \frac{\partial h_{2s}(k)}{\partial x_s(k)}\frac{\partial x_s(k)}{\partial \psi_k} + \frac{\partial h_{2s}(k)}{\partial y_s(k)}\frac{\partial y_s(k)}{\partial \psi_k} + \frac{\partial h_{2s}(k)}{\partial z_s(k)}\frac{\partial z_s(k)}{\partial \psi_k} \tag{.128}$$

$$\frac{\partial h_{2s}(k)}{\partial \rho_k} = \frac{\partial h_{2s}(k)}{\partial x_s(k)}\frac{\partial x_s(k)}{\partial \rho_k} + \frac{\partial h_{2s}(k)}{\partial y_s(k)}\frac{\partial y_s(k)}{\partial \rho_k} + \frac{\partial h_{2s}(k)}{\partial z_s(k)}\frac{\partial z_s(k)}{\partial \rho_k} \tag{.129}$$

$$\frac{\partial h_{2s}(k)}{\partial \phi_k} = \frac{\partial h_{2s}(k)}{\partial x_s(k)}\frac{\partial x_s(k)}{\partial \phi_k} + \frac{\partial h_{2s}(k)}{\partial y_s(k)}\frac{\partial y_s(k)}{\partial \phi_k} + \frac{\partial h_{2s}(k)}{\partial z_s(k)}\frac{\partial z_s(k)}{\partial \phi_k} \tag{.130}$$

$$\mathbf{x}_s(k) = \begin{bmatrix} x_s(k) \\ y_s(k) \\ z_s(k) \end{bmatrix} = T_s(\mathbf{x}(k) - \boldsymbol{\xi}_s(k))$$
$$= \begin{bmatrix} T_{s_{11}} & T_{s_{12}} & T_{s_{13}} \\ T_{s_{21}} & T_{s_{22}} & T_{s_{23}} \\ T_{s_{31}} & T_{s_{32}} & T_{s_{33}} \end{bmatrix} \begin{bmatrix} x(k) - \xi_s(k) \\ y(k) - \eta_s(k) \\ z(k) - \zeta_s(k) \end{bmatrix} \qquad (.131)$$

Given that (5.2) can be written as therefore

$$x_s(k) = T_{s_{11}}(x(k) - \xi_s(k)) + T_{s_{12}}(y(k) - \eta_s(k)) + T_{s_{13}}(z(k) - \zeta_s(k)) \quad (.132)$$
$$y_s(k) = T_{s_{21}}(x(k) - \xi_s(k)) + T_{s_{22}}(y(k) - \eta_s(k)) + T_{s_{23}}(z(k) - \zeta_s(k)) \quad (.133)$$
$$z_s(k) = T_{s_{31}}(x(k) - \xi_s(k)) + T_{s_{32}}(y(k) - \eta_s(k)) + T_{s_{33}}(z(k) - \zeta_s(k)) \quad (.134)$$

and

$$\begin{array}{lll} \frac{\partial x_s(k)}{\partial x(k)} = T_{s_{11}}, & \frac{\partial x_s(k)}{\partial y(k)} = T_{s_{12}}, & \frac{\partial x_s(k)}{\partial y(k)} = T_{s_{13}} \\ \frac{\partial y_s(k)}{\partial x(k)} = T_{s_{21}}, & \frac{\partial y_s(k)}{\partial y(k)} = T_{s_{22}}, & \frac{\partial y_s(k)}{\partial y(k)} = T_{s_{23}} \\ \frac{\partial z_s(k)}{\partial x(k)} = T_{s_{31}}, & \frac{\partial z_s(k)}{\partial y(k)} = T_{s_{32}}, & \frac{\partial z_s(k)}{\partial y(k)} = T_{s_{33}} \end{array} \quad (.135)$$

$$\frac{\partial x_s(k)}{\partial \psi_k} = \frac{\partial T_{s_{11}}}{\partial \psi_k}(x(k) - \xi_s(k)) + \frac{\partial T_{s_{12}}}{\partial \psi_k}(y(k) - \eta_s(k)) + \frac{\partial T_{s_{13}}}{\partial \psi_k}(z(k) - \zeta_s(k)) \quad (.136)$$

$$\frac{\partial x_s(k)}{\partial \rho_k} = \frac{\partial T_{s_{11}}}{\partial \rho_k}(x(k) - \xi_s(k)) + \frac{\partial T_{s_{12}}}{\partial \rho_k}(y(k) - \eta_s(k)) + \frac{\partial T_{s_{13}}}{\partial \rho_k}(z(k) - \zeta_s(k)) \quad (.137)$$

$$\frac{\partial x_s(k)}{\partial \phi_k} = \frac{\partial T_{s_{11}}}{\partial \phi_k}(x(k) - \xi_s(k)) + \frac{\partial T_{s_{12}}}{\partial \phi_k}(y(k) - \eta_s(k)) + \frac{\partial T_{s_{13}}}{\partial \phi_k}(z(k) - \zeta_s(k)) \quad (.138)$$

$$\frac{\partial y_s(k)}{\partial \psi_k} = \frac{\partial T_{s_{21}}}{\partial \psi_k}(x(k) - \xi_s(k)) + \frac{\partial T_{s_{22}}}{\partial \psi_k}(y(k) - \eta_s(k)) + \frac{\partial T_{s_{23}}}{\partial \psi_k}(z(k) - \zeta_s(k)) \quad (.139)$$

$$\frac{\partial y_s(k)}{\partial \rho_k} = \frac{\partial T_{s_{21}}}{\partial \rho_k}(x(k) - \xi_s(k)) + \frac{\partial T_{s_{22}}}{\partial \rho_k}(y(k) - \eta_s(k)) + \frac{\partial T_{s_{23}}}{\partial \rho_k}(z(k) - \zeta_s(k)(k)) \quad (.140)$$

$$\frac{\partial y_s(k)}{\partial \phi_k} = \frac{\partial T_{s_{11}}}{\partial \phi_k}(x(k) - \xi_s(k)) + \frac{\partial T_{s_{22}}}{\partial \phi_k}(y(k) - \eta_s(k)) + \frac{\partial T_{s_{23}}}{\partial \phi_k}(z(k) - \zeta_s(k)(k)) \quad (.141)$$

$$\frac{\partial z_s(k)}{\partial \psi_k} = \frac{\partial T_{s_{31}}}{\partial \psi_k}(x(k) - \xi_s(k)) + \frac{\partial T_{s_{32}}}{\partial \psi_k}(y(k) - \eta_s(k)) + \frac{\partial T_{s_{33}}}{\partial \psi_k}(z(k) - \zeta_s(k)(k)) \quad (.142)$$

$$\frac{\partial z_s(k)}{\partial \rho_k} = \frac{\partial T_{s_{31}}}{\partial \rho_k}(x(k) - \xi_s(k)) + \frac{\partial T_{s_{32}}}{\partial \rho_k}(y(k) - \eta_s(k)) + \frac{\partial T_{s_{33}}}{\partial \rho_k}(z(k) - \zeta_s(k)(k)) \quad (.143)$$

$$\frac{\partial z_s(k)}{\partial \phi_k} = \frac{\partial T_{s_{31}}}{\partial \phi_k}(x(k) - \xi_s(k)) + \frac{\partial T_{s_{32}}}{\partial \phi_k}(y(k) - \eta_s(k)) + \frac{\partial T_{s_{33}}}{\partial \phi_k}(z(k) - \zeta_s(k)(k)) \quad (.144)$$

$$\frac{\partial h_{1_s}(k)}{\partial x_s(k)} = \frac{z_s(k)}{z_s(k)^2 + x_s(k)^2} \tag{.145}$$

$$\frac{\partial h_{1_s}(k)}{\partial y_s(k)} = 0 \tag{.146}$$

$$\frac{\partial h_{1_s}(k)}{\partial z_s(k)} = -\frac{x_s(k)}{x_s(k)^2 + z_s(k)^2} \tag{.147}$$

$$\frac{\partial h_{1_s}(k)}{\partial \dot{x}_s(k)} = \Delta t \frac{\partial h_{1_s}(k)}{\partial x_s(k)} \tag{.148}$$

$$\frac{\partial h_{1_s}(k)}{\partial \dot{y}_s(k)} = 0 \tag{.149}$$

$$\frac{\partial h_{1_s}(k)}{\partial \dot{z}_s(k)} = \Delta t \frac{\partial h_{1_s}(k)}{\partial z_s(k)} \tag{.150}$$

$$\frac{\partial h_{2_s}(k)}{\partial x_s(k)} = -\frac{x_s(k) y_s(k)}{\sqrt{(x_s(k)^2 + z_s(k)^2)}(x_s(k)^2 + y_s(k)^2 + z_s(k)^2)} \tag{.151}$$

$$\frac{\partial h_{1_s}(k)}{\partial x_s(k)} = \frac{z_s(k)}{z_s(k)^2 + x_s(k)^2} \tag{.152}$$

$$\frac{\partial h_{1_s}(k)}{\partial y_s(k)} = 0 \tag{.153}$$

$$\frac{\partial h_{1_s}(k)}{\partial z_s(k)} = -\frac{x_s(k)}{x_s(k)^2 + z_s(k)^2} \tag{.154}$$

$$\frac{\partial h_{2_s}(k)}{\partial x_s(k)} = -\frac{x_s(k) y_s(k)}{\sqrt{(x_s(k)^2 + z_s(k)^2)}(x_s(k)^2 + y_s(k)^2 + z_s(k)^2)} \tag{.155}$$

$$\frac{\partial h_{2_s}(k)}{\partial y_s(k)} = \frac{\sqrt{x_s(k)^2 + z_s(k)^2}}{x_s(k)^2 + y_s(k)^2 + z_s(k)^2} \tag{.156}$$

$$\frac{\partial h_{2_s}(k)}{\partial z_s(k)} = -\frac{z_s(k) y_s(k)}{(x_s(k)^2 + y_s(k)^2 + z_s(k)^2)(\sqrt{x_s(k)^2 + z_s(k)^2})} \tag{.157}$$

$$\frac{\partial h_{2_s}(k)}{\partial \dot{x}_s(k)} = \Delta t \frac{\partial h_{2_s}(k)}{\partial x_s(k)} \tag{.158}$$

$$\frac{\partial h_{2_s}(k)}{\partial \dot{y}_s(k)} = \Delta t \frac{\partial h_{2_s}(k)}{\partial y_s(k)} \tag{.159}$$

$$\frac{\partial h_{2_s}(k)}{\partial \dot{z}_s(k)} = \Delta t \frac{\partial h_{2_s}(k)}{\partial z_s(k)} \tag{.160}$$

$$\frac{\partial T_{s_{11}}}{\partial \psi_k} = -\sin\psi_k \cos\rho_k \tag{.161}$$

$$\frac{\partial T_{s_{12}}}{\partial \psi_k} = -\sin\psi_k \sin\rho_k \sin\phi_k - \cos\psi_k \cos\phi_k \tag{.162}$$

$$\frac{\partial T_{s_{13}}}{\partial \psi_k} = -\sin\psi_k \sin\rho_k \cos\phi_k + \cos\psi_k \sin\phi_k \tag{.163}$$

$$\frac{\partial T_{s_{21}}}{\partial \psi_k} = \cos\psi_k \cos\rho_k \tag{.164}$$

$$\frac{\partial T_{s_{22}}}{\partial \psi_k} = \cos\psi_k \sin\rho_k \sin\phi_k - \sin\psi_k \cos\phi_k \tag{.165}$$

$$\frac{\partial T_{s_{23}}}{\partial \psi_k} = \cos\psi_k \sin\rho_k \cos\phi_k + \sin\psi_k \sin\phi_k \tag{.166}$$

$$\frac{\partial T_{s_{31}}}{\partial \psi_k} = 0 \tag{.167}$$

$$\frac{\partial T_{s_{32}}}{\partial \psi_k} = 0 \tag{.168}$$

$$\frac{\partial T_{s_{33}}}{\partial \psi_k} = 0 \tag{.169}$$

$$\frac{\partial T_{s_{11}}}{\partial \rho_k} = -\cos\psi_k \sin\rho_k \tag{.170}$$
$$\frac{\partial T_{s_{12}}}{\partial \rho_k} = \cos\psi_k \cos\rho_k \sin\phi_k \tag{.171}$$
$$\frac{\partial T_{s_{13}}}{\partial \rho_k} = \cos\psi_k \cos\rho_k \cos\phi_k \tag{.172}$$
$$\frac{\partial T_{s_{21}}}{\partial \rho_k} = -\sin\psi_k \sin\phi_k \tag{.173}$$
$$\frac{\partial T_{s_{22}}}{\partial \rho_k} = \sin\psi_k \cos\rho_k \sin\phi_k \tag{.174}$$
$$\frac{\partial T_{s_{23}}}{\partial \rho_k} = \sin\psi_k \cos\rho_k \cos\phi_k \tag{.175}$$
$$\frac{\partial T_{s_{31}}}{\partial \rho_k} = -\cos\phi_k \tag{.176}$$
$$\frac{\partial T_{s_{32}}}{\partial \rho_k} = -\sin\rho_k \sin\phi_k \tag{.177}$$
$$\frac{\partial T_{s_{33}}}{\partial \rho_k} = -\sin\rho_k \cos\phi_k \tag{.178}$$
$$\frac{\partial T_{s_{11}}}{\partial \phi_k} = 0 \tag{.179}$$
$$\frac{\partial T_{s_{12}}}{\partial \phi_k} = \cos\psi_k \sin\rho_k \cos\phi_k + \sin\psi_k \sin\phi_k \tag{.180}$$
$$\frac{\partial T_{s_{13}}}{\partial \phi_k} = -\cos\psi_k \sin\rho_k \sin\phi_k + \sin\psi_k \cos\phi_k \tag{.181}$$
$$\frac{\partial T_{s_{21}}}{\partial \phi_k} = 0 \tag{.182}$$
$$\frac{\partial T_{s_{22}}}{\partial \phi_k} = \sin\psi_k \sin\rho_k \cos\phi_k - \cos\psi_k \sin\phi_k \tag{.183}$$
$$\frac{\partial T_{s_{23}}}{\partial \phi_k} = -\sin\psi_k \sin\rho_k \sin\phi_k - \cos\psi_k \cos\phi_k \tag{.184}$$
$$\frac{\partial T_{s_{31}}}{\partial \phi_k} = 0 \tag{.185}$$
$$\frac{\partial T_{s_{32}}}{\partial \phi_k} = \cos\psi_k \cos\phi_k \tag{.186}$$
$$\frac{\partial T_{s_{33}}}{\partial \phi_k} = -\cos\rho_k \sin\phi_k \tag{.187}$$

Bibliography

[1] "FTM-20 in the Ballistic Missile Defense System," AEGIS Ballistic Missile Defense System, Tech. Rep., approved For Public Release 13-MDA-7168 (5 Feb 13).

[2] Y. Bar-Shalom, X.-R. Li, and T. Kirubarajan, *Estimation with Applications to Tracking and Navigation: Theory, Algorithms and Software*. J. Wiley and Sons, 2001.

[3] Y. Bar-Shalom, P. K. Willett, and X. Tian, *Tracking and Data Fusion*. YBS Publishing, 2011.

[4] M. Basseville, "A genetic algorithm based multi-dimensional data association algorithm for multi-sensor multi-target tracking," *Mathematical and Computer Modelling*, vol. 26, no. 4, Dec. 1997.

[5] D. Belfadel, R. W. Osborne, and Y. Bar-Shalom, "A Minimalist Approach to Bias Estimation for Passive Sensor Measurements with Targets of Opportunity," in *Proc. SPIE Conf. Signal and Data Processing of Small Targets,* #8857-13, San Diego, California, Aug. 2013.

[6] ——, "Bias Estimation for Optical Sensor Measurements with Targets of Opportunity," in *Proc. FUSION Conf.*, Istanbul, Turkey, July 2013.

[7] ——, "Bias Estimation and Observability for Optical Sensor Measurements with Targets of Opportunity," *Journal of Advances in Information Fusion*, vol. 9, no. 2, pp. 59–74, Dec. 2014.

[8] ——, "Bias estimation for space-based optical sensors with targets of opportunity," in *Proc. SPIE Conf. Signal and Data Processing of Small Targets,* #9092-25, Baltimore, MD, May. 2014.

[9] ——, "Bias Estimation for Moving Optical Sensor Measurements with Targets of Opportunity," *Journal of Advances in Information Fusion*, June 2015.

[10] X. Benlian and W. Zhiquan, "Biased Bearings-Only Parameter Estimation for Bistatic System," *Journal of Electronics (China)*, vol. 24, no. 3, May 2007.

[11] S. V. Bordonaro, P. Willett, and Y. Bar-Shalom, "Tracking with Converted Position and Doppler Measurements," in *Proc. SPIE Conf. Signal and Data Processing of Small Targets,* #8137-12, San Diego, CA, Aug. 2011.

[12] ——, "Consistent Linear Tracker with Position and Range Rate Measurements," in *Proc. Asilomar Conf.*, Asilomar, CA, Nov. 2012.

[13] ——, "Unbiased Tracking with Converted Measurements," in *Proc. 2012 IEEE Radar Conference*, Atlanta, GA, May 2012.

[14] ——, "Unbiased Tracking with Converted Measurements," in *Proc. 51st IEEE Conf. on Decision and Control*, Maui, HI, Dec. 2012.

[15] T. M. Clemons and K.-C. Chang, "Effect of Sensor Bias on Space-based Bearings-only tracker," in *Proc. SPIE Conf. Signal and Data Processing of Small Targets,* #6968, San Diego, California, Aug. 2008.

[16] ——, "Sensor Calibration using In-Situ Celestial Observations to Estimate Bias in Space-Based Missile Tracking," *IEEE Tans. on Aerospace and Electronic Systems*, vol. 48, no. 2, pp. 1403–1427, April 2012.

[17] J. B. Collins and J. K. Uhlmann, "Efficient gating in data association with multivariate distributed states," *IEEE Trans. Aerosp. Electron. Syst.*, vol. 28, no. 3, 1992.

[18] D. F. Crouse, R. Osborne, III, K. Pattipati, P. Willett, and Y. Bar-Shalom, "2D Location Estimation of Angle-Only Sensor Arrays Using Targets of Opportunity," in *Proc. 13th International Conference on Information Fusion*, Edinburgh, Scotland, July 2010.

[19] S. Deb, M. Yeddanapudi, K. Pattipati, and Y. Bar-Shalom, "A generalized S-D assignment algorithm for multisensor-multitarget state estimation," *IEEE Trans. Aerosp. Electron. Syst.*, vol. 33, no. 2, Dec. 1997.

[20] B. D. Kragel, S. Danford, S. M. Herman, and A. B. Poore, "Bias Estimation Using Targets of Opportunity," *Proc. SPIE Conf. on Signal and Data Processing of Small Targets,* #6699, Aug. 2007.

[21] ——, "Joint MAP Bias Estimation and Data Association: Algorithms," *Proc. SPIE Conf. on Signal and Data Processing of Small Targets,* #6699-1E, Aug. 2007.

[22] B. D. Kragel, S. Danford, and A. B. Poore, "Concurrent MAP Data Association and Absolute Bias Estimation with an Arbitrary Number of Sensors," *Proc. SPIE Conf. on Signal and Data Processing of Small Targets,* #6969-50, May 2008.

[23] X. Lin, Y. Bar-Shalom, and T. Kirubarajan, "Exact Multisensor Dynamic Bias Estimation with Local Tracks," *IEEE Tans. on Aerospace and Electronic Systems*, vol. 40, no. 2, pp. 576–590, April 2004.

[24] R. W. Osborne, III, and Y. Bar-Shalom, "Statistical Efficiency of Composite Position Measurements from Passive Sensors," in *Proc. SPIE Conf. on Signal Proc., Sensor Fusion, and Target Recognition,* #8050-07, Orlando, FL, April 2011.

[25] ——, "Statistical Efficiency of Composite Position Measurements from Passive Sensors," *IEEE Tans. on Aerospace and Electronic Systems*, vol. 49, no. 4, pp. 2799–2806, Oct. 2013.

[26] K. R. Pattipati, S. Deb, Y. Bar-Shalom, and R. Washburn, "A new relaxation algorithm and passive sensor data association," *IEEE Trans. Automat. Contr.*, vol. 37, no. 2, pp. 198–213, Apr. 1992.

[27] R. Robertson, "A set of greedy rounding randomized adaptative local search procedure (grasp) implementation for the multidimensional assignment problem," *Computational Optimization and Applications*, vol. 19, Dec. 2001.

[28] I. STK Systems Tool Kit are registered trademarks of Analytical Graphics, *https://www.agi.com.*

[29] P. P. A. Storms and F. C. R. Spieksma, "An LP-based algorithm for the data association problem in multitarget tracking," *Computers and Operations Research*, vol. 30, no. 7, 2003.